Estimation of State of Charge (SOC) and Water Loss for Absorbed Glass Mat Lead Acid Battery

by

Nan Cao

A thesis submitted to the Graduate Faculty of
Auburn University
in partial fulfillment of the
requirements for the Degree of
Master of Science

Auburn, Alabama
Aug 01, 2015

Keywords: state of charge, water loss, Coulomb counting,
equivalent circuit model, extend Kalman filter, AGM

Approved by

Song-Yul Choe, Chair, Professor of Mechanical Engineering
Roy Knight, Assistant Professor of Mechanical Engineering
John Hung, Professor of Electrical and Computer Engineering

Abstract

Accurate and fast estimation of state of charge (SOC) and water loss during battery operations plays an important role in the prevention of over-charge and over-discharge and optimal control strategy of charging, which requires a model that has great performance in accuracy, algorithm robustness, computational efficiency, numerical stability, and cost. For SOC estimation, most researchers focus on electric equivalent circuit model (ECM) and electrochemical model. The latter is based on electrochemical and thermal principles which are capable of representing the details of cell behavior, it is more accurate. However, it cannot be applied to real time applications, due to high computational time. The ECM is relatively simple, but limited to represent a narrow range of operating behaviors not considering the effects of temperature and aging. Therefore, there is a need for the development of a method that considers the effects of temperature and aging and also has real time capability. In water loss estimation, the qualitative analysis is proposed.

A Second order ECM with an extended Kalman filter (EKF) is used to estimate the SOC of an AGM lead acid battery. Considering the model parameter dependence on temperature and aging, the EKF is designed to identify model parameters online. Because the ECM shows poor performance when the battery is under constant voltage (C.V.) charging, the new EKF and Coulomb counting are combined. Then, given the relationship between capacity and temperature, the capacity-temperature model is added to the new method. With this proposed method, SOC estimation error can be reduced to 3% at various temperatures and aging processes.

In water loss estimation, this thesis is the first to propose and test a method to measure the mass of the decomposed water of an AGM lead acid battery. Through calibration of the reaction rate of decomposed water, a water loss estimation algorithm is presented. The comparison between

simulation and experimental results proves the accuracy of this water loss estimation method. The algorithm shows that water loss can be minimized by limiting the maximum voltage and temperature during charging.

Acknowledgments

I would like to express my gratitude to my advisor, Dr. Song-yul Choe, for offering me this research opportunity. Under his guidance I am able to develop strong problem solving skills. Under his influence I have learned how to face the challenges and choices in my life. I believe that these skills will serve me well in the rest of my life. I would also like to acknowledge committee members Dr. Roy W. Knight and Dr. John Hung for their encouragement and insightful comments.

Many thanks to my colleagues Dr. Xueyan Li, Dr. Meng Xiao, Dr. Rujian Fu, Yinyin Zhao, Xinchen Zhao, Yilin Yin, and Yumeng Gao. They provided valuable advice and practical support concerning battery application technology, model development, electronics design, and control theory. Additional thanks to Dr. Meng Xiao for teaching me a lot of electrochemical knowledge that I would have never touched.

I would also like to thank my parents, older sister, and my parents-in-law. They are always supporting me and encouraging me.

Finally, I would like to thank my daughter, Evelyn Cao, who always makes me happy. I would like to convey my deep appreciation to my wife, Dr. Xueyan Li. In life, she gives me inestimable love and patience. In research, she gives me unswerving support.

Table of Contents

List of Tables

List of Figures

Nomenclature

C_1	Equivalent capacitor of the first R-C circuit of ECM, [F]
C_2	Equivalent capacitor of the second R-C circuit of ECM, [F]
C_{H2SO4}	Concentration of H_2SO_4 , [mol/L]
E	Equilibrium potential of electrode, [V]
E^0	Standard potential of the electrode, [V]
F	Faraday constant
δ^0_{Pb}	Electrochemical equivalent weight per Ah of Pb, [g/Ah]
g^{eq}_{Pb}	Equivalent weight of Pb, [g]
I	Current of the battery, [A]
I_{1a}	Current at R_1, [A]
I_{1b}	Current at C_1, [A]
I_{2a}	Current at R_2, [A]
I_{2b}	Current at C_2, [A]
P	Pressure, [Pa]
Q_{max}	Maximum charge capacity at full charge, [Ah]
Q_{max25}	Maximum charge capacity at full charge at 25^{o}C, [Ah]
Q_{rated}	Rated charge capacity, [Ah]
$Q_{releasable}$	Dischargeable charge capacity, [Ah]
R	Universal (or ideal)gas constant, [Ω]
R_0	Equivalent resistance in ECM, [Ω]
R_1	Equivalent resistance of the first R-C circuit of ECM, [Ω]
R_2	Equivalent resistance of the second R-C circuit of ECM, [Ω]

T	Temperature, [^{o}C] or [K]
U_2, U_3	Voltage of the second R-C circuit of ECM, [V]
V_t	Terminal voltage of the battery, [V]
x	State vector
z	Measurement vector
α	Activity
ΔG^0	Change of Gibbs free energy, [cal]
Δt	Sample time, [s]
ΔSOC	Change of the SOC in one sampling period
ΔSOC_{max}	Max. change of the SOC in one sampling period
$\Delta R_{0,max}$	Max. change of R_0 of ECM in one sampling period
κ	Equilibrium constant of the electrochemical reaction
κ_c	Reaction rate of water loss in charging
κ_s	Reaction rate of water loss in discharging and self-discharging
w_k	Process noise
v_k	Measurement noise
$\hat{x}_k$	Posteriori estimate of the state in step k.

Chapter 1: Introduction

1.1 Background

Increased amounts of electronic devices in vehicles and electrically driven actuators used for improvement of fuel economy has changed operating conditions for batteries. The performance of conventional lead acid batteries used for start, lights, and ignition (SLI) should be improved to meet those new electrical loads requirements. The battery itself should deliver more power over a long cycle life and ensure less maintenance. Absorbed Glass Mat (AGM) lead acid battery is one of the lead acid technologies widely used for those applications because of increased power and energy density, and longer cycle life than regular flooded and maintenance free type lead acid batteries. In addition, the prediction of the states of batteries has obtained more attention because of new electric load profiles that electronic devices and actuators consume. State-of-Charge (SOC) allows the Battery Management System (BMS) to protect the battery from overcharging or over-discharging, and finally reduce battery failure. Moreover, the information of SOC can also be used to make better control strategies to regenerate energy from braking or output power for acceleration, and save fuel. The water loss should also be monitored, since lack of water in the electrolyte decreases ion conductivity, and affects battery performance. The amount of water loss can be used as a sign for replacement of the battery.

1.1.1 AGM lead acid battery

AGM lead acid battery is a type of the valve-regulated lead acid (VRLA) battery that has small gas channels in the electrolyte, the oxygen generated in the positive electrode during overcharging or float-charging can be transported to the negative electrode and reused. This process of recombination is called closed oxygen cycle (COC) that can substantially reduce the water loss,

since the water consumed for side reactions during charging can be compensated by regeneration from the reaction of hydrogen and oxygen. As a result, it becomes maintenance-free [1]. In fact, the AGM lead acid battery is completely sealed and there is no way to refill the water, and too much water loss will lead to battery failure. Consequently, water loss is one of the most important operational parameters although the amount of decomposed water is less than conventional lead acid batteries. Although lack of water affects battery performance due to a decrease of ion conductivity of the electrolyte, lack of water causes accelerated side reactions and faster battery degradation, which leads to shorter battery cycle life.

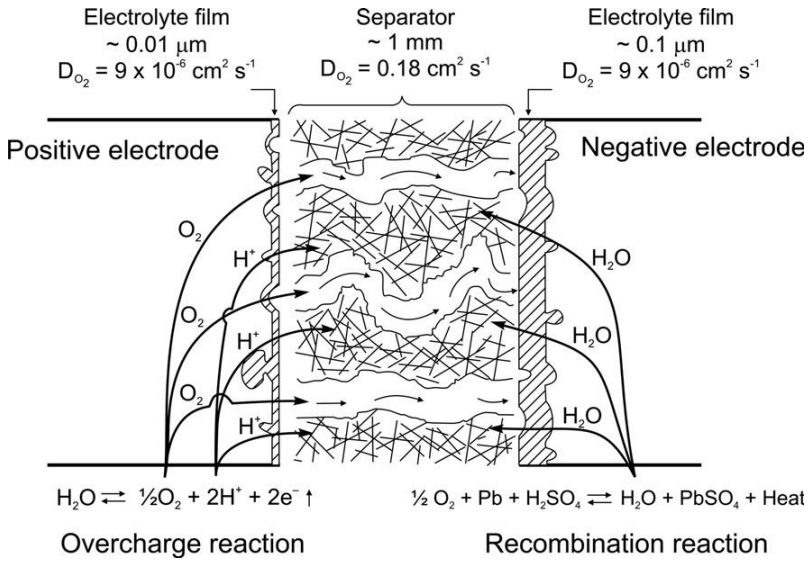

Figure 1: Schematic representation of the internal COC in AGM lead acid battery [1].

1.1.2 Definition of State of Charge (SOC)

SOC is defined as the ratio between the dischargeable charge capacity in a cell ($Q_{releasable}$) and the maximum charge capacity at full charge (Q_{max}). For a fresh battery, Q_{max} is the rated charge capacity (Q_{rated}); Q_{max} decreases as the cell ages. SOC can be expressed in percentage as equation (1), and the value can vary between 0 to 100%.

$$SOC = \frac{Q_{releasable}}{Q_{rated}} \times 100\%, \tag{1}$$

where Q has a unit of ampere-hours (Ah). $Q_{\text{releasable}}$ and $Q_{\max}$ are measurements of electrons inside of the battery.

1.1.3 The measurement and estimation method of SOC

Lead acid batteries use three major materials, lead (Pb), lead oxide (PbO_2) and sulfuric acid (H_2SO_4) and are called Pb\ PbO_2\ H_2SO_4 system. The main reaction of the battery is as follows,

$$Pb + PbO_2 + 2H_2SO_4 \underset{charge}{\overset{discharge}{\rightleftharpoons}} 2PbSO_4 + 2H_2O. \tag{2}$$

For reduction and oxidation of the reaction, electrons, sulfate ions (SO_4^{2-}) and hydrogen ions (H^+) are participated. The current can be determined by electrons that flow through an external circuit or ions that are transported through the electrolyte from anode to cathode, which are called electron current and ion current respectively.

This process is depicted in Figure 2. The orange plates are electrodes, the blue is the electrolyte, the black dots are the sulfate ions (SO_4^{2-}), the white dots are the hydrogen ions (H^+), and the yellow dots are electrons. When the current flows externally from negative to positive, H^+ is transported to and consumed at the anode internally, while the electrons move from cathode to anode externally. During the discharging reaction, the concentrations of SO_4^{2-} , H^+, Pb, and PbO_2 decrease.

SOC can be estimated by either the number of ions present in active material or the number of electrons or change of mass of active materials.

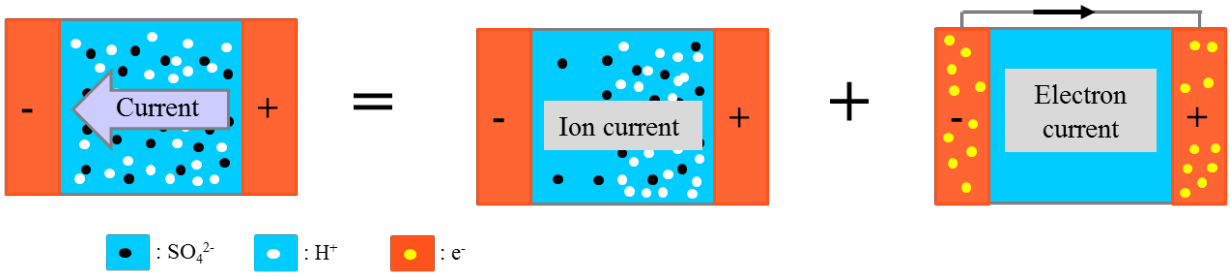

Figure 2: Currents in a micro cell.

SOC estimation can be classified according to following principles, as summarized in Table 1.

Table 1: Classification of SOC estimation method

Principle	**Method**		**Application**
Ion concentration	Direct measurement of ion concentration in electrolyte		Lab
	Open circuit voltage (OCV)		Industry
	Electrochemical model	Full order model (FOM)	Lab / Industry
		Reduced order model (ROM)	
Ion concentration & Active material	Impedance		Lab
	Empirical model		Industry
	Equivalent circuit model (ECM)		Industry
Active material	Direct measurement of quantity of active materials in anode and cathode		Lab
	Resistance		Lab
Electrons	Coulomb counting		Industry

1.2 Literature review

According to the description in subsection 1.1.3, SOC estimation can be classified according to the following principles, as summarized in Table 1.

In Table 1 the method of SOC estimation can be classified in three types, which will be discussed in more details in the following subsection 1.2.1-1.2.3.

1.2.1 Ion concentration

Theoretically, ion concentrations like protons, H^+, can be directly measured using sensors. However, the sensors are very expensive and difficult to integrate in the glass mat of the battery because the electrolyte is absorbed by the glass mat and no liquid electrolyte is presented. Moreover, ion concentration in the electrolyte is not always in an equilibrium state when the battery is in operation.

Open circuit voltage (OCV) can be used for estimation of SOC. After the battery is rested sufficiently, the concentration is uniformly distributed and the terminal voltage becomes the OCV that represents the difference of equilibrium potentials of two electrodes. The equilibrium potential of an electrode is a function of stoichiometric number and ion concentrations. The number of ions in the negative electrode can be used to calculate SOC.

OCV can be measured by charging or discharging a cell with a low current for a finite time and rest periods until fully charged or discharged [2]. SOC is then obtained by integrating the current during loading, which is called the Coulomb counting method. A corresponding SOC to OCV results in a relationship for OCV-SOC [3] that can be experimentally produced and stored in a lookup table for online application. However, if there is current continuously flowing from or into the battery, the equilibrium state cannot be reached, which results in erroneous prediction of OCV [3].

It is assumed that there is no OCV-SOC relationship change during cycling of the battery, if SOC is expressed with relative capacity [4]. Temperature dependence is considered in multiple

lookup tables. A typical OCV-SOC curve of lead acid battery is plotted in Figure 3, where the red circles are the data points measured, and the blue line is fitting result with fifth order polynomial.

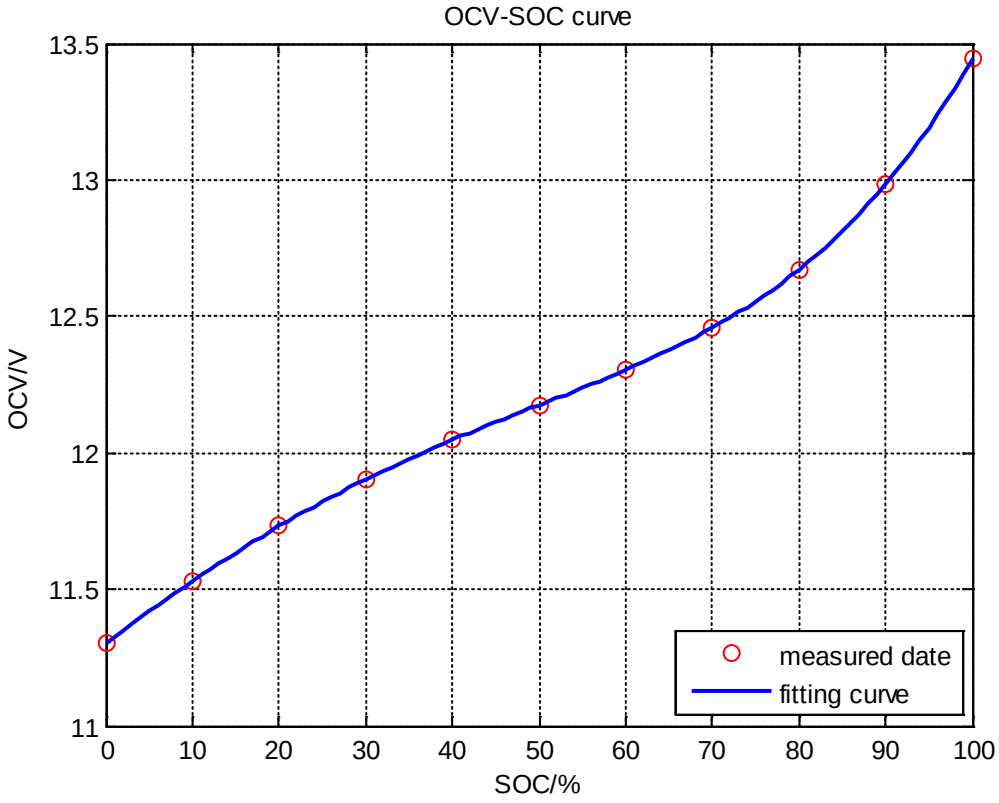

Figure 3: Typical OCV-SOC curve of lead acid battery.

In general, the OCV method is relatively accurate only under the condition that the battery reaches an equilibrium state after a long rest. The direct measurement of OCV does not need any extra models. In contrast, OCV can be estimated based on models during operations.

1.2.2 Active material

Another potential direct measurement method is based on the measurement of active material of the anode or the cathode. The weight of active materials is determined based on design specification on the capacity of the battery.

One coulomb (C) is the amount of electric charge carried by a current of 1 A flowing for 1 s through the cross-section of an electric conductor (1C = 1As), Therefore, the unit ampere-hour is adopted, $1\text{Ah} = 3600\text{C}$. We also know $1\text{F} = 96{,}500\text{C/mol}$.

The quantity of electricity (electric charge) of 1F can be expressed in Ah, like equation,

$$Q_{1F} = \frac{96{,}500\text{C/mol}}{3600\text{s/h}} = 26.80\text{Ah/mol}. \tag{3}$$

The atomic weight of Pb is equal to 207.21 g/mol. Two electrons of each Pb atom take part in the electrochemical reactions of charge or discharge in lead acid battery. The equivalent weight of Pb, g_{Pb}^{eq} is equal to,

$$g_{Pb}^{eq} = 207.12\text{g/mol} / 2 = 103.61\text{g/mol}. \tag{4}$$

We denote as δ^0_{Pb} the electrochemical equivalent weight per Ah of a given active material,

$$\delta_{Pb}^{0} = 103.61\text{g/mol} / 26.8\text{Ah/mol} = 3.866\text{g} \cdot \text{Ah}^{-1}. \tag{5}$$

The equation means when 1Ah of electricity flows through the lead acid battery, 3.866g Pb are oxidized at the negative plates during discharge or released during charge of the battery.

Similarly, the δ^0_{PbO2} is equal to 4.463 g/Ah and the δ^0_{H2SO4} is equal to 3.66 g/Ah. According to the density of the anode or cathode, the SOC can be calculated. Therefore, the battery needs to be opened and cannot be used anymore with this method. It can only be used in a lab to analyze the active material of the anode and the cathode.

Due to the fact that the $Pb/PbSO_4$ and $PbO_2/PbSO_4$ have different resistances, another method is presented. Resistance (R) is voltage divided by a DC current, written as $R=\Delta V/\Delta I$. In application, the voltage change and current in a short time can be used to calculate the R, and a lookup table

can be built to estimate SOC. Multiple lookup tables are needed to cover the range of expected temperatures.

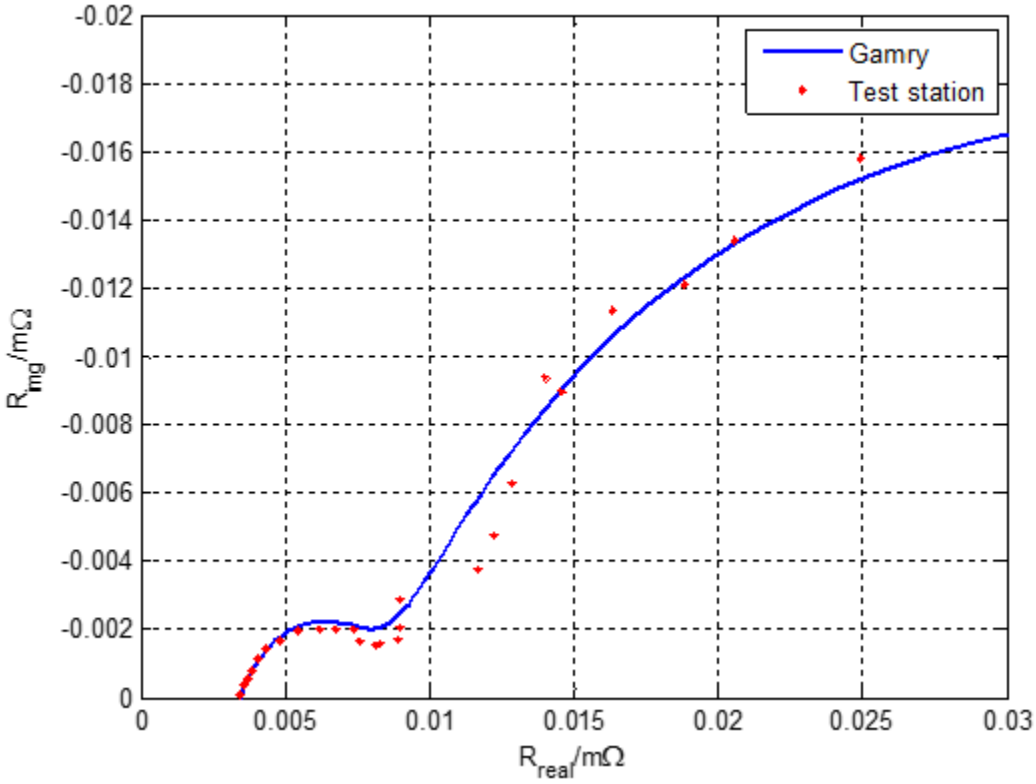

Figure 4: Nyquist plot of the AGM lead acid battery.

The Impedance model, the electrochemical model, and the equivalent circuit model are based on ion concentration and active material. The resistance and diffusion of H_2SO_4 solution are based on the concentration of the solution. Considering both ion concentration and active material, another method, Impedance model, is proposed. Impedance (Z) can be calculated with voltage divided by an AC current, written as $Z = \frac{V}{I}$, where $V = |V|e^{j(\omega t - \phi I)}$ and $I = |I|e^{j(\omega t - \phi I)}$. This equation is similar to the resistance model except there is a phase change. Impedance of the battery is measured by 1mHz to 1KHz AC signal [1]. This measurement is accomplished with the use of

an Electrochemical Impedance Spectroscopy (EIS) machine manufactured by Gamry. The Nyquist plot of an AGM lead acid battery is shown in Figure 4. When the EIS curves of the battery at different SOCs are fitted to a battery ECM, the parameters of ECM over SOC may be extracted and saved in a lookup table [5].

In application, the parameters of ECM are measured using an impedance spectroscope and curve fitting. The SOC is obtained by the lookup table. A severe drawback of the *Z* method is that a specific AC current is required which is difficult to achieve during real time application [6].

1.2.3 Electron

Coulomb counting calculates SOC by counting the number of electrons by integrating the measured current over time, resulting in units of ampere-seconds [7]. The method is very easy to implement, but has several drawbacks [8]. On one hand, it is difficult to find out the initial SOC experimentally, thus history data is needed, which may already have an offset error [3]. On the other hand, since this method is based on current integration, any sensor offset errors will accumulate and further reduce estimation accuracy [9]. The initial SOC is defined to be zero or one hundred percent when the battery is fully discharged or charged. The side reactions like self-discharge would lead to the initial error as well.

1.3 Experimental Setup

The author designed and constructed several battery test stations at Auburn University. Those test stations can be used to charge and discharge a battery with any desired current profile and ambient temperature, including the EIS measurement of the AGM lead acid battery. All of experiments have conducted with AGM lead acid battery, which specifications are as shown in Table 2.

Table 2: Specifications of the AGM lead acid battery in experiments

Manufacturer	Johnson Control Inc.
Part Number:	H6-AGM
Capacity @20Hr	70Ah
Cold Cranking Amps (CCA) @0^{o}F	680A
Weight:	21.1Kg
Battery Height:	190mm
Battery Length:	278mm
Battery Width:	175mm
Rated Voltage:	12V
Operated Voltage:	10.5-14.5V

1.3.1 Test equipment

A test station wiring diagram is show in Figure 5, and Figure 6 shows a photograph of the test station. The equipment are set on a metal rack with one shelf for the computer, one for the electronic load, one for the power supply, and one for the data acquisition (DAQ) board, over-charge and over-discharge protector, and DC power supply, with the computer peripherals on top. The capability and specifications of the test station are shown in Table 3.

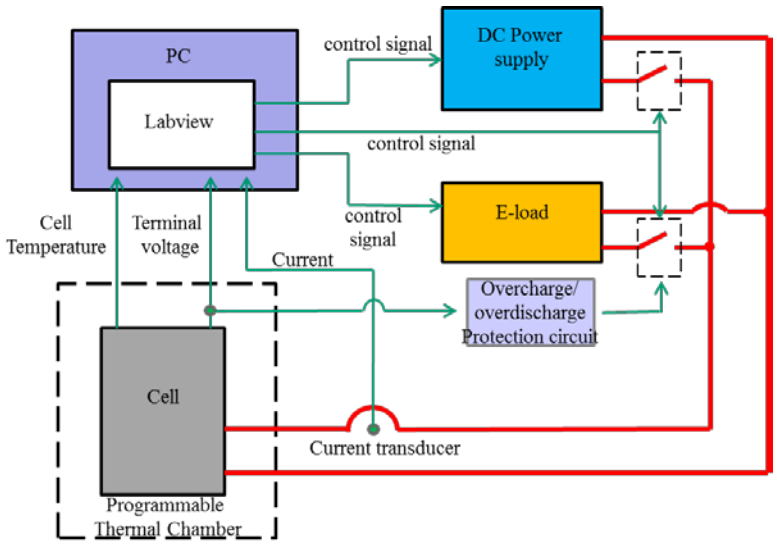

Figure 5: Test station wiring diagram.

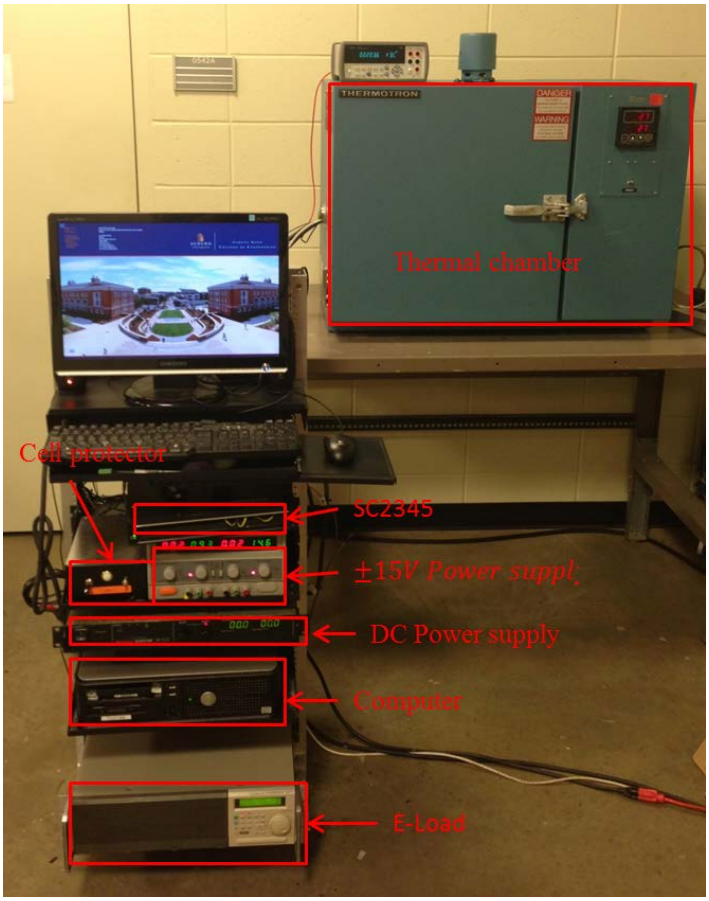

Figure 6: Test station photograph.

Table 3: Performance of the test station

Term		**Values**
Max. charge current		50A
Max. discharge current		125A
Range of the ambient temperature		-20~60 ºC
Data acquisition	Channel	16 Analog input channels 24 Digital input/output channels 2 Analog output channels
	Frequency	625 kS/s
	Resolution	1 mA (current) 0.01mV (voltage)
Frequency of EIS		1mHz~1kHz

1.3.2 Software programming

National Instruments LabVIEW software is used to control the test station. The program works in four modes, including constant current (C.C.), constant voltage (C.V.), constant capacity (C.Q.) charging/discharging, and EIS mode ranging from 1mHz to 1kHz.

A screenshot of the front control panel is shown in Figure 7.

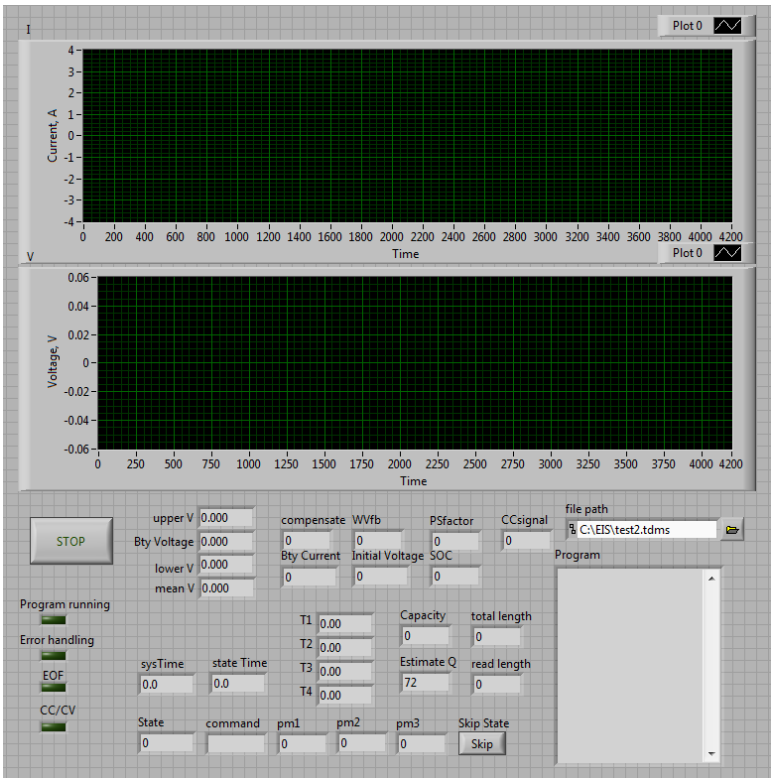

Figure 7: LabVIEW front panel screenshot.

1.4 Structure

The basic structure of the thesis is shown as following:

1. Introduction

This section involves the research background, literature review, and experiment setup.

2. SOC estimation

In section 2.1, the equivalent circuit model is introduced. The state of the battery is then analyzed in section 2.2. The principles of Kalman filter are introduced in section 2.3. A new method that combined Kalman filter and online parameter identification is also introduced in this section. The experimental results and analysis are shown in the last section of this chapter.

3. Improvement of SOC estimation method

In this chapter, the SOC estimation method is improved considering C.V. charge mode and capacity-temperature model, and a novel SOC estimation method is presented in section 3.1 and section 3.2. In the last section, the experimental results and analysis are shown.

4. Water loss estimation

The subsection 4.1 describes the principles of water loss of a lead acid battery. The subsection 4.2 introduces the experiment setup. Based on the results of those experiments, the algorithm of water loss estimation is developed. In subsection 4.3. The results of water loss estimation are shown.

5. Conclusion

Chapter 2: SOC estimation

A review of published papers on estimation of State-of-charge (SOC) has revealed that the estimation methods for the lead acid battery can be classified based on the usage of models or not. Coulomb Counting and Open Circuit Voltage (OCV) or Impedance model, Empirical model, Equivalent circuit model (ECM) and electrochemical full order and reduced order model (FOM and ROM) are the typical methods. Advantages and disadvantages of the methods are summarized in Table 4.

The Coulomb counting and OCV based estimation of SOC do not need any models and the accuracy is relatively low. The empirical model requires many experiments and has difficulty finding the set of parameters, while ECM, FOM and ROM can be used to estimate OCV and as a result, the SOC of the battery. Accurate construction of the models is required and is very challenging because of cell characteristics determined by complex chemical reactions inside of the cell. By modeling each reaction with partial differential equations, the dynamics of the cell can be clearly described. The chemical reaction rate inside each of the electrodes is dependent on SOC, temperature, and the capacity of the battery. The mass or charge diffusion needs to be considered since the exchange current density is not always evenly distributed in each electrode. In the publications [10-12], electrochemical and thermal models are preferred for such applications. Since such models are described based on the electrochemical and thermal principles and use coupled partial differential equations, high computational time is needed and it is not efficient for real time application. Therefore, ECM is preferred by industries.

Table 4: Overview of SOC estimation methods

Technique	**Principles**	**Advantage**	**Disadvantage**
Coulomb counting	$SOC(t) = SOC(0) - \frac{\int_0^t \eta i dt}{Q_{\max}} \times 100\%$	Easy implementation and low cost	Measurement errors accumulate Unable to estimate initial SOC Self-discharge not accounted for
OCV	OCV-SOC values stored in lookup table	Easy implementation and low cost	Ohmic voltage drop and over potentials must be removed Highly sensitive to temperature and aging Identical batteries may have slight variations in OCV curve
Impedance	Impedance is a function of SOC at a certain temperature	Provides insight in to dynamics of multiple internal components	Highly sensitive to temperature, current and aging Requires constant AC amplitude
Empirical model	$V_t = OCV - f(SOC)$	Easy implementation Fast calculation	Can only be used under certain conditions
ECM	Voltage source: $OCV = f(SOC)$ Resistance and capacity	Simple to construct RC circuit Relatively low computational power required	The parameters of ECM are highly sensitive to temperature and aging Unable to provide physical characteristics of the battery
FOM and ROM	Ion concentration Over-potential Heat generation	Describes physical cell limitations and heat generation rate	Relatively high computational power required

2.1 Equivalent circuit model

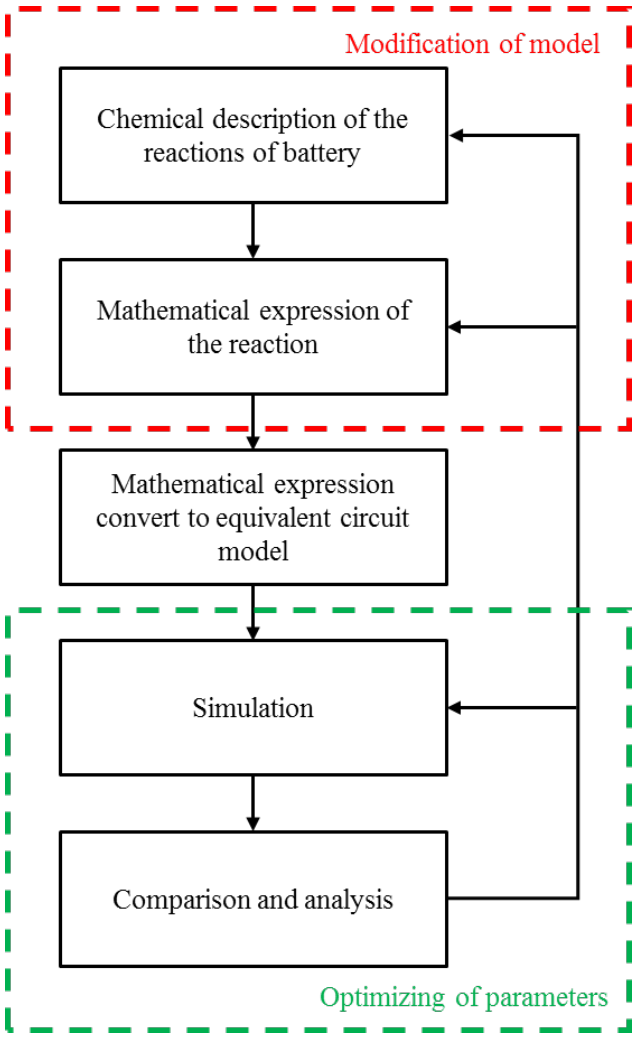

Figure 8: Creation of an equivalent circuit model (ECM).

The principle of equivalent circuit model is shown in Figure 8. There are two major difficulties in model application. First, to improve model accuracy, the order of the model should be high, which would lead to model complexity. Second, some mechanism cannot be completely described by the circuit model, including constant voltage charging and over discharging.

2.1.1 Simple model

The Simple battery model and the correctional model are widely used in battery power estimation. The simple battery model consists of open circuit voltage (OCV), equivalent resistance (R_0), and terminal voltage (Vt), as shown in Figure 9. This model's application is limited by the requirement of SOC estimation accuracy, since the resistance dependence to SOC and aging is not considered.

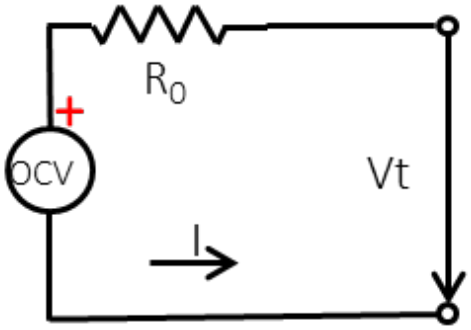

Figure 9: Simple model of lead acid battery.

The simple model of the lead acid battery is shown in Figure 9. The resistance of the battery is not a constant, but a variable which depends on battery SOC. The resistance can be calculated with the following equation.

$$ESR = \frac{R_0}{SOC^{k}}. \qquad (6)$$

where R_0 is the initial resistance when the battery is fully charged; k is a function of current rate, which is determined by electrode geometry, porosity, and additives in the electrolyte.

2.1.2 Thevenin model

Another widely used model is the Thevenin model, which consists of a voltage source E_0, internal resistor R_0, capacitor C_1 of the electrode, and R_1 responsible for activation overpotential

between electrode and electrolyte, as shown in Figure 9. The disadvantage of this model is that it does not consider the effects of current direction and side reactions on battery performance.

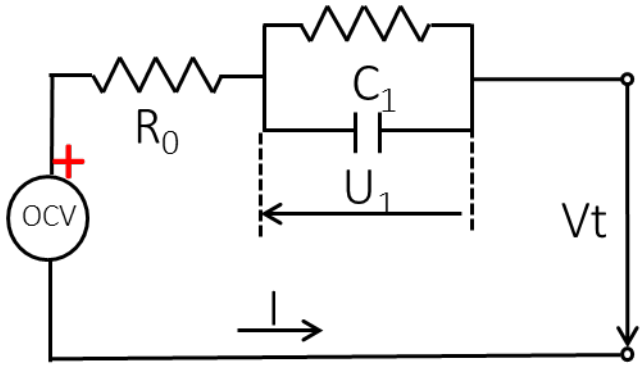

Figure 10: Thevenin battery model.

Figure 10 shows an improved Thevenin model, which takes consideration of internal resistance for self-discharge and the double layer effects, but still ignores the effects caused by current direction.

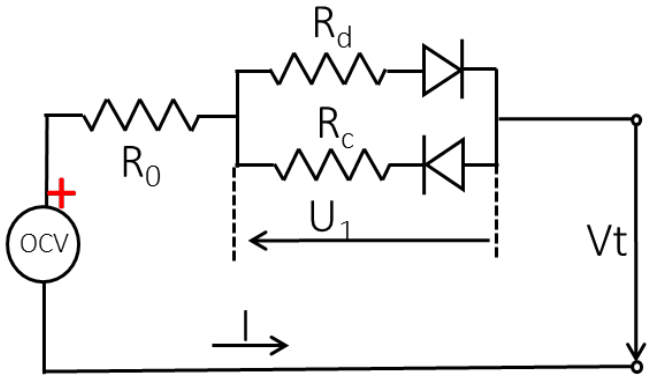

Figure 11: Resistive Thevenin battery model.

The Resistive Thevenin model is shown in Figure 11. The model is developed based on the following assumptions:

1. The electrode is composed of active materials.

2. The resistance of the electrode is constant during discharging.
3. The battery is discharged at a constant current.
4. Polarization resistance is a linear function of the current density of active materials.

The internal resistance during charging and discharging is represented by two separate resistors together with diodes. However, the transient behavior of the capacitor is not considered in this model.

2.1.3 Dynamic model

To build the dynamic model, current, voltage, and temperature need to be considered. This model consists of parallel resistor-capacitor connected in series, and the resistors and capacitors are functions of SOC, temperature, and current direction. The parameters can be measured offline then stored in a look-up table, or be estimated online. The equivalent circuit model proposed in this work is shown in Figure 12.

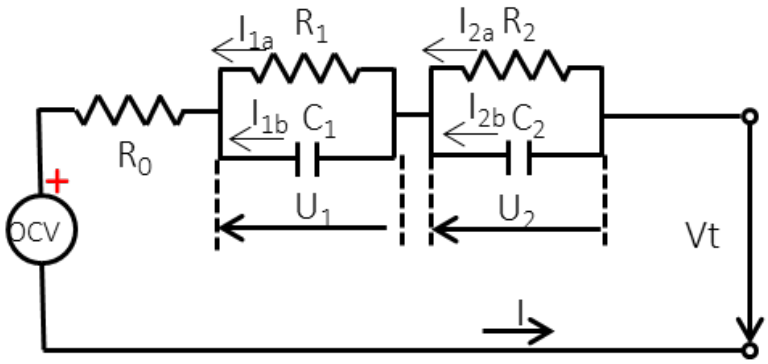

Figure 12: Equivalent circuit model.

2.2 Battery states analysis

2.2.1 Battery states during loading

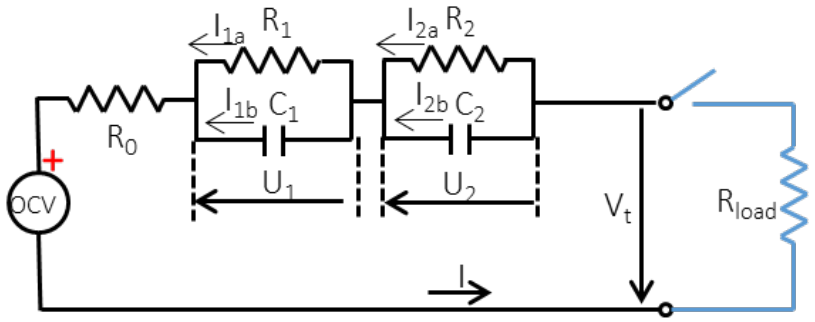

Figure 13: Discharging from rest.

As shown in Figure 13, at the instant of t=0, the switch is closed and the battery starts discharging. The voltage of the first R-C circuit is U_1. The current over the resistance R_1 and the capacitor, C_1 is I_{1a} and I_{1b} . According to Ohm's law, the current, I_{1a} and I_{1b} can be expressed as,

$$I_{1a} = \frac{U_1}{R_1}; \tag{7}$$

$$I_{1b} = C_1 \frac{dU_1}{dt}; \tag{8}$$

$$I = I_{1a} + I_{1b}. \tag{9}$$

Combining equation (7)-(9) results in

$$\frac{dU_1}{dt} + \frac{U_1}{R_1 C_1} = \frac{I}{C_1}. \tag{10}$$

With the boundary conditions of $U_1(0) = 0$ and $U_1(\infty) = IR$, the solution becomes,

$$U_1 = IR_1\left(1 - e^{\frac{-t}{R_1C_1}}\right). \tag{11}$$

Similarly, the voltage of second R-C circuit (U_2) is given as,

$$U_2 = IR_2\left(1 - e^{\frac{-t}{R_2C_2}}\right). \tag{12}$$

Finally, the terminal voltage of the battery can be calculated with the following equation,

$$V_t(t) = OCV(SOC) - IR_1\left(1 - e^{\frac{-t}{R_1C_1}}\right) - IR_2\left(1 - e^{\frac{-t}{R_2C_2}}\right) - IR_0 \tag{13}$$

2.2.2 Battery state during relaxation

Initially, the battery is either charging or discharging at a time instant t and then the switch is open. There is no current flowing in and out of the battery. The relationship between voltage and current in a parallel resistor-capacitor circuit can be described by Equation (6), but with different boundary conditions, $U_1(0) = U_{1,0}$ and $U_1(\infty) = 0$, the solution becomes,

$$U_1 = U_{1,0}e^{\frac{-t}{R_1C_1}}, \tag{14}$$

$$U_2 = U_{2,0}e^{\frac{-t}{R_2C_2}}. \tag{15}$$

Finally, the terminal voltage of the battery can be expressed as,

$$V_t(t) = OCV(SOC) - U_{1,0}e^{\frac{-t}{R_1C_1}} - U_{2,0}e^{\frac{-t}{R_2C_2}} - IR_0. \tag{16}$$

2.2.3 Discretization

The equations derived for the ECM second order system above are nonlinear in time domain. For a discrete system, the equation should be discretized to obtain a difference equation. If the

sample time (Δt) is small enough at a time instant t_k, the change of current during the time interval can be assumed to be constant, the voltage equation for the first R-C circuit can be converted into a discrete equation for the sampling interval from k and k+1 ,

$$U_1[k] = IR_1\left(1 - e^{\frac{-t}{R_1C_1}}\right); \tag{17}$$

According to $f(x) = f(x_0) + f'(x_0)\cdot(x - x_0)$, the voltage of R-C circuit in k+1 time can be written as an equation (18).

$$\begin{aligned} U_1[k+1] &= U_1[k] + \left.\frac{\partial U_1}{\partial t}\right|_k \Delta t \,. \\ &= U_1[k] + IR_1 \cdot \left(-\frac{1}{R_1C_1}\right)\cdot\left(-e^{-\frac{t}{R_1C_1}}\right)\cdot\Delta t + IR_1\frac{\Delta t}{R_1C_1} - IR_1\frac{\Delta t}{R_1C_1} \\ &= U_1[k] - IR_1\frac{\Delta t}{R_1C_1}\left(1 - e^{-\frac{t}{R_1C_1}}\right) + \frac{I}{C_1}\Delta t \\ &\quad - U_1[k]\left(1 - \frac{\Delta t}{R_1C_1}\right) + \frac{I}{C_1}\Delta t \end{aligned} \tag{18}$$

Likewise, the voltage equation of the second R-C circuit at time step k+1 can also be rewritten as follows,

$$U_1[k+1] = \left(1 - \frac{\Delta t}{R_1C_1}\right)U_1[k] + \frac{\Delta t}{C_1}I \,, \tag{19}$$

$$U_2[k+1] = \left(1 - \frac{\Delta t}{R_2C_2}\right)U_1[k] + \frac{\Delta t}{C_2}I \,. \tag{20}$$

Likewise, the equations to describe terminal voltage during rest can also be discretized as,

$$U_1[k+1] = U_1[k]\left(1 - \frac{\Delta t}{R_1C_1}\right), \tag{21}$$

$$U_2[k+1] = U_2[k]\left(1 - \frac{\Delta t}{R_2 C_2}\right), \tag{22}$$

Finally, the equation (16) for the battery terminal voltage is rewritten using difference equation,

$$V_t[k+1] = OCV[k] - U_1[k]\left(1 - \frac{\Delta t}{R_1 C_1}\right) - U_2[k]\left(1 - \frac{\Delta t}{R_2 C_2}\right) - I\left(R_0 - \frac{\Delta t}{C_1} - \frac{\Delta t}{C_2}\right). \tag{23}$$

2.3 Parameter identification

2.5.1 Offline Determination of parameters

All resistors and capacitors in the model are not constant, but dependent on SOC, current direction, temperature, and aging of the battery. There are two approaches to identify the parameters, offline and online estimation. For offline measurement of the parameters of R_0, R_1, R_2, C_1, and C_2, the battery is fully charged at first. A constant pulse current is then applied and the terminal voltage response is measured until the battery is almost fully discharged. Each of the pulses consist of a two hours' discharging at 1/20 C-rate (3.5A) with a four hours' relaxation. The example of one pulse is shown in Figure 14.

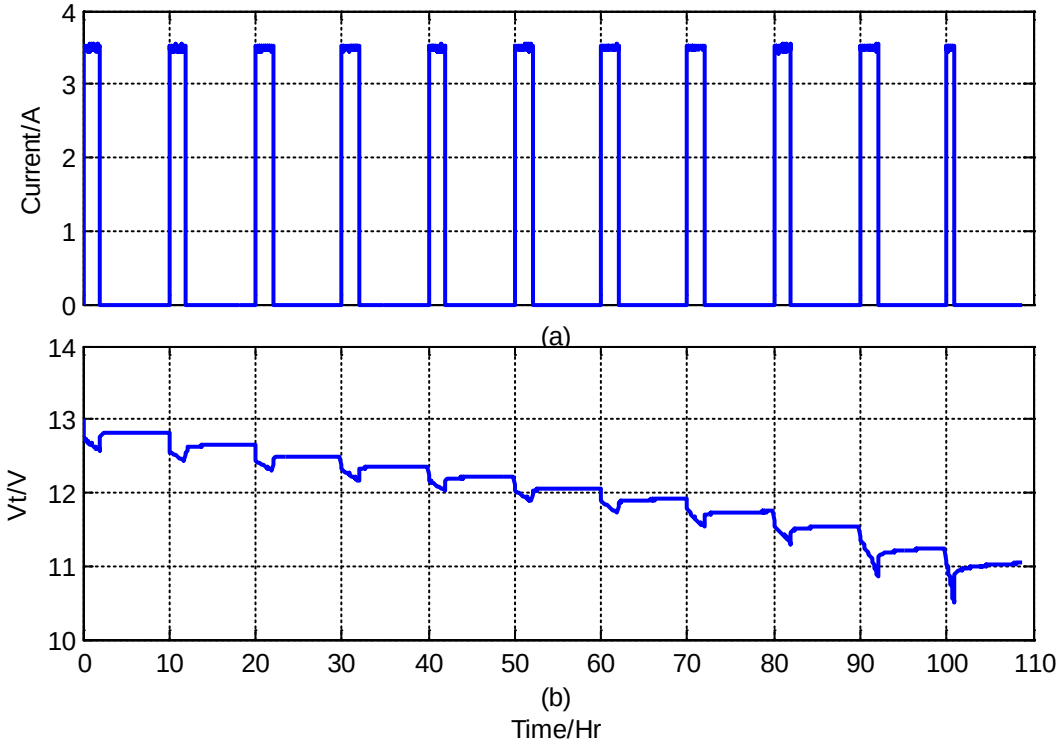

Figure 14: Measurement of model parameters using current pulse discharging.

The internal resistance R_0 can be extracted from the voltage difference obtained before and after the instant that the discharge current is off. According to Ohm's law, R_0 is the voltage divided by the current. The remaining voltage change is used to extract the two parallel RC parameters using the following equation,

$$\mathrm{OCV} - V_t - IR_0 = U_1{}^k e^{\frac{-\Delta t}{R_1 C_1}} + U_2{}^k e^{\frac{-\Delta t}{R_1 C_1}}. \tag{24}$$

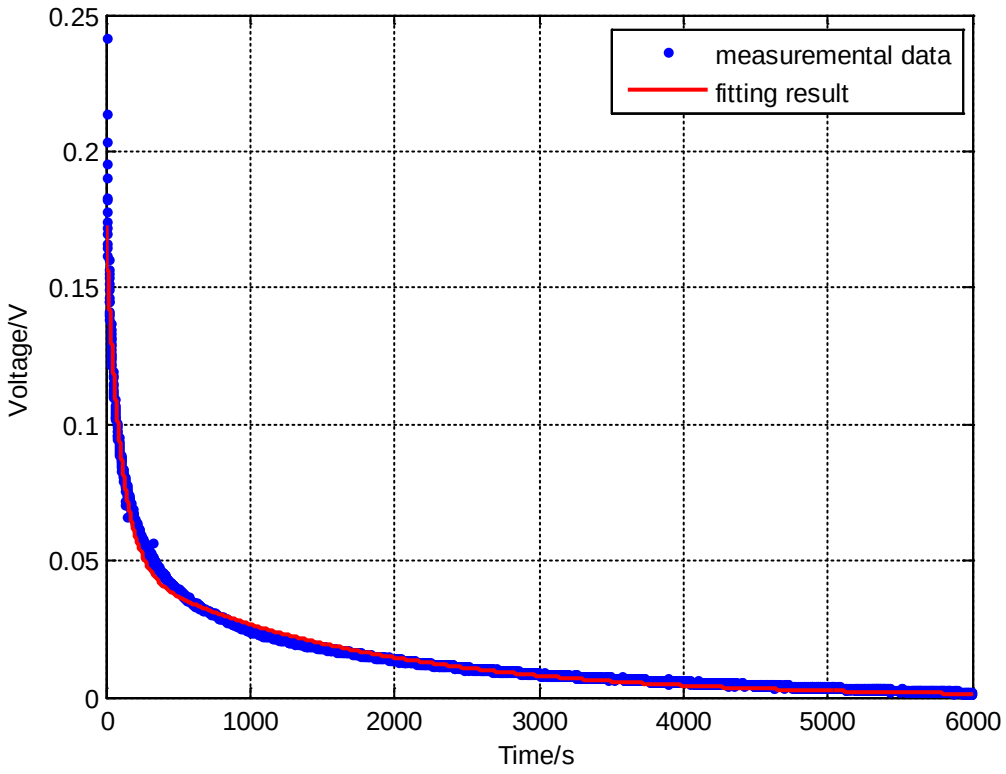

Figure 15: Curve fitting.

After four hours' relaxation, it can be assumed that the battery reaches an equilibrium state, thus the measured terminal voltage can be considered the OCV at a specific SOC. The voltage difference is a second order exponential equation $y = a \cdot e^{b \cdot x} + c \cdot e^{d \cdot x}$. With the help of the Curve Fitting toolbox in Matlab, the parameters can be found with the nonlinear least square method. Figure 15 shows a comparison of curve fitting results, where the blue dots are experimental data points and the red line is from the curve fit.

With the pulse discharge and relaxation method, the parameters of the ECM can be estimated offline. At 25 ^{o}C, the values of the resistors and capacitors of a fresh battery as a function of SOC are shown as the circles in Figure 16. In order to apply this relationship between the parameters

and SOC of the battery in the ECM, they are fitted by fifth order polynomials, and the fitting results are shown in the solid lines of Figure 16. The results show that at both high and low SOC resistance is high, while capacitance is low. The similar method is then applied for charging, and the results of C.C. and C.V. charging are shown in Figure 17 and Figure 18, respectively. Although both Figure 17 and Figure 18 show results during charging, the parameters are very different, because they are at constant current and constant voltage mode. When comparing the parameters at discharging and charging, the results show similar trend with SOC changes, but the parameter values are very different, thus two sets of parameters are used in the model for discharging and charging separately.

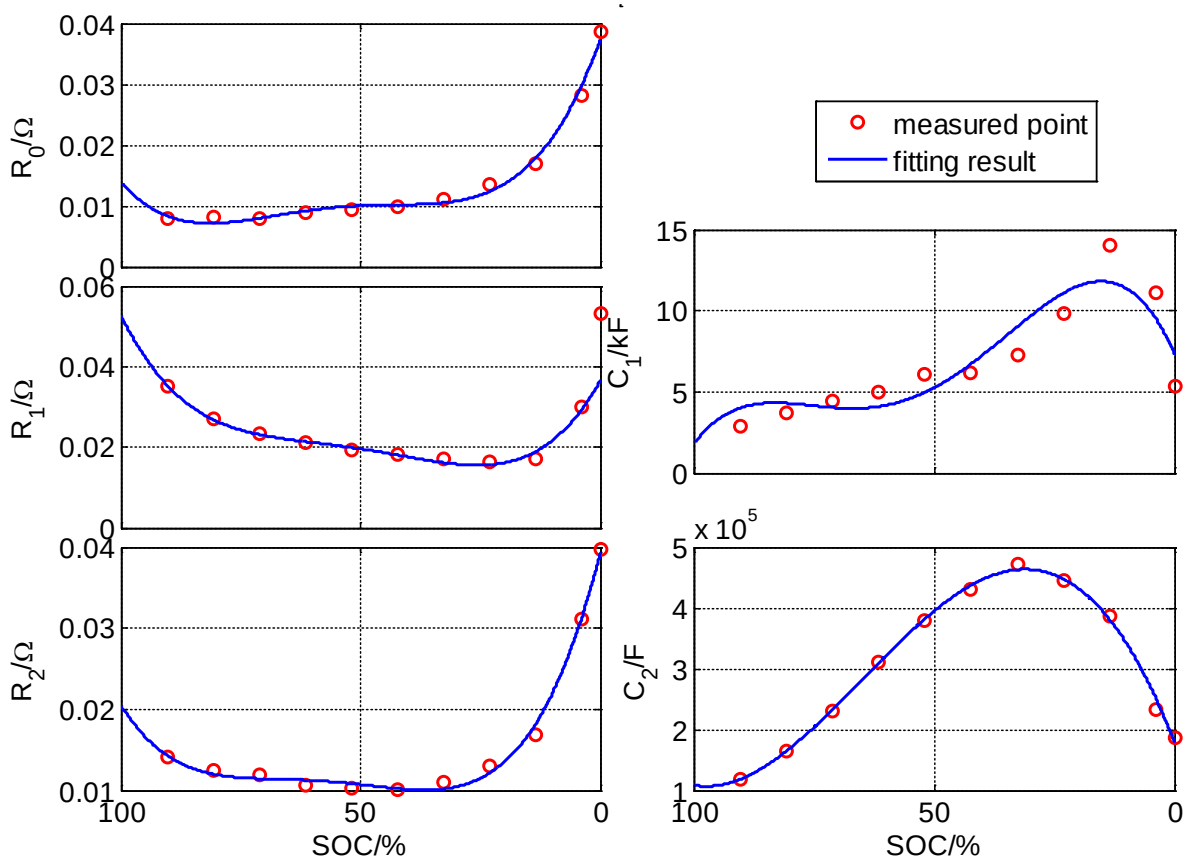

Figure 16: ECM five parameters of a fresh battery from offline estimation at 25°C during discharging.

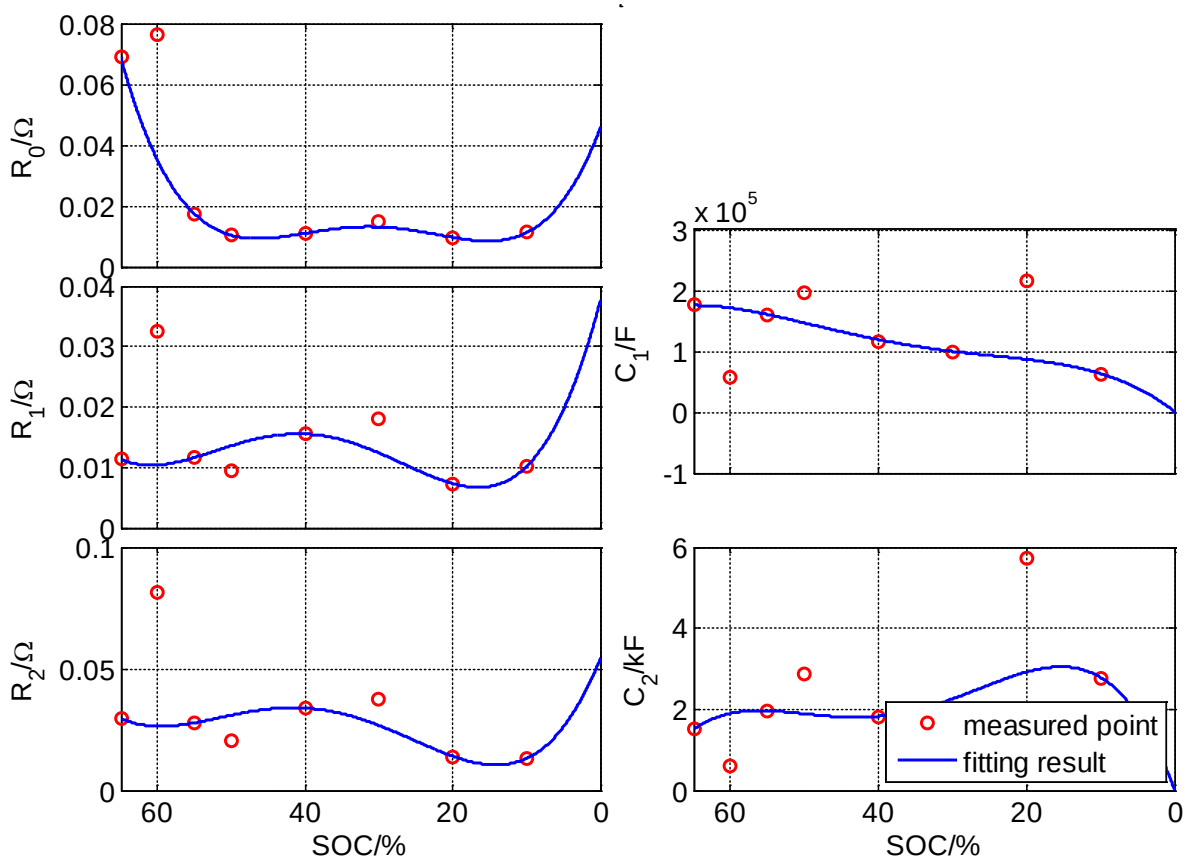

Figure 17: ECM five parameters of a fresh battery from offline estimation at 25ºC during charging (low SOC).

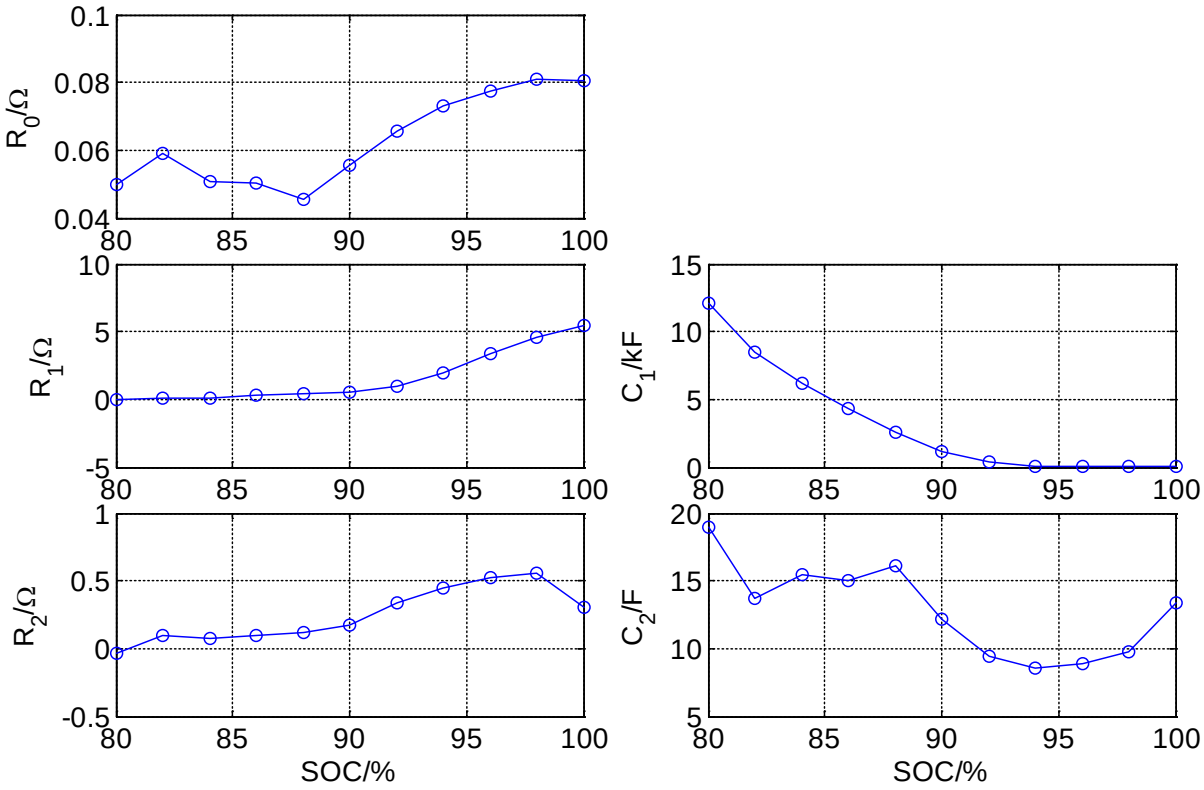

Figure 18: ECM five parameters of a fresh battery from offline estimation at 25°C during charging (high SOC).

2.5.2 Temperature dependence of parameters

The same method is then applied to obtain the parameters of the ECM at various temperatures. The results are shown in Figure 19. At different SOCs, temperatures, and charge directions, the battery shows different performance. In order to accurately mimic the performance of the battery under different load conditions, the model parameters are set to different values according to the load conditions.

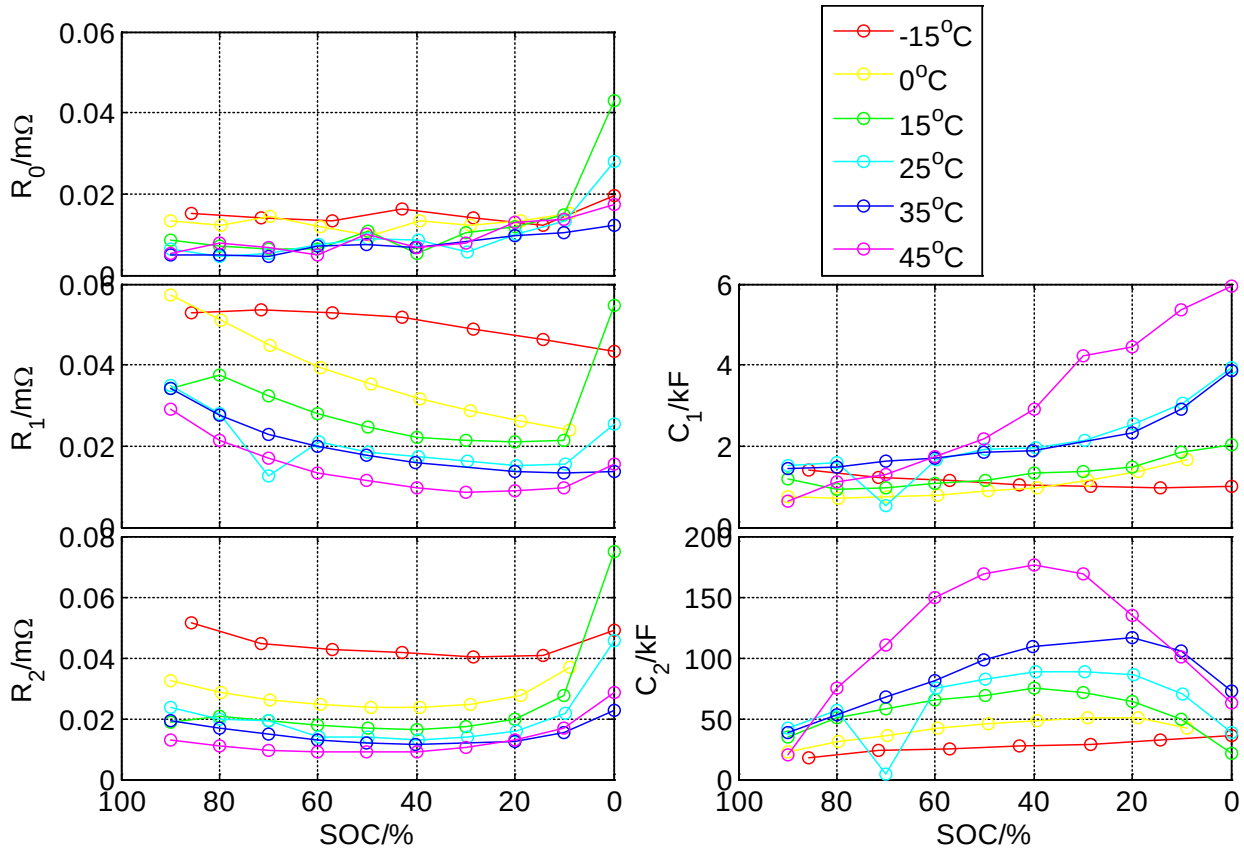

Figure 19: Parameters of the ECM during discharging a fresh battery at different temperatures, which are identified with offline parameter estimation algorithm.

Besides the pulse method mentioned in the previous section, EIS can also be used to extract the parameters of the battery. The measured EIS curves at different temperatures are shown in Figure 20, where the battery is set to 50% SOC at 25°C. By fitting these curves with model, the RC parameters can be extracted, and the results are shown in Figure 21.

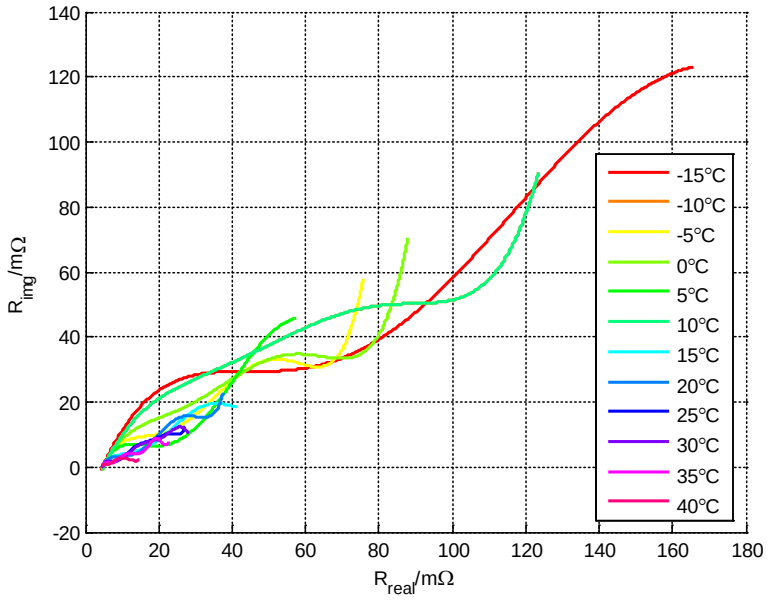

Figure 20: EIS Nyquist plot of a fresh battery at 50% SOC at different temperatures.

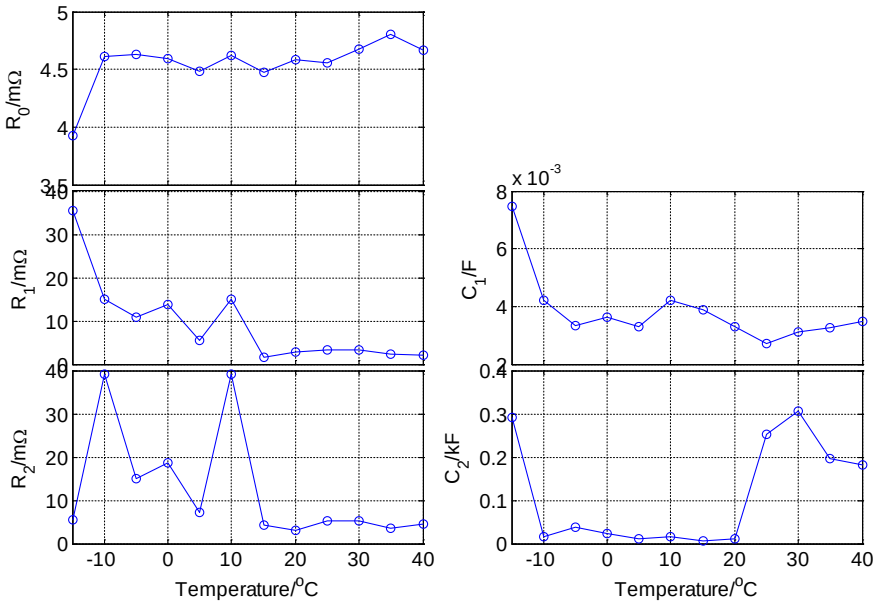

Figure 21: Parameters extracted from Nyquist plots of a fresh battery at 50% SOC at different temperatures.

2.5.3 Aging dependence of parameters

An experiment is designed to obtain aging dependent parameters of the battery. Figure 22 shows the aging profile of a cycle that consists of CC and CV discharging and charging. At the beginning of the aging profile, the fully charged battery is discharged at 75A, until the terminal voltage reaches the manufacturer's V_{min} of 10.5V. The battery is then discharged at constant voltage (10.5V), until the discharging current reaches 3.5A. Then, the battery is charged with 45A, until the terminal voltage reaches 14.5V. The battery is then charged in C.V. model, until the charging current reaches 7A. Then, the battery rests four hours. The above profile shows one full cycle to age the battery, and more details is shown in Figure 23, where capacity and parameters are measured at room temperature. For aging tests, the ambient temperature is set to be constant, and the following process is applied to battery, that includes capacity test, parameter test, and 8 times aging cycles, until the capacity of the battery fade reaches 35%. The capacity test consists of C.C. charge (1/5 C-rate) and C.V. charge (14.3V) during twenty four hours, four hours' rest, C.C. discharge (1/20 C-rate), and four hours' rest. The capacity is measured by the C.C. discharge method. The parameter measurements are described in section 2.5.1.

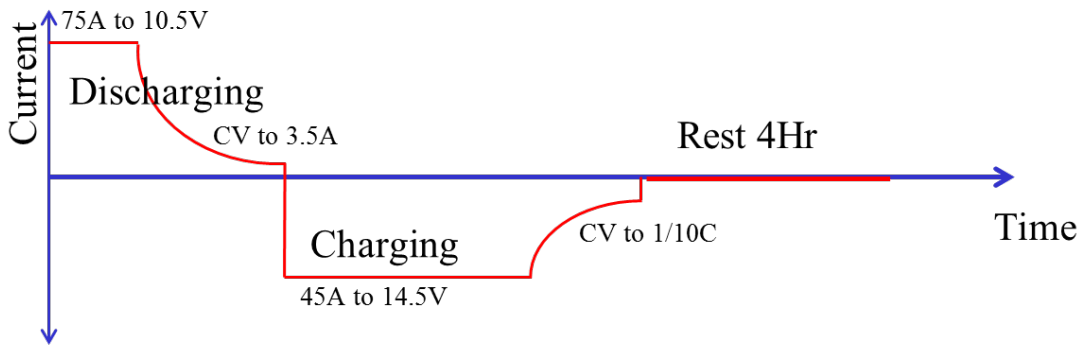

Figure 22: Aging profile.

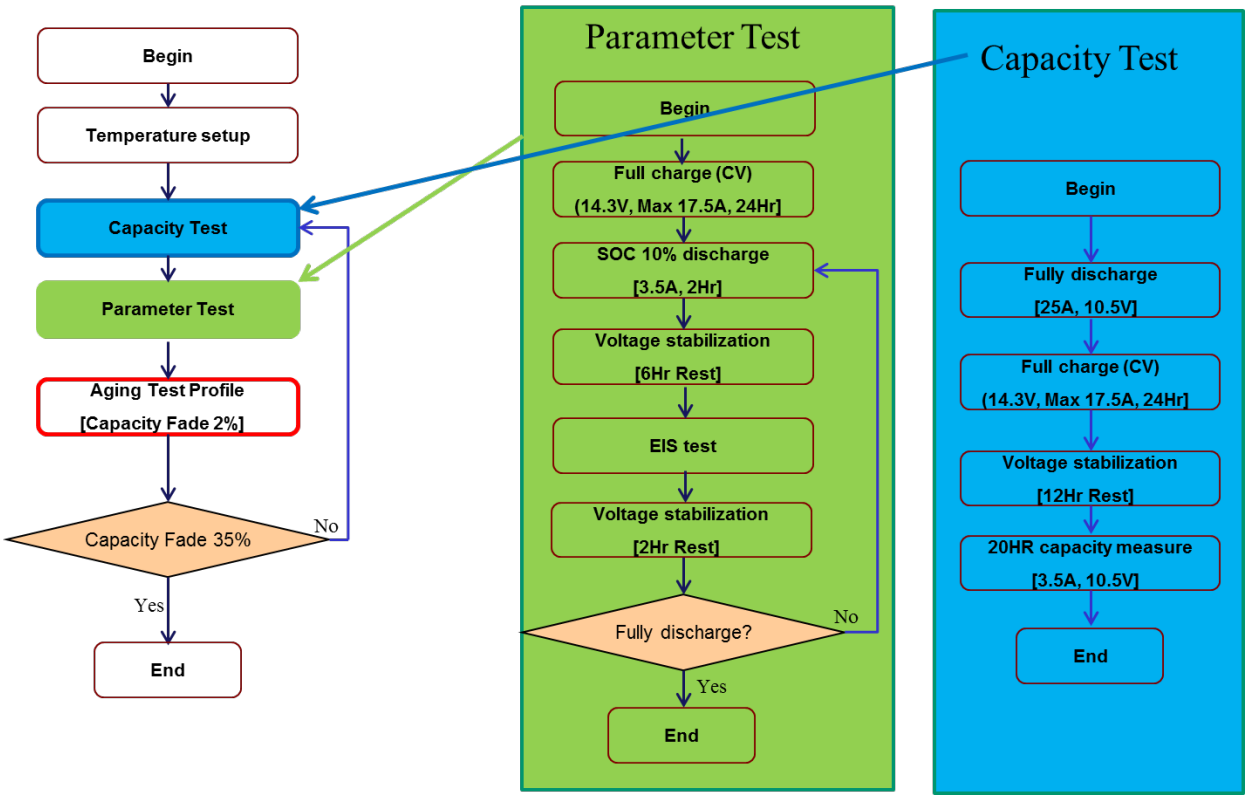

Figure 23: Flowchart of the aging tests.

The parameters of the battery at different aging states can be obtained and are shown in Figure 24. When the battery is being aged, the impedances are measured at different aging states, and the Nyquist plot of the impedances are shown in Figure 26. With curve fitting, the parameters at 50% SOC at different aging states can be obtained as shown in Figure 27.

Compared with the results from the pulse method, the results from EIS show a similar trend that when the battery is being aged, the resistance increases and the capacitance decreases.

From the above analysis, the parameters of the battery are affected by SOC, temperature, charging direction, charging mode, and aging process. It is very difficult to build a lookup table for the parameters considering all these factors. Therefore, an online parameter identification algorithm is employed to estimate the parameters of the model and to estimate SOC.

After the battery is used to estimate parameters under the pulses, it is cycled with charging and discharging profile to be aged. Once aged, the performance of the battery is different, and the parameters of the ECM are different from those of a fresh battery. An example of the parameters of the battery at different aging states is shown in Figure 25, where the SOC of the battery at each measurement is 50%. When capacity fade is larger, the resistance increases and capacitance decreases. Therefore, when building a model to mimic the battery, different sets of parameters should be used for the battery at different aging states.

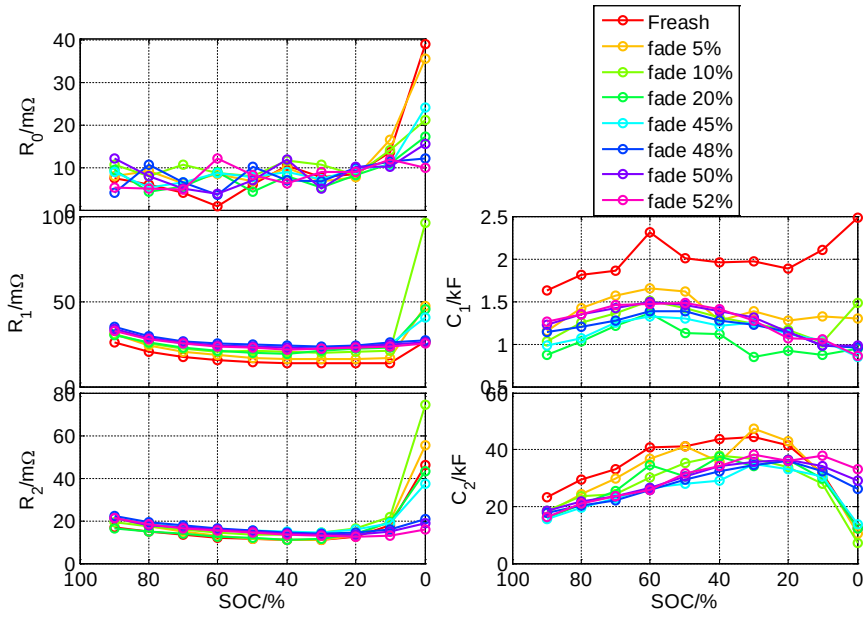

Figure 24: Parameters from pulse discharge of the battery at different aging states and different SOCs at 25°C.

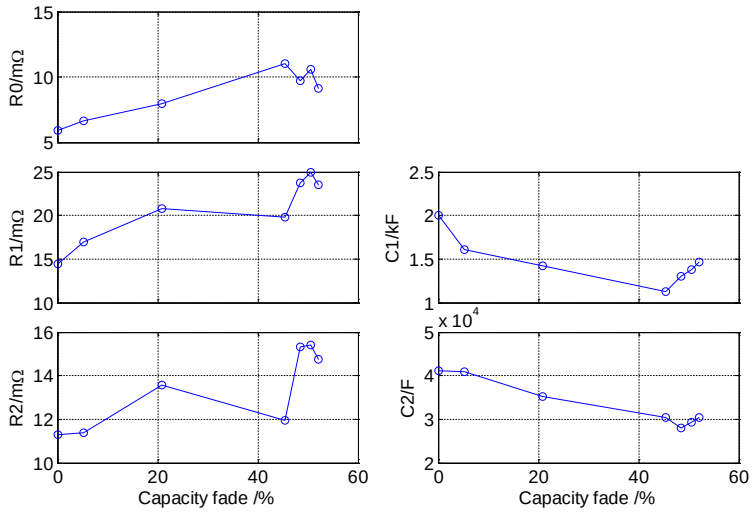

Figure 25: Parameters of equivalent circuit model for EIS at different aging states extracted from EIS measurements at 50% SOC at 25ºC.

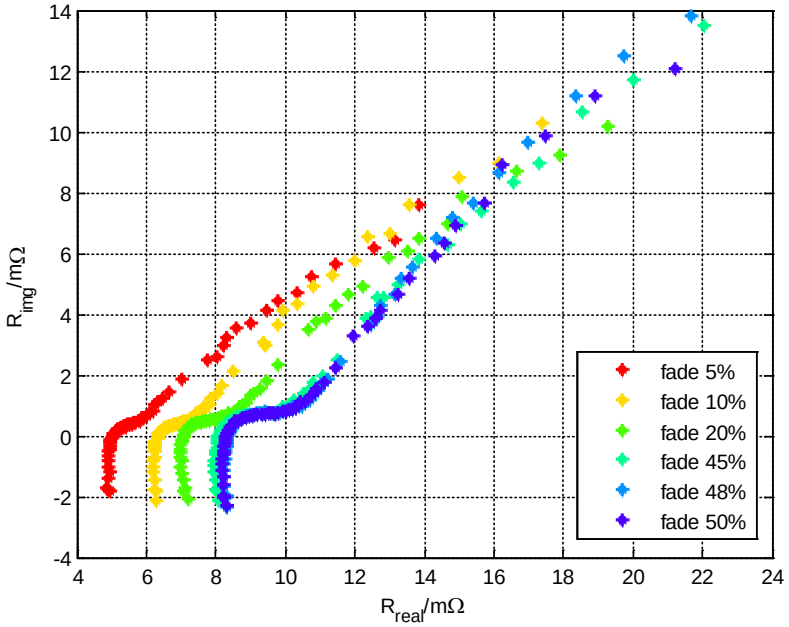

Figure 26: Nyquist plot of the battery at different aging states, 50% SOC, 25ºC.

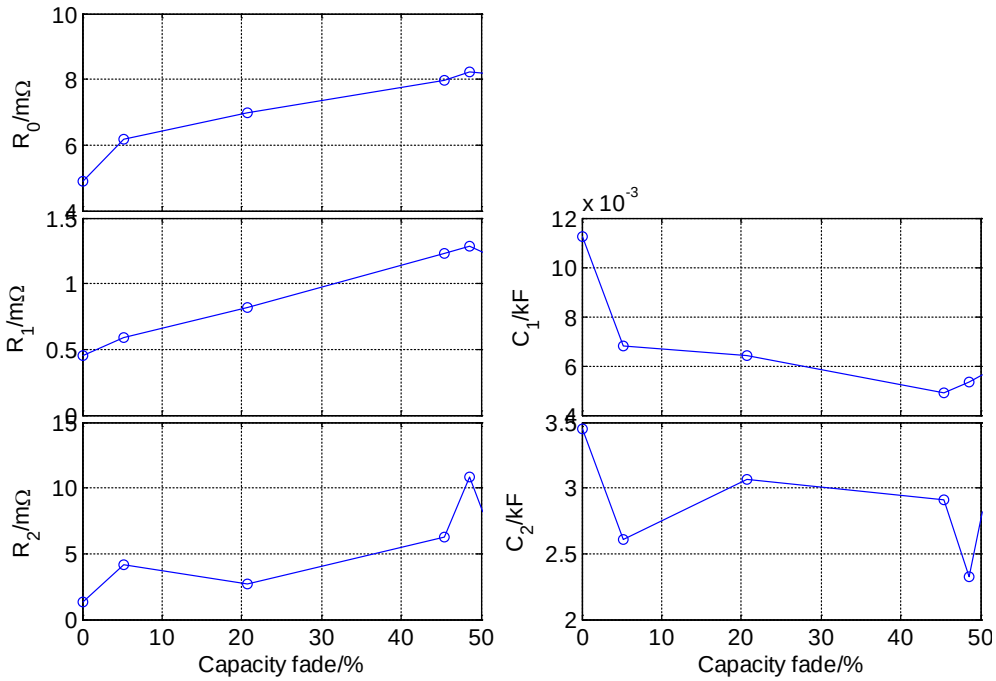

Figure 27: Parameters of equivalent circuit model for EIS at different aging states extracted from EIS measurements at 50% SOC at 25°C.

2.4 Kalman filter

As shown in the previous chapter, the parameters measured offline have shown their dependency upon different operating conditions. The model cannot follow dynamics of the battery. Therefore, Kalman filter is used to compensate the model errors caused by parameter variations.

2.4.1 Introduction of EKF

Kalman Filter is a recursive solution originally used for the discrete-data linear filter problem and has been extensively used for many other applications. The Kalman filter consists of a set of mathematical equations that provides an efficient computational (recursive) mean of estimating the state of a process, in a way that minimizes the mean of the squared error. The filter is very

powerful in several aspects by supporting estimations of past, present, and even future states, even though the precise nature of the modeled system is unknown.

When a second order ECM is used in SOC estimation, the linear Kalman Filter cannot be applied directly because of nonlinear parameters of the ECM. Therefore, the model needs to be linearized before applying the Kalman filter. This method is called extended Kalman Filter (EKF). If all models contain variables that cannot be directly measured, the choice of error variances, Q and R might be difficult. If improperly chosen, the SOC variable of the ECM oscillates and might diverge. Therefore, the model is very important for EKF.

This proposed model is a second order ECM that shows accurate response with relatively simple structure. Other Kalman filter techniques include Sigma-Point Kalman filter (SPKF) [13, 14], unscented Kalman filter (UKF) [15], adaptive extended Kalman filter (AEKF)[2, 10], adaptive unscented Kalman filter (AUKF) [2], and dual Kalman filter (DKF) [16]. All Kalman filter typically require significant computational time [17].

The second order ECM combined with an EKF is proposed [18]. The internal resistance of battery (R_0) is the only one estimated online because of major cause for voltage drop. AEKF based on an improved Thevenin' model, as shown in Figure 12, is proposed [10]. The authors attempt to estimate parameters of the model online, where state variables include [U_1, U_2, V_t, $1/R_1$, $1/C_1$, $1/R_2$, $1/C_2$]$^{\mathrm{T}}$. Others extended the EKF based on "filter state" cell model, where SOC and the parameters of the model are estimated online [19]. The filter state model is an empirical one that is a function of current direction, SOC and temperature, which requires many experiments to obtain coefficients for the equations.

Assume the process has a state vector $x \in R^n$. The process is governed by the non-linear equation,

$$x_{k+1} = f\left(x_k, u_k, w_k\right), \tag{25}$$

with a measurement $z \in R^n$ that is,

$$z_k = h\left(x_k, v_k\right), \tag{26}$$

where the random variable w_k and v_k represent the process and measurement noise. An approximated state and measurement vector can be described as,

$$\tilde{x}_{k+1} = f\left(\hat{x}_k, u_k, w_k\right), \tag{27}$$

$$\tilde{z}_k = h\left(\tilde{x}_{k,v_k}\right), \tag{28}$$

where $\hat{x}_k$ is a posteriori estimate of the state from a previous time step k+1.

The following are the new governing equations that linearize an estimate about equation (27) and (28),

$$x_{k+1} \approx \tilde{x}_{k+1} + \mathbf{A}\left(x_k - \hat{x}_k\right) + \mathbf{W}w_k, \tag{29}$$

$$z_k \approx \tilde{z}_k + \mathbf{H}\left(x_k - \tilde{x}_k\right) + \mathbf{V}v_k, \tag{30}$$

where

- x_{k+1} and z_k are the actual state and measurement vectors;
- $\tilde{x}_{k+1}$ and $\tilde{z}_k$ are the approximate state and measurement vectors from equation (27) and (28);
- $\hat{x}$ is a posteriori estimate of the state at step k;
- the random variable, w_k and v_k represent the process and measurement noise as in equation (27) and (28);
- $\mathbf{A}$ is the Jacobian matrix of partial derivatives of $f(-)$ with respect to χ, that is $\mathbf{A}_{[i,j]} = \frac{\partial f_{[i]}}{\partial x_{[j]}}\left(\hat{x}_k, u_k, 0\right)$;

- $\mathbf{W}$ is the Jacobian matrix of partial derivatives of $f(-)$ with respect to w, $\mathbf{W}_{[i,j]} = \frac{\partial f_{[i]}}{\partial w_{[j]}}(\hat{x}_k, u_k, 0)$;
- $\mathbf{H}$ is the Jacobian matrix of partial derivatives of $h(-)$ with respect to x, $\mathbf{H}_{[i,j]} = \frac{\partial h_{[i]}}{\partial x_{[j]}}(\tilde{x}_k, 0)$;
- $\mathbf{V}$ is the Jacobian matrix of partial derivatives of $h(-)$ with respect to v, $\mathbf{V}_{[i,j]} = \frac{\partial h_{[i]}}{\partial v_{[j]}}(\tilde{x}_k, 0)$.

The prediction error and the measurement error is defined as,

$$\tilde{e}_{x_k} \equiv x_k - \tilde{x}_k \approx \mathbf{A}(x_{k-1} - \hat{x}_{k-1}) + \varepsilon_k, \tag{31}$$

$$\tilde{e}_{z_k} \equiv z_k - \tilde{z}_k \approx \mathbf{H}\tilde{e}_k + \eta_k. \tag{32}$$

The posteriori state estimates for the original non-linear process as,

$$\begin{aligned} \hat{x}_k &= \tilde{x}_k + \hat{e}_k \\ &= \tilde{x}_k + \mathbf{K}_k \tilde{e}_{z_k} \\ &= \tilde{x}_k + \mathbf{K}_k (z_k - \tilde{z}_k) \end{aligned} \tag{33}$$

The complete set of EKF is shown in Table 5 and Table 6.

Table 5: Discrete Kalman filter time update equation

$\hat{\mathbf{x}}_k^- = f(\hat{\mathbf{x}}_{k-1}, u_{k-1}, 0)$
$\mathbf{P}_{k+1}^- = \mathbf{A}_k \mathbf{P}_k \mathbf{A}_k^{\mathrm{T}} + \mathbf{W}_k \mathbf{Q}_k \mathbf{W}_k^{\mathrm{T}}$

Table 6: Discrete Kalman filter measurement update equation

$\mathbf{K}_k = (\mathbf{P}_k^- \mathbf{H}_k^{\mathrm{T}})(\mathbf{H}_k \mathbf{P}_k^- \mathbf{H}_k^{\mathrm{T}} + \mathbf{V}_k \mathbf{R}_k \mathbf{V}_k^{\mathrm{T}})^{-1}$
$\hat{\mathbf{x}}_k = \hat{\mathbf{x}}_k^- + \mathbf{K}_k (\mathbf{z}_k - h(\hat{\mathbf{x}}_k^-, 0))$

$$\mathbf{P}_k = (1 - \mathbf{K}_k \mathbf{H}_k)\mathbf{P}_k^-$$

The complete picture of the operation of EKF is shown in Figure 28 and the block diagram of EKF is shown in Figure 29.

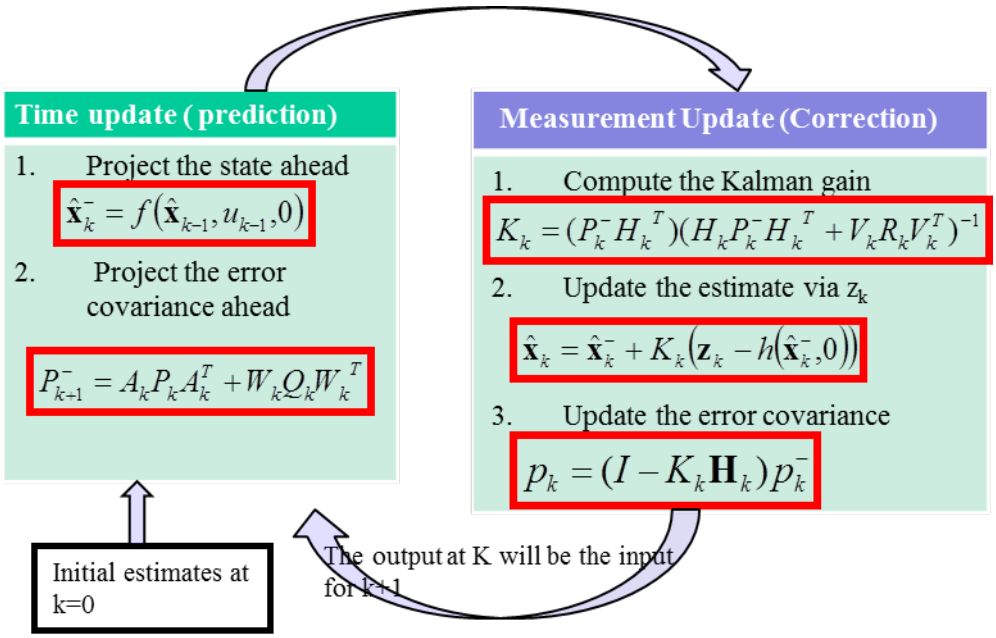

Figure 28: Complete picture of the operation of the EKF.

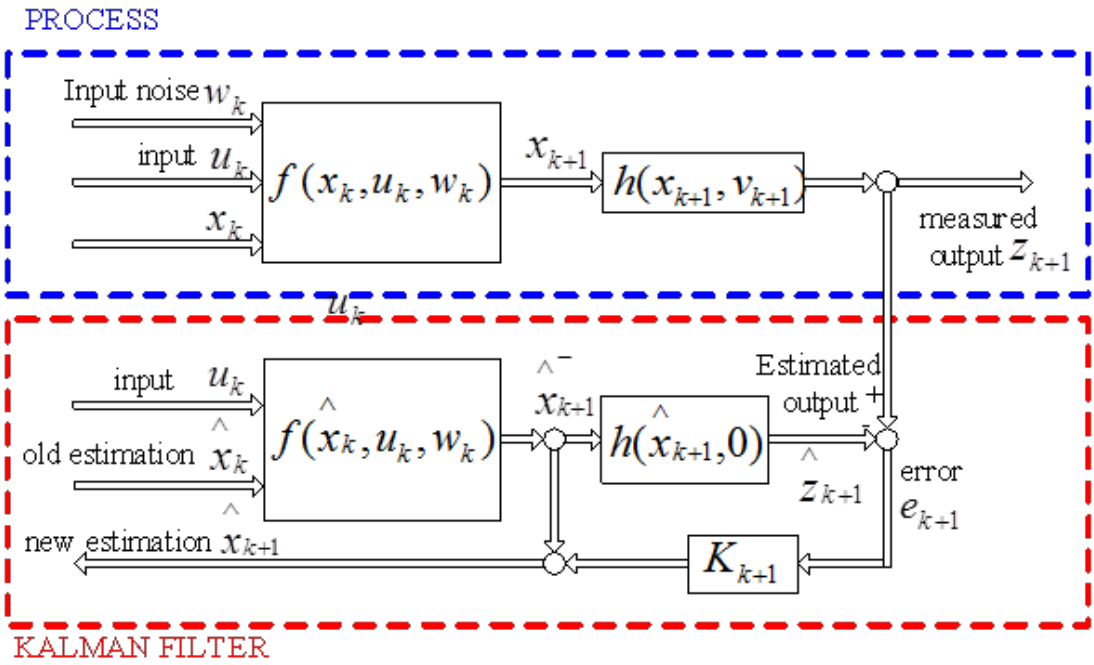

Figure 29: Block diagram of the EKF.

2.4.2 Application of Kalman Filter

For SOC estimation based on the ECM, the parameters vary severely and need to be estimated accurately for ensuring less errors in the SOC estimation. Therefore, the parameters of the ECM and the SOC are defined as the states to be estimated by the EKF. For the ECM based EKF system, the input, *u*, is the current (*I*) and the output, *z*, is the terminal voltage (V_t). As a result, the number of states for the system results in eight parameters, [*SOC*, U_1, U_2, R_0, R_1, C_1, R_2, C_2,]^T.

The change of the SOC during one sampling period, Δt can be calculated by the following equation,

$$\Delta SOC = \frac{I \cdot \Delta t}{Q_{\max}} . \tag{34}$$

In a vehicle, the normal discharge current is less than 35A, while the max charge current is 75A. Therefore, the maximum change of the SOC during one sampling period is

$$\Delta SOC_{\max} = \frac{75A \times 0.1s}{70Ah \times 3600s/h} \approx 2.98 \times 10^{-5}.$$

From Figure 16, the maximum slope of R_0 over SOC, $\partial R_0/\partial$SOC is 0.2167 Ω. Thus, the maximum change of R_0 during one sampling period can be calculated,

$$\Delta R_{0\max} = \frac{\partial R_0}{\partial SOC} \cdot \Delta SOC_{\max} = 0.2167\Omega \times 2.98 \times 10^{-5} \approx 6.46 \times 10^{-6}\Omega.$$

The max rate of change of R_0 during one sampling period is

$$\frac{\Delta R_{0,\max}}{\min(R_0)} = \frac{6.46 \times 10^{-6}\Omega}{0.0072\Omega} \approx 9 \times 10^{-4}.$$

Similarly, the rate of change of R_1 is $\Delta R_{1,\max}/\min(R_1) \approx 4.12 \times 10^{-4}$, the rate of change of C_1 is $\Delta C_{1,\max}/\min(C_1) \approx 6.53 \times 10^{-4}$, the rate of change of R_2 is $\frac{\Delta R_{2,\max}}{\min(R_2)} \approx 6.84 \times 10^{-4}$, and the rate of change of $C2$ is $\frac{\Delta C_{2,\max}}{\min(C_2)} \approx 2.25 \times 10^{-4}$. During one sampling period that is assumed to be 0.1s, the changes of parameters of ECM are very small, so negligible.

$$R_0[k+1] = a_1 R_0[k]$$

$$R_1[k+1] = a_2 R_1[k]$$

$$C_1[k+1] = a_3 C_1[k]$$

$$R_2[k+1] = a_4 R_2[k]$$

$$C_2[k+1] = a_5 C_2[k]$$

where a_1 to a_5 are chosen to be close to 1.

The linearized state equation and the output variable are as follows,

$$\begin{bmatrix} SOC_{k+1} \\ U_{1,k+1} \\ U_{2,k+1} \\ R_{0,k+1} \\ R_{1,k+1} \\ C_{1,k+1} \\ R_{2,k+1} \\ C_{2,k+1} \end{bmatrix} = \begin{bmatrix} SOC_k - \dfrac{I_k \Delta t}{Q_{\max}} \\ \left(1 - \dfrac{\Delta t}{R_{1,k} C_{1,k}}\right) U_{1,k} + \dfrac{\Delta t}{C_{1,k}} I_k \\ \left(1 - \dfrac{\Delta t}{R_{2,k} C_{2,k}}\right) U_{2,k} + \dfrac{\Delta t}{C_{2,k}} I_k \\ a_1 R_{0,k} \\ a_2 R_{1,k} \\ a_3 C_{1,k} \\ a_4 R_{2,k} \\ a_5 C_{2,k} \end{bmatrix} \tag{35}$$

$$V_{t,k+1} = OCV\left(SOC_{k+1}\right) - U_{1,k+1} - U_{2,k+1} - I_k R_{0,k+1}, \tag{36}$$

,where Q_{max} is the maximum capacity of the battery, and a_1-a_5 are the changing rate of the parameters in the ECM.

After a linearization, equation (35) and (36) can be rewritten in a state space form as,

$$x_{k+1} = \mathbf{A} x_k + \mathbf{B} u_k , \tag{37}$$

$$z_{k+1} = \mathbf{C} x_{k+1} , \tag{38}$$

where,

$$\mathbf{A}=\begin{bmatrix} 1 & 0 & 0 & 0 & 0 & 0 & 0 & 0 \\ 0 & \left(1-\frac{\Delta t}{R_1C_1}\right) & 0 & 0 & \frac{\Delta tU_1}{R_1^{\,2}C_1} & \frac{\Delta tU_1}{R_1C_1^{\,2}} & 0 & 0 \\ 0 & 0 & \left(1-\frac{\Delta t}{R_2C_2}\right) & 0 & 0 & 0 & \frac{\Delta tU_2}{R_2^{\,2}C_2} & \frac{\Delta tU_2}{R_2C_2^{\,2}} \\ 0 & 0 & 0 & a_1 & 0 & 0 & 0 & 0 \\ 0 & 0 & 0 & 0 & a_2 & 0 & 0 & 0 \\ 0 & 0 & 0 & 0 & 0 & a_3 & 0 & 0 \\ 0 & 0 & 0 & 0 & 0 & 0 & a_4 & 0 \\ 0 & 0 & 0 & 0 & 0 & 0 & 0 & a_5 \end{bmatrix}$$

$$\mathbf{B}=\begin{bmatrix} -\frac{\Delta t}{Q_{\max}} & 0 & 0 & 0 & 0 & 0 & 0 & 0 \end{bmatrix}^T$$

$$\mathbf{C}=\begin{bmatrix} \frac{\partial OCV}{\partial SOC} & -1 & -1 & -I & 0 & 0 & 0 & 0 \end{bmatrix}.$$

For SOC estimation, the system should be observable to apply EKF, where the rank of the observability matrix of (39) is examined. If the matrix has a full rank, the system becomes observable.

$$rank\left(\begin{bmatrix} \mathbf{C} \\ \mathbf{CA} \\ \mathbf{CA}^2 \\ \\ \mathbf{CA}^{n-1} \end{bmatrix}\right) \tag{39}$$

To meet the requirements of observability, the coefficients of a_1-a_5 must have different values. Therefore, a_1=1, a_2 = 0.995, a_3=0.99, a_4=1.005, and a_5=1.01 are chosen.

The first term in equation (36) presents the relationship between SOC and OCV that are obtained experimentally. A fully charged battery is discharged at a 1/20 C-rate for two hours and

then rested for four hours while T_{amb} remains a constant 25°C. Until the terminal voltage reached the manufacturer's V_{min} of 10.5V, this process is repeated. The SOC at the end of each pulse is calculated using Coulomb counting. The terminal voltage at the end of each rest is regarded as OCV at that SOC, because the four hours is considered to be sufficient for the battery to reach a state of chemical equilibrium. The terminal voltage profile of OCV discharge pulses is shown in Figure 30.

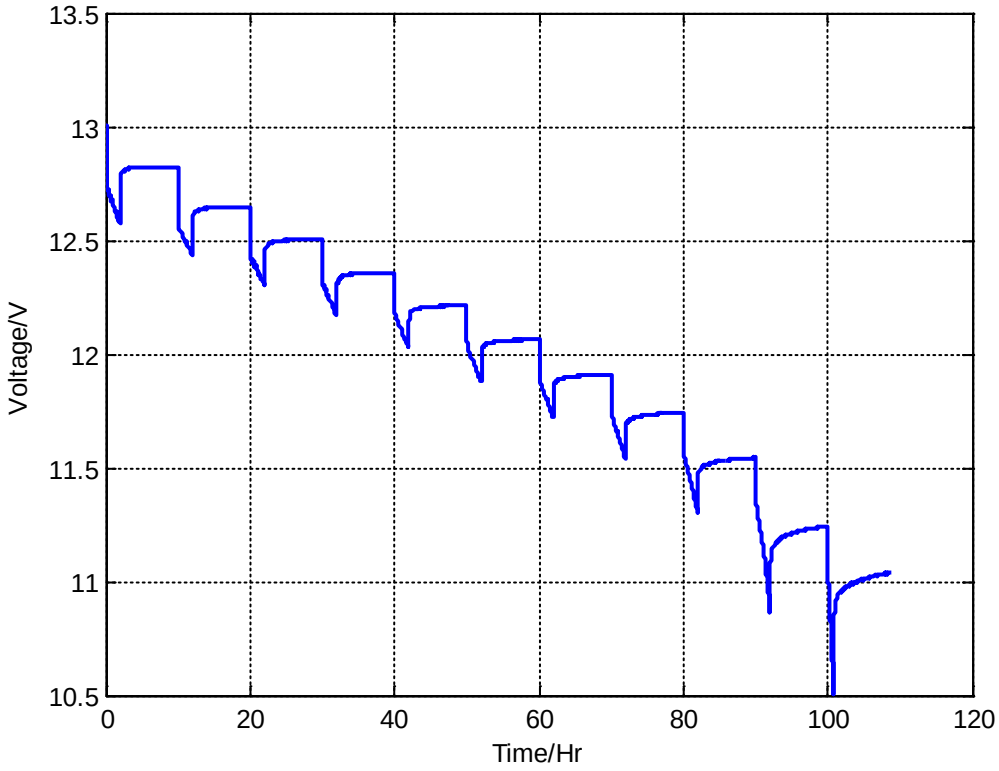

Figure 30: Terminal voltage during OCV measurement.

Initial value of SOC is 100%, and the maximum capacity of the battery (Q_{max}) is measured experimentally beforehand. To minimize any measurement errors, a high accurate current sensor is used in this test and calibrated beforehand. Both measured OCVs and SOCs are then linked to generate the OCV-SOC curve, as shown in Figure 31.

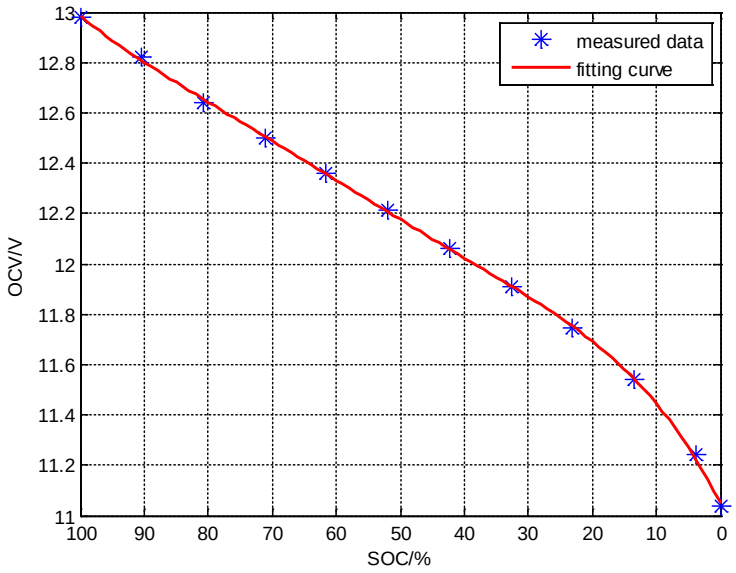

Figure 31: OCV-SOC curve.

In application, the OCV/SOC curve is fitted with the fifth order of polynomial. The coefficients are shown in Table 7.

$$OCV(x) = b_1 x^5 + b_2 x^4 + b_3 x^3 + b_4 x^2 + b_5 x + b_6 \tag{40}$$

Table 7: Coefficients of the OCV/SOC function

Coefficient	b_1	b_2	b_3	b_4	b_5	b_6
Value	7.134	-21.21	24.36	-13.44	5.086	11.05

According the above function, the $\frac{\partial \text{OCV}}{\partial \text{SOC}}$, as a function of SOC, can be calculated as shown in Figure 32.

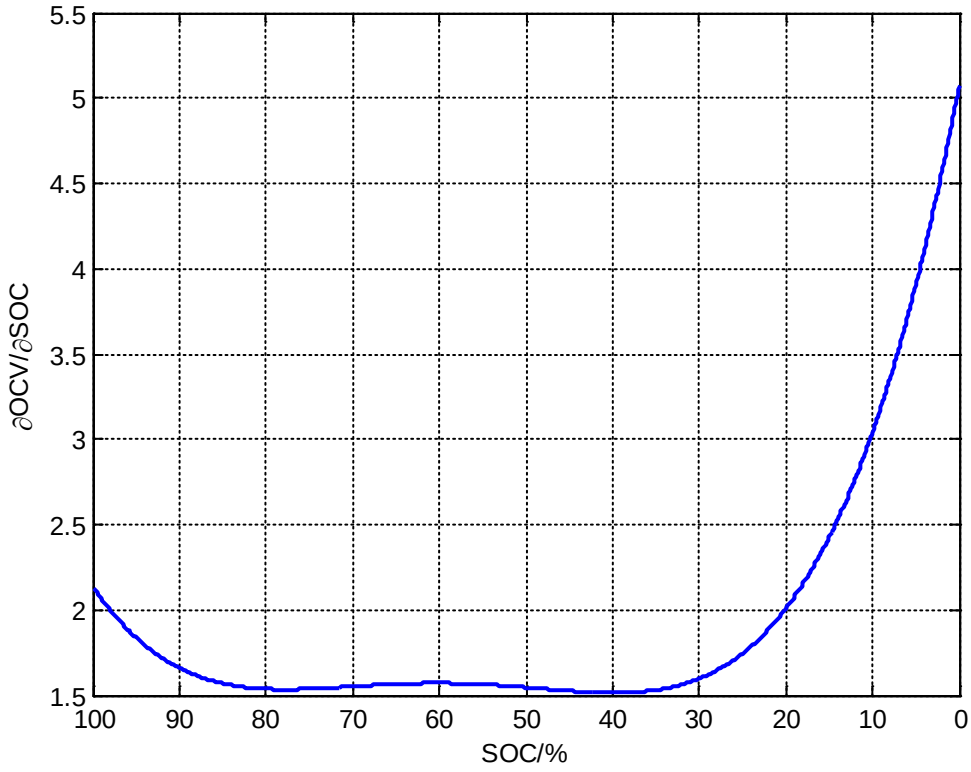

Figure 32: $\frac{\partial \mathrm{OCV}}{\partial \mathrm{SOC}}$-SOC curve.

2.5 Results and analysis

2.5.1 SOC estimation with offline identification method

To test the performance of the proposed SOC estimation algorithm, a series of tests are designed, including full discharge, full charge, pulse discharge, and three types of different drive cycles. The load profile of these tests is plotted in the following sections. During the tests experimental data is collected, including time, current, voltage, and temperature. There are four thermocouples used to measure the temperature at cathode, anode, battery housing surface, and the ambient. Before all the tests start, SOC of the battery is set to be 100% with equilibrium state, so the polarization of R-C circuit is 0. One of the main tasks of the EKF is to correct initial SOC that the ECM might has based on the error between the battery and the ECM voltage. To test the

performance of the ECM based EKF, the initial SOC of the model is set to be 79%, which results in an error of 21%. The estimated SOC is then compared with the true SOC, where the true SOC during each test is calculated by Coulomb counting with an initial SOC obtained from an OCV/SOC look-up table. Then, the SOC information is used to detect whether the battery is at a Fully Charge or End of Discharge, or to forward it for other algorithms.

The parameters of the ECM can be estimated offline. However, the accuracy of SOC estimation is limited to loading conditions. For example, the voltage, current, and temperature of a fresh battery during full discharging are plotted in Figure 33, and the true SOC and estimated SOC are plotted in Figure 34. When SOC is high or low, the estimation error is large, because the parameters have been changed quickly at both high and low SOC ranges.

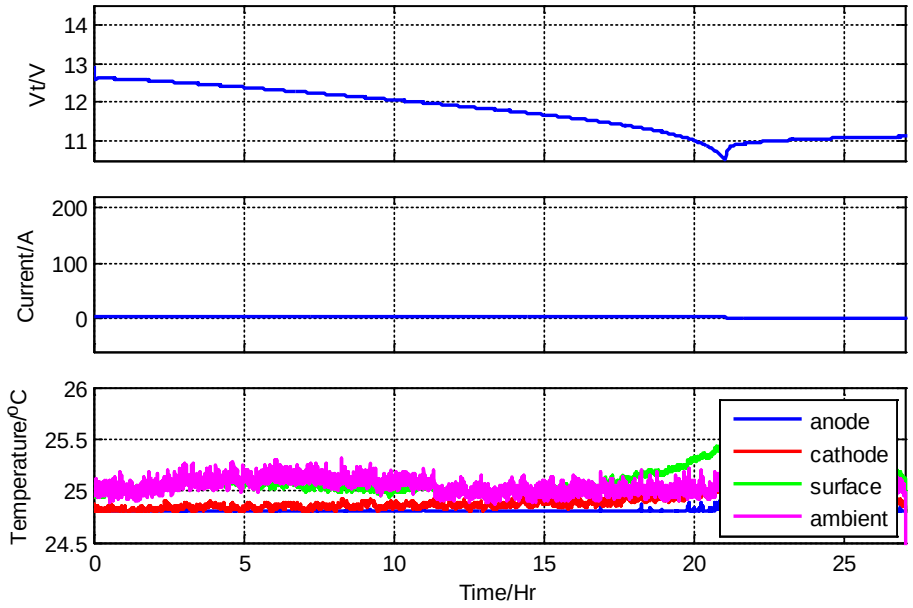

Figure 33: Discharging and rest.

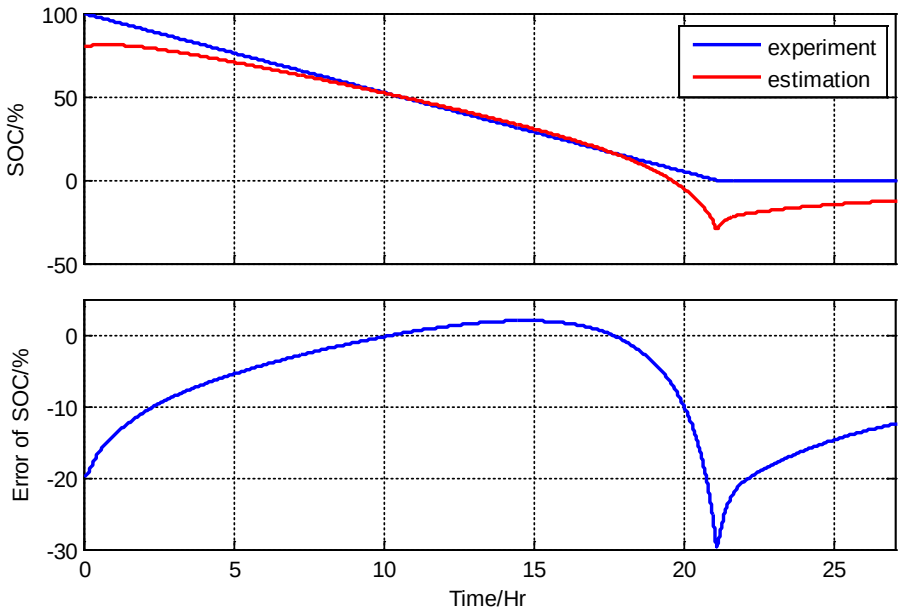

Figure 34: Simulated SOC and its error of a fresh battery using offline parameters during discharging and rest at 25^{o}C.

Figure 35 shows the voltage, current, and temperature of a fresh cell during a full cycle that consists of constant current charging, constant voltage charging, rest, constant current discharging, and another rest. The comparison of experimental and simulation SOC are shown in Figure 36. For most of the tests, the estimation results have been matched well with experimental results. However, the error becomes large at high and low SOC ranges, especially when there are changes of current direction. Moreover, the error is large during charging at C.V. mode, where the current is getting smaller.

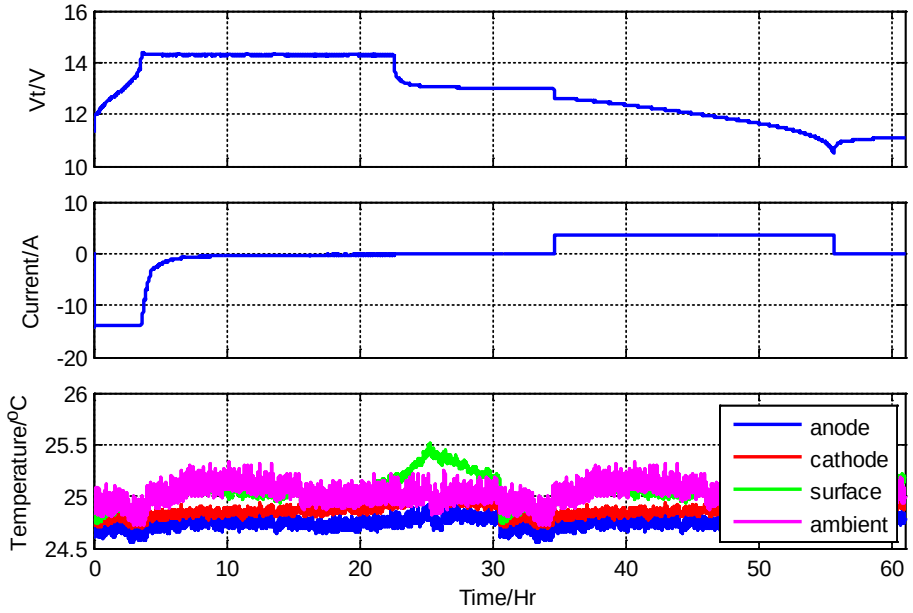

Figure 35: Single cycle at 25°C.

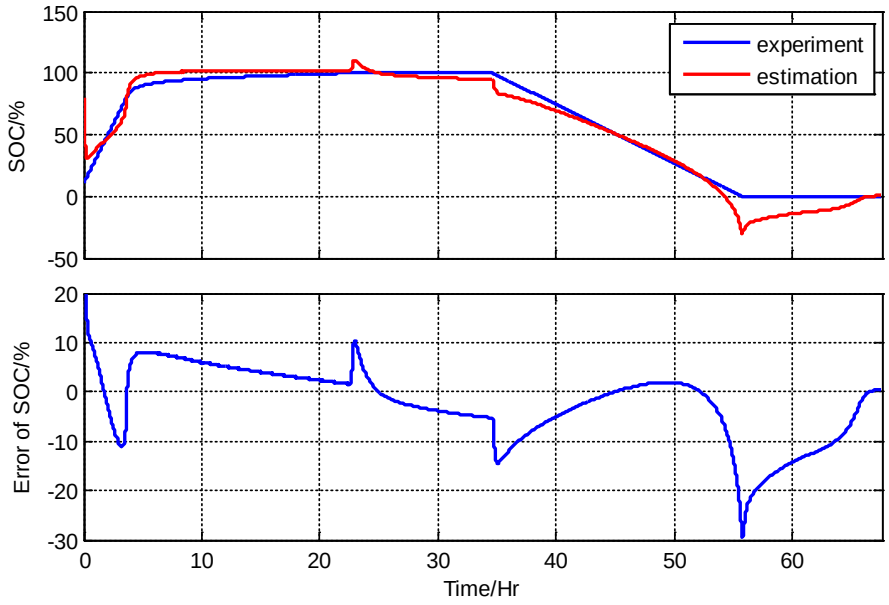

Figure 36: Simulated SOC and its error of a fresh battery using offline parameters during single cycle at 25°C.

The algorithm is also tested during pulse discharge, and the results are shown in Figure 37 and Figure 38. Similarly, the accuracy is good in the medium range of SOC, while the error becomes large at both high and low SOC ranges.

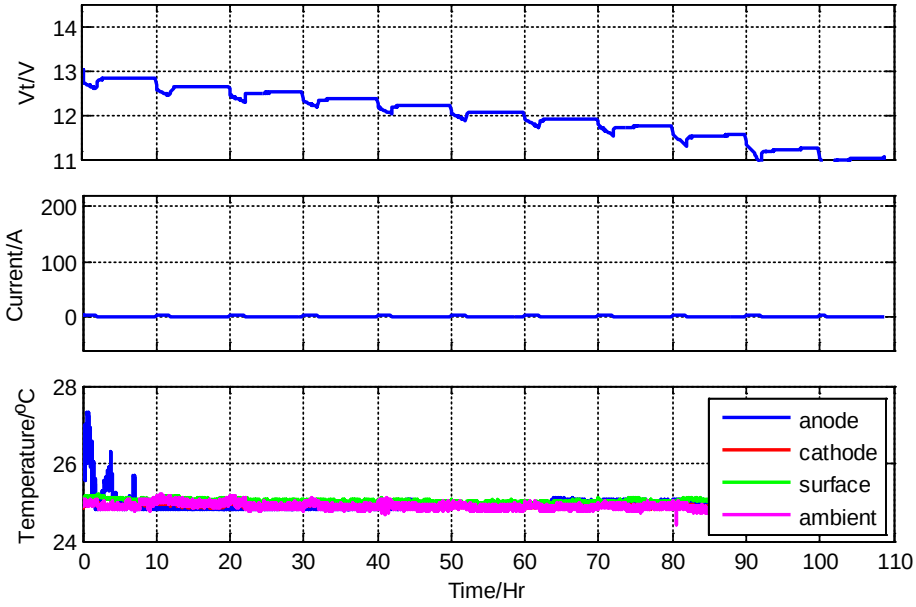

Figure 37: Pulse discharging

The results of all the above tests have shown that the accuracy particularly at both high and low SOC ranges needs to be improved. Since the parameters of the ECM change quickly in those ranges, an online parameter identification method is used to reduce SOC errors.

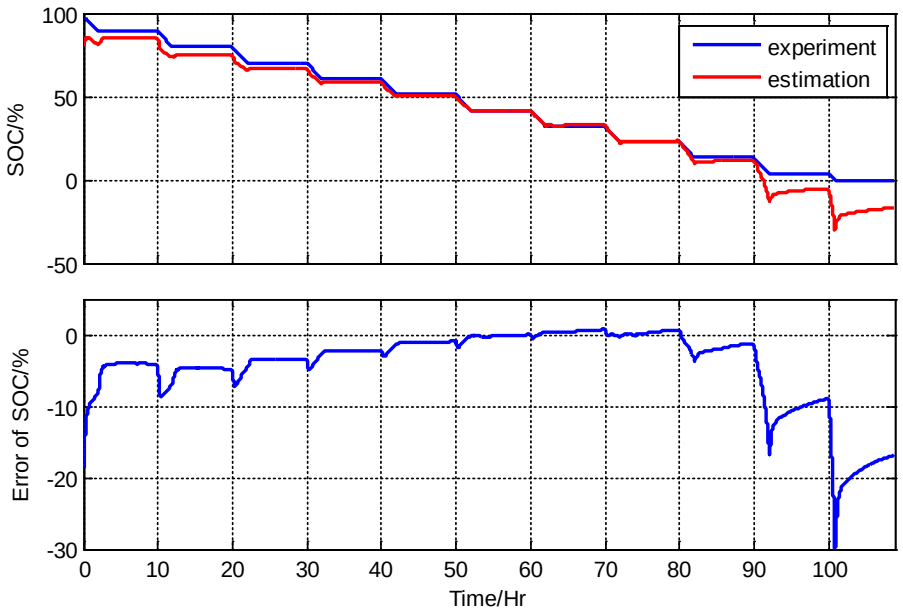

Figure 38: Simulated SOC and its error of a fresh battery using the offline parameters estimation during pulse discharging at 25^{o}C.

2.5.2 Reduction of SOC estimation errors using online parameter identification

Performance of the new algorithm with the online parameter identification algorithm is evaluated for all the three tests conducted in 2.5.1.

The simulation results of SOCs and estimation errors are shown in Figure 39, Figure 40, and Figure 41. Compared with the SOC estimation results in 2.5.1, the errors of the estimation with the online parameter algorithm is further reduced that becomes less than 3%. Inaccuracy of SOC and low SOC ranges or those caused by changes in the current direction are improved. . In addition, initial SOC errors are also reduced.

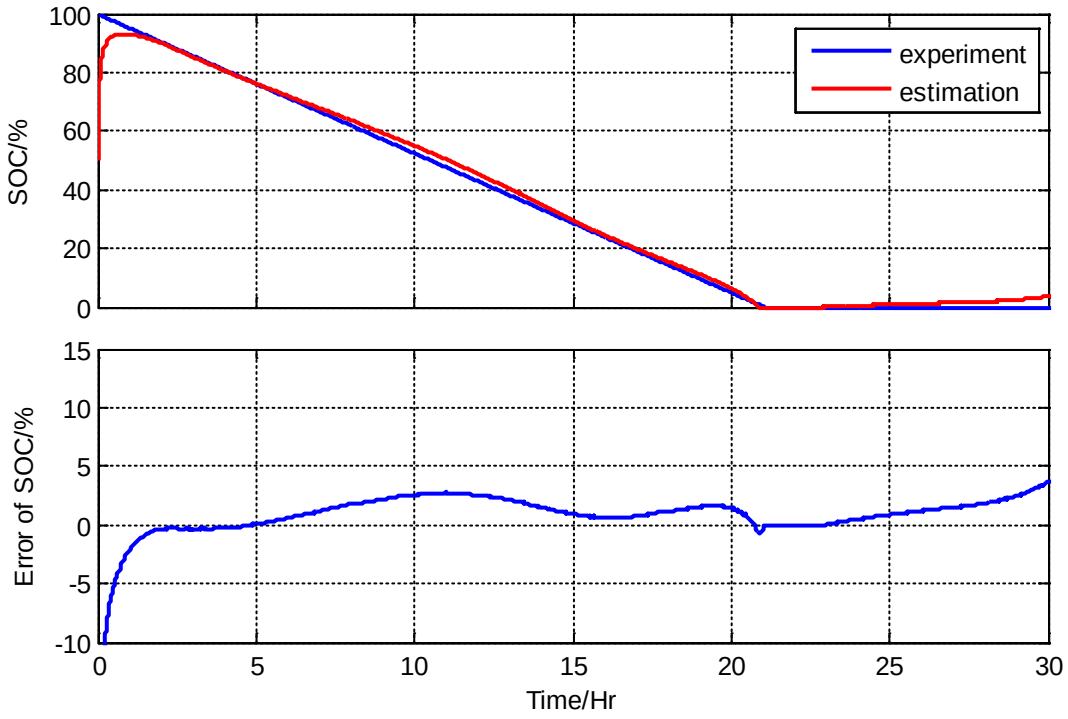

Figure 39: Simulated SOC and its error of a fresh battery using online parameter estimation during discharging and rest at 25^{o}C.

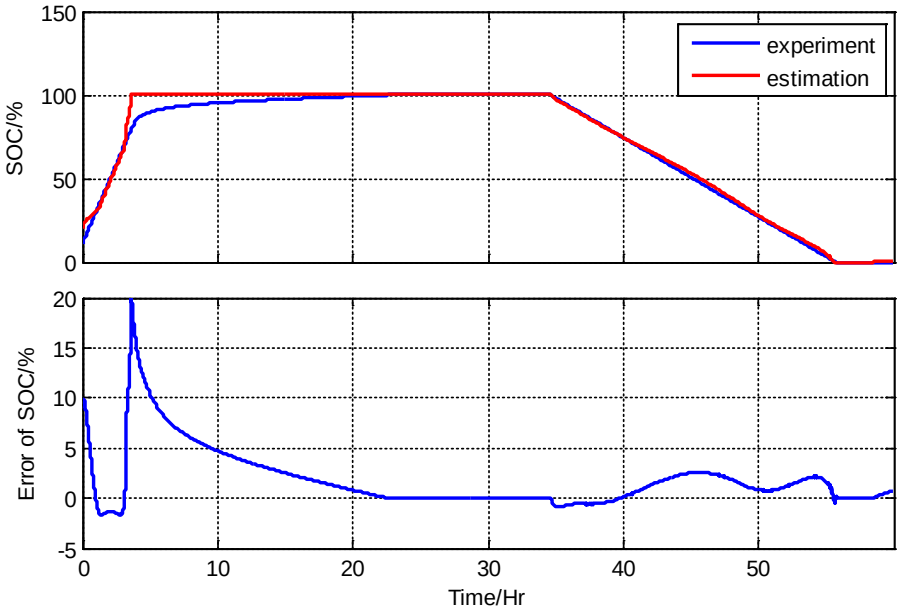

Figure 40: Simulated SOC and its error of a fresh battery using online parameter estimation during a single cycle at 25^{o}C.

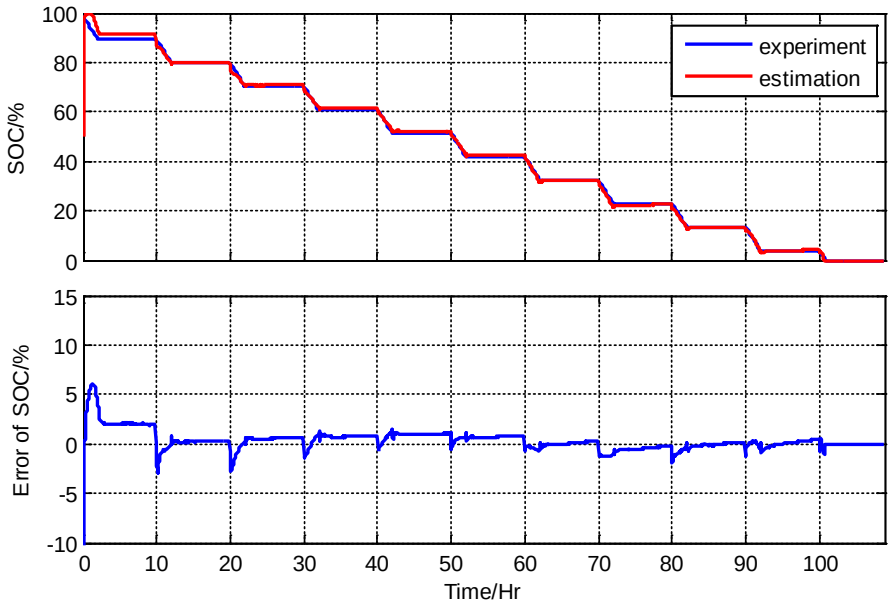

Figure 41: Simulated SOC and its error of a fresh battery using online parameter estimation during pulse discharging at 25^{o}C.

ECM with the online parameter estimation algorithm is also tested using three cycles obtained from a vehicle. The estimation results of parameters of the ECM are shown in Figure 42, where the blue and red curves are the parameters with online and offline identification method, respectively.

The comparison shows that the two sets of parameters tend to stay close, but there are some discrepancies when the current changes direction. Figure 42 proves the online parameters identification algorithm works for a fresh battery at 25^{o}C. The voltage, current, and temperature during drive cycle I are plotted in Figure 43, and the SOC estimation results and error are plotted in Figure 44. The proposing algorithm can accurately estimate the SOC of the battery with errors that are less than 3% throughout the drive cycle. However, the estimation error during charging at C.V. mode is still very large, which needs to be improved.

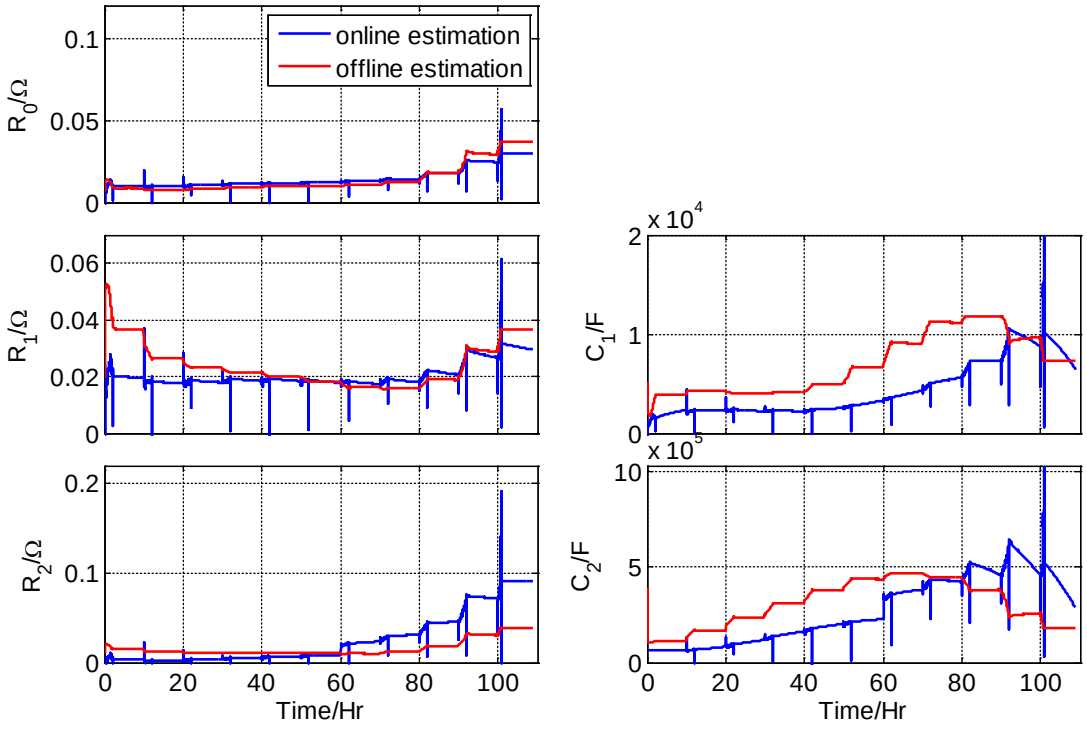

Figure 42: Estimated ECM parameters of a fresh battery during pulse discharging at 25°C.

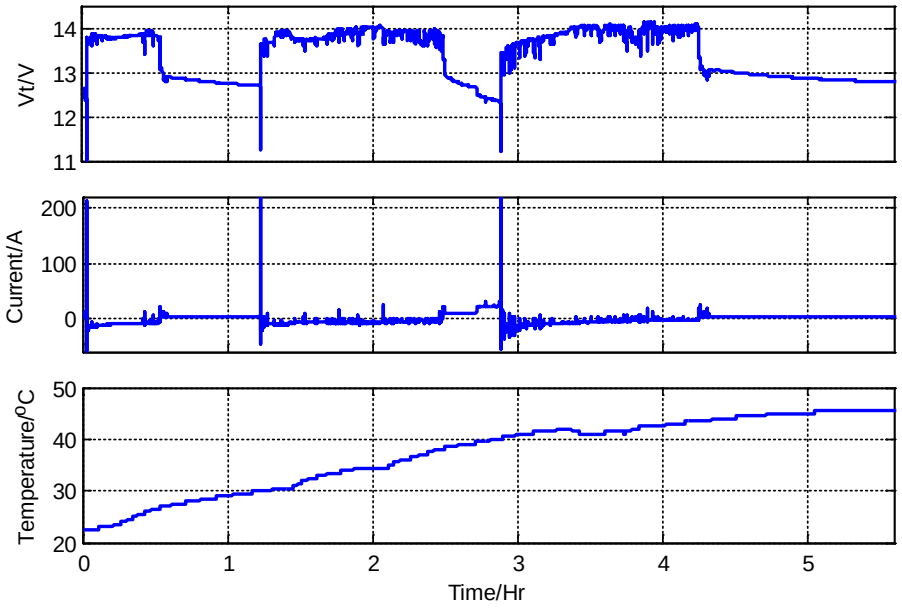

Figure 43: Drive cycle I.

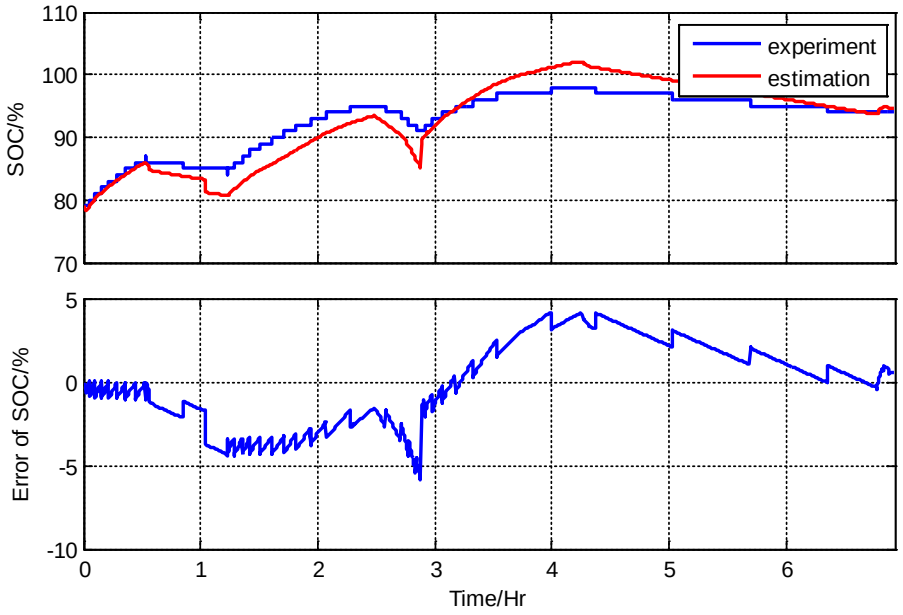

Figure 44: Simulated SOC and its error of a fresh battery using online parameters during drive cycle I at 25^{o}C.

2.5.3 Sensitivity analysis of parameter coefficients

In equation (35), the values of a_1 to a_5 should all be close to 1 because the change of the parameters with respect to time is very slow. The larger the value is, the faster is the increase of the parameter. Likewise, the smaller the value is, the faster is the decrease of the parameter. For both cases, the stability of the battery model can become worse, and it takes more time for the parameters to reach its true value, although there is a correction with EKF. The following values are tested during a pulse discharge, where the experimental data of voltage, current, and temperature are shown in Figure 37, and the parameter estimation and SOC estimation are shown in the following sequence:

1. a_1=1, a_2 = 1.02, a_3=0.99, a_4=1.005, and a_5=1.01 (Figure 42 and Figure 41);
2. a_1=1, a_2 = 1.03, a_3=0.99, a_4=1.005, and a_5=1.01 (Figure 45 and Figure 46);
3. a_1=1, a_2 = 0.97, a_3=0.99, a_4=1.005, and a_5=1.01 (Figure 47 and Figure 48);

4. a_1=1, a_2 = 1.04, a_3=0.99, a_4=1.005, and a_5=1.01 (Figure 49 and Figure 50);
5. a_1=1, a_2 = 1, a_3=1, a_4=1, and a_5=1 (Figure 51 and Figure 52);
6. a_1=1.01, a_2 = 1.01i, a_3=1.01, a_4=1.01, and a_5=1.01 (Figure 63 and Figure 54);

In this work, the parameters are set as shown in 1, and the estimation results of parameters of the ECM are shown in Figure 42 and Figure 41. The errors of SOC estimation results are less than 3%. Then the value of a1 is changed to 1.03, 0.97, and 1.04, while all the others are kept the same result. From Figure 45 to Figure 50, the results show that if a1 is set too large or too small, the parameter estimation becomes inaccurate, which leads to an inaccurate SOC estimation. Then, the parameters are set as the same value 1 or 1.01, the results are shown in Figure 51 and Figure 54. Due to the matrices A and C of the model, if a1 to a5 have the same value, the observability of the model becomes vulnerable, especially for parameters, C1 and C2.

Based on the response time of the model and the accuracy of the SOC estimation, the parameters of a1 to a5 are optimized.

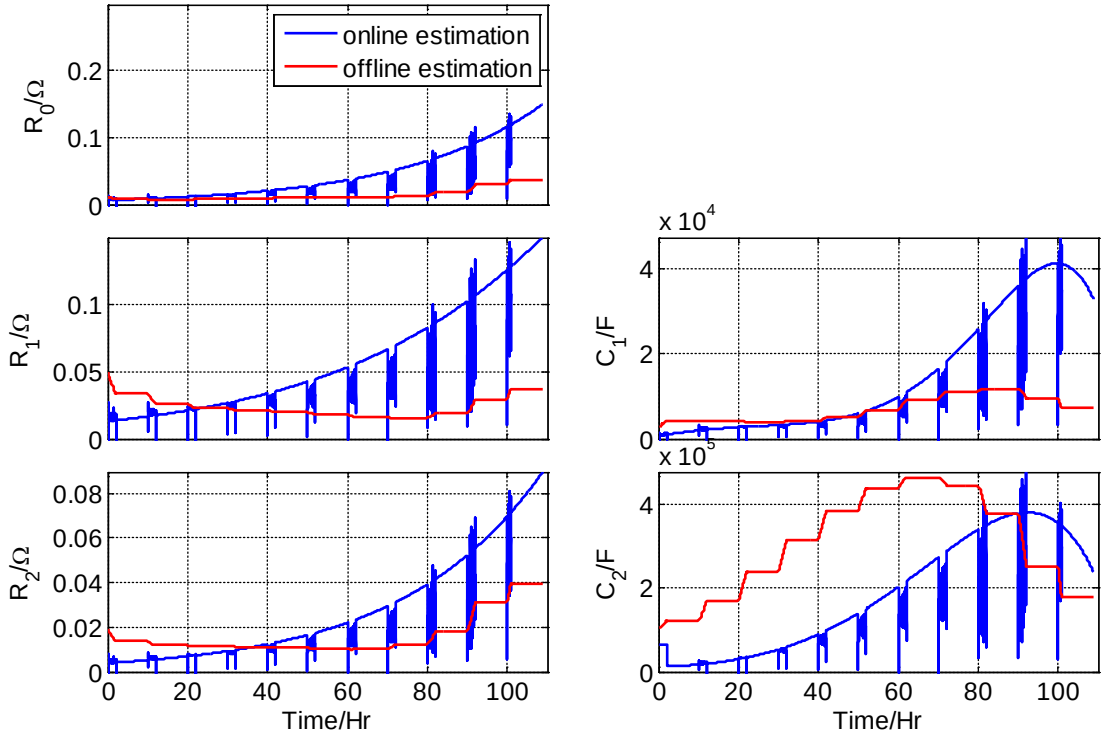

Figure 45: Parameter estimation (a_1=1, a_2 = 1.03, a_3=0.99, a_4=1.005, and a_5=1.01)

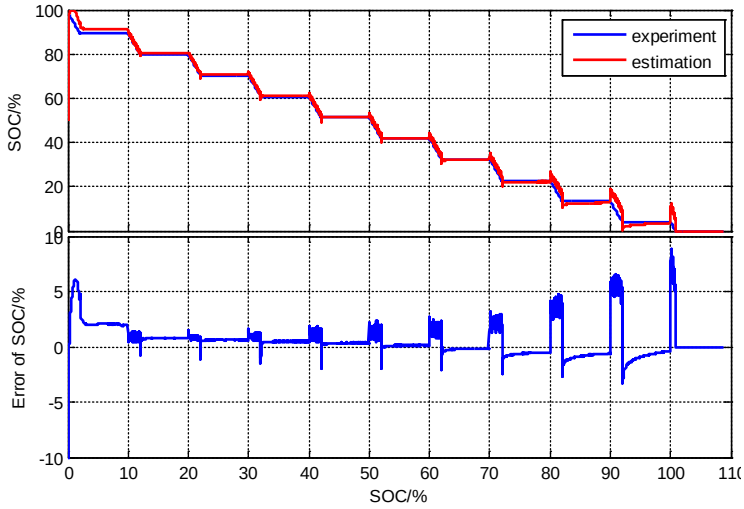

Figure 46: SOC estimation (a_1=1, a_2 = 1.03, a_3=0.99, a_4=1.005, and a_5=1.01)

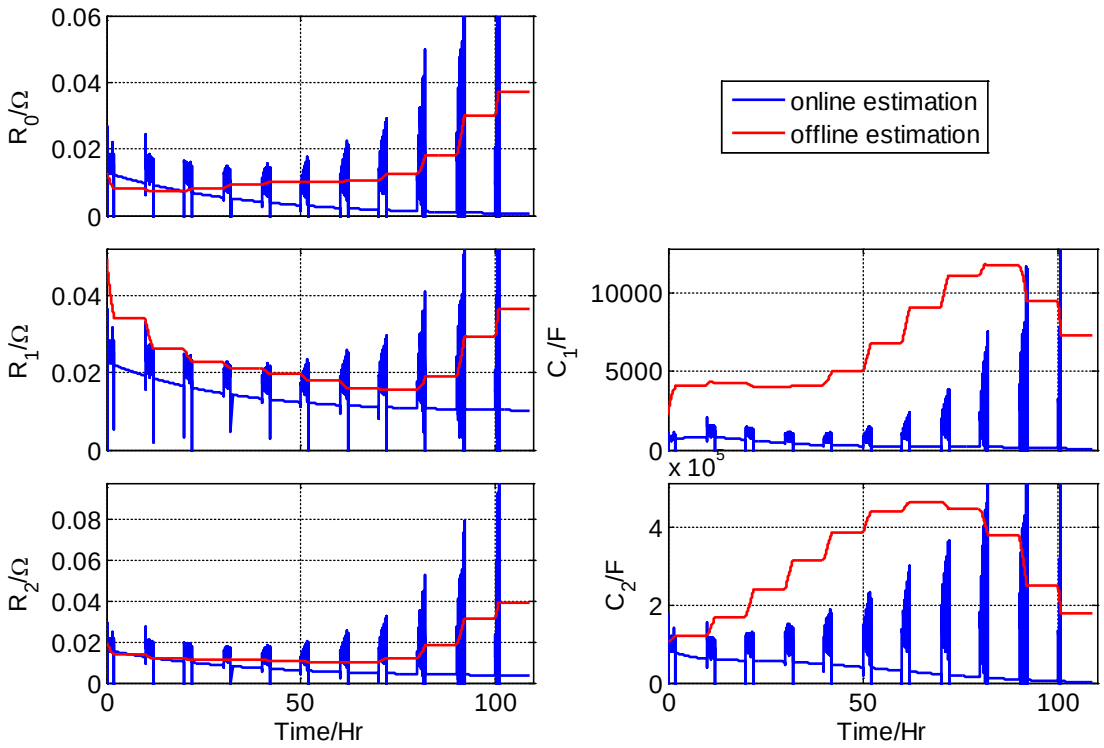

Figure 47: Parameter estimation (a_1=1, a_2 = 0.97, a_3=0.99, a_4=1.005, and a_5=1.01)

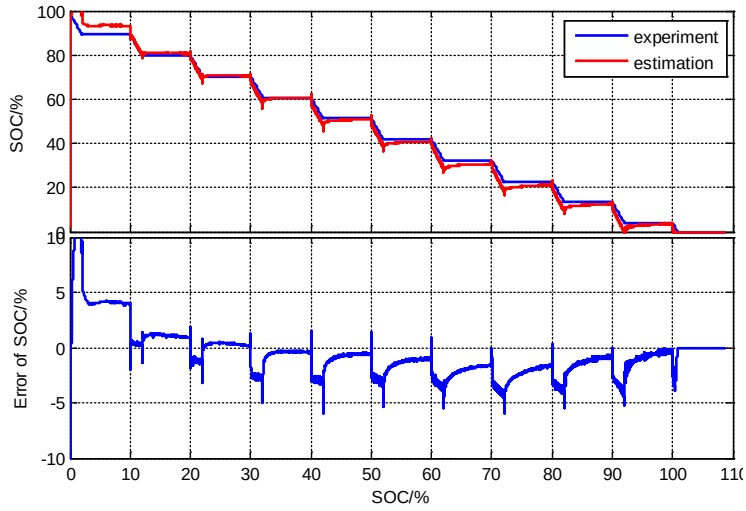

Figure 48: SOC estimation (a_1=1, a_2 = 0.97, a_3=0.99, a_4=1.005, and a_5=1.01)

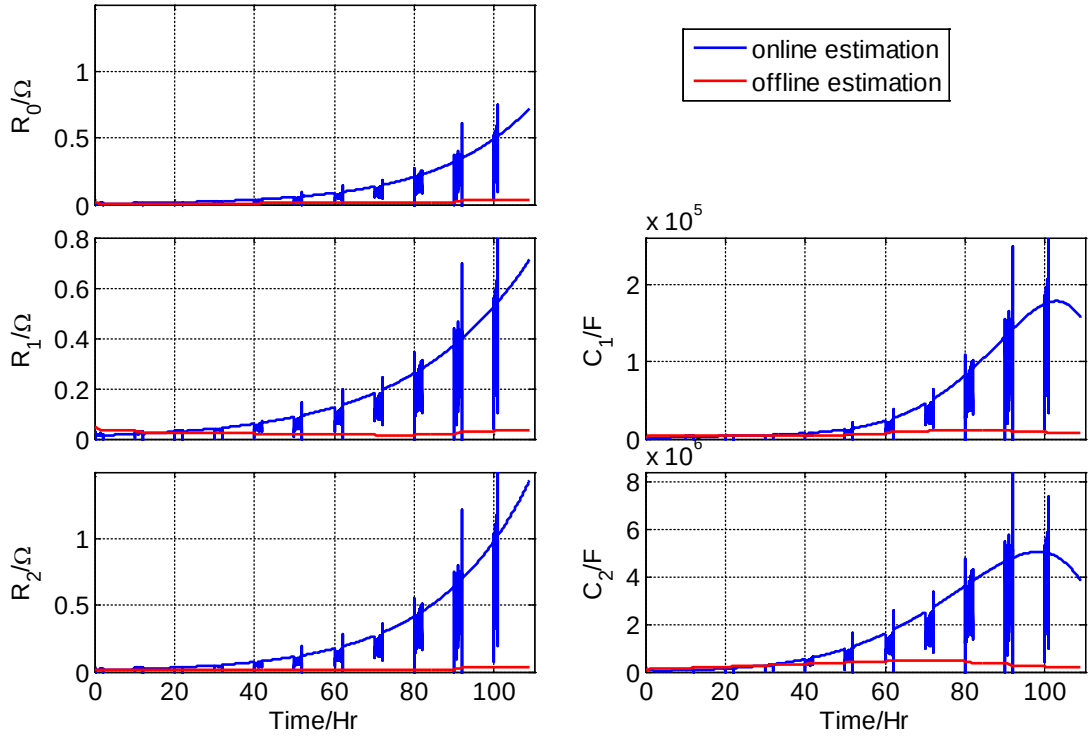

Figure 49: Parameter estimation (a_1=1, a_2 = 1.04, a_3=0.99, a_4=1.005, and a_5=1.01)

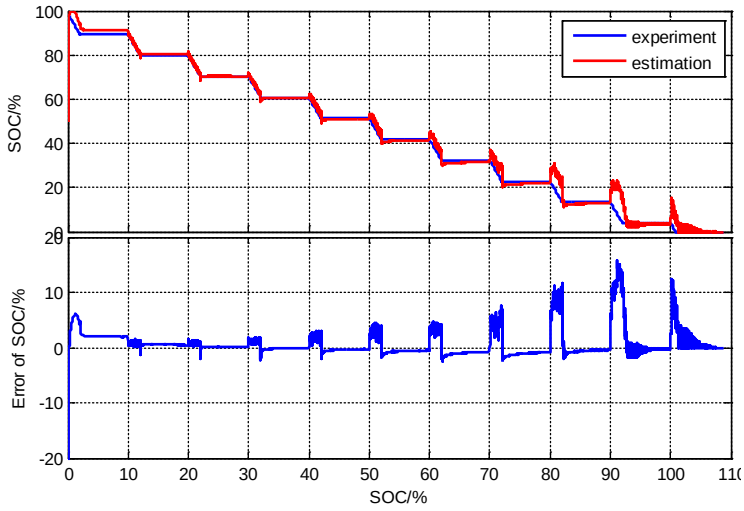

Figure 50: SOC estimation (a_1=1, a_2 = 1.04, a_3=0.99, a_4=1.005, and a_5=1.01)

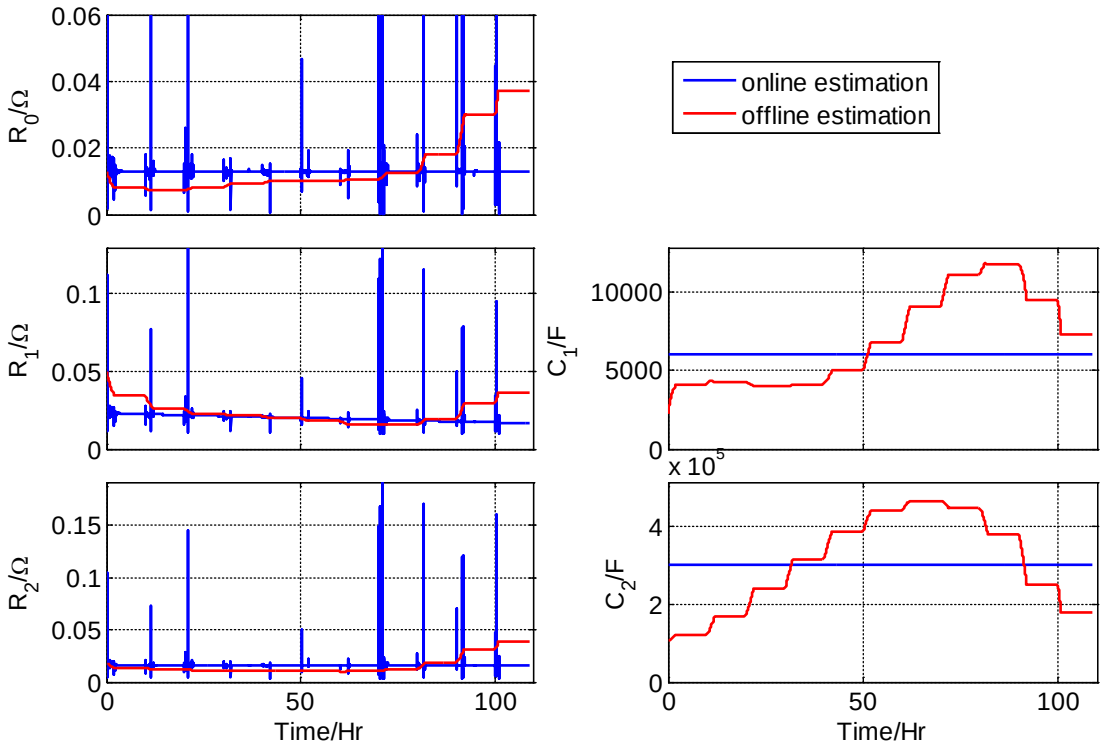

Figure 51: Parameter estimation (a_1=1, a_2 = 1, a_3=1, a_4=1, and a_5=1)

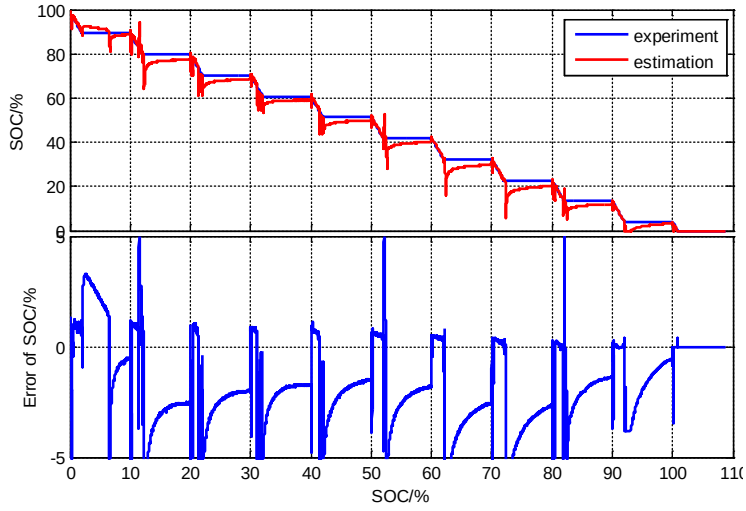

Figure 52: SOC estimation (a_1=1, a_2 = 1, a_3=1, a_4=1, and a_5=1)

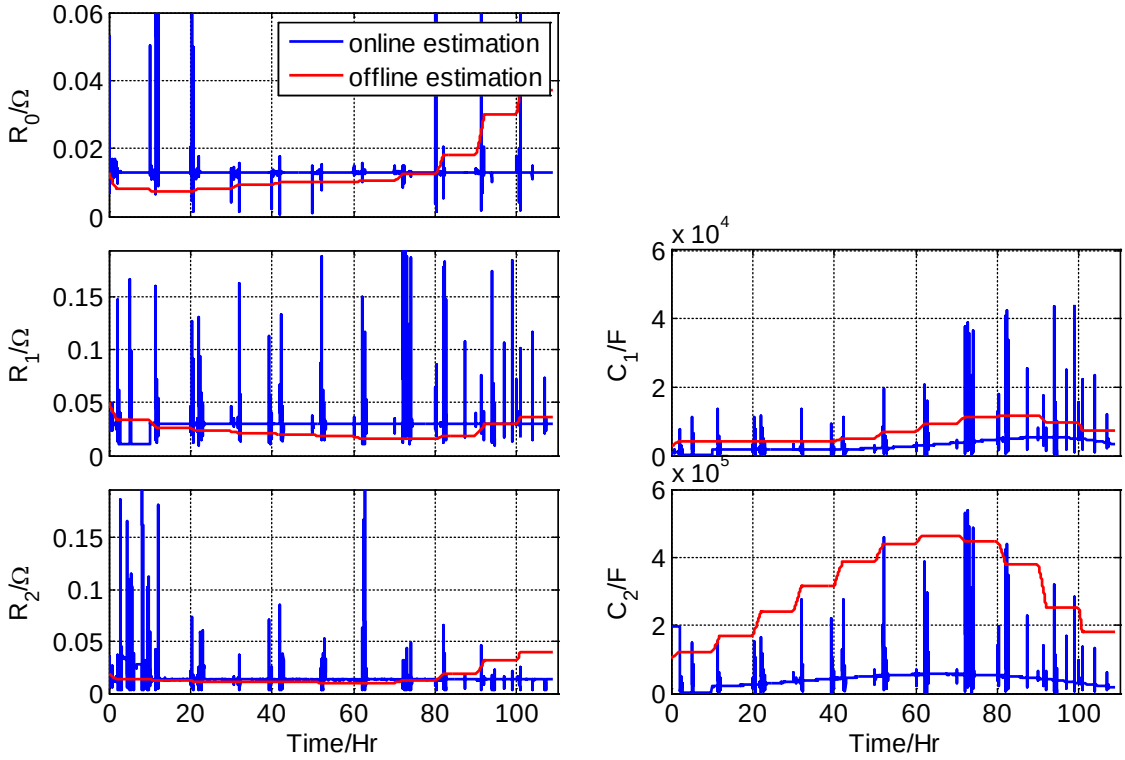

Figure 53: Parameter estimation (a_1=1.01, a_2 = 1.01, a_3=1.01, a_4=1.01, and a_5=1.01)

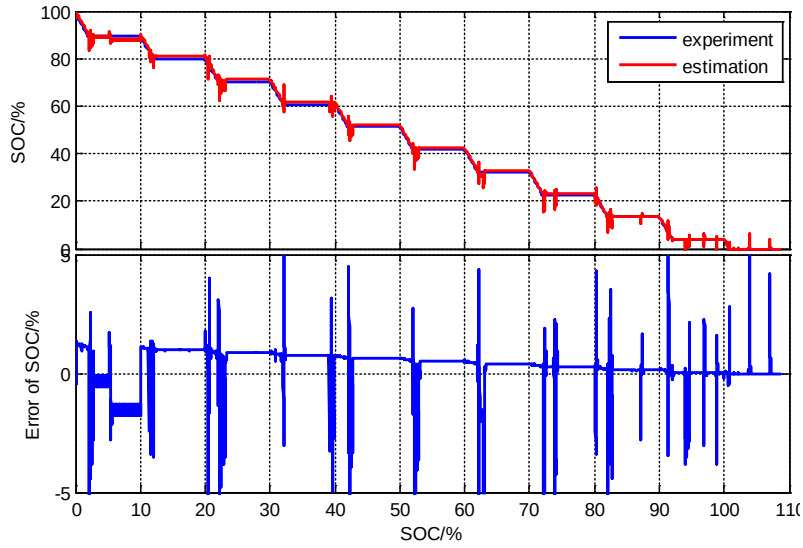

Figure 54: SOC estimation (a_1=1.01, a_2 = 1.01i, a_3=1.01, a_4=1.01, and a_5=1.01)

In this chapter, the SOC estimation algorithm with the ECM based EKF is described, where these parameters in the model are identified online and offline method. The batteries used to collect experimental data and test the algorithm are AGM lead acid batteries. The simulation results of SOC under four load profiles show that the ECM based EKF with online parameter identification works well at constant temperature except for C.V. charge. Although the parameter identification is considered with temperature change, the EKF cannot consider the change of capacity with temperature. The following chapters introduces how the SOC estimation algorithm can be further improved.

Chapter 3: Improvement of SOC estimation

In chapter 2, an ECM based EKF algorithm for SOC estimation was discussed. The parameters of the ECM were identified by an online or offline estimation methods. However, the EKF cannot accurately estimate the parameters under certain operating conditions, when the battery is charged in C.V. mode, or when there is a significant temperature change. This chapter focuses on how to improve this algorithm for SOC estimation. A novel combined SOC estimation method based on extended Kalman filter and Coulomb counting for starting engines, lighting and ignition (SLI) system is proposed, as it can effectively consider effects of parameter changes of ECM caused during C.V. charging, by varying temperature and aging process. In section 3.1, the principles of this proposed method are described. In section 3.2, improvements of the method considering temperature and aging are described. In section 3.3, results of SOC estimation and analysis using this method are described.

3.1 SOC estimation during C.V. charging

As shown in Chapter 2, the SOC estimation during C.V. charging is not accurate because of rapid changes of the parameters changes. When the terminal voltage of the battery reaches 14.3V, the current is reduced, so that the terminal voltage can be kept equal to or less than 14.3V. To measure the parameters in C.V. charging mode, the following experiment has been made.

1. Charge the battery with 14A C.C. mode to 14.3V at room temperature
2. Keep 14.3V C.V. charging, when the capacity increases 7Ah, followed by four hours' rest to relax the battery, and record the data.
3. Repeat step 2, until the total charged capacity is equal to capacity of the battery

The same parameter estimation method described in section 2.3 is applied to obtain the parameters, as shown in Figure 18. It turns out that RC parameters change significantly with time, therefore, the online identification method cannot identify the parameters accurately.

In Chapter 1.1.3, Coulomb counting is introduced as a possible solution for the SOC estimation. Coulomb counting is pretty simple. However, initial SOC errors and measurement errors of the current sensor cause errors that cannot be removed. On the other hand, these errors can be corrected by the model based EKF that does not work well for the CV charging mode. Therefore, a combination of these two methods is proposed to estimate SOC accurately under any loading conditions, even with an initial error.

The principle of the combined two methods is shown in Figure 55. The charging and discharging status of the battery is first monitored. When the battery is discharged or charged in C.C. mode, and the voltage is less than 14V, the ECM based EKF is applied to estimate SOC. Once the battery voltage reaches 14V and the battery is in C.V. charging mode, the ECM based EKF stops estimating. Instead, the SOC is estimated with Coulomb counting until the battery stops C.V. charging more than 50s, then the ECM based EKF resumes. More details of this combination method are shown in the flowchart of Figure 56. The initial SOC is set to be 50%. The initial values of parameters of ECM are the same values of a fresh battery at 50% SOC. The EKF is applied after 50s. The initial errors are reduced. The terminal voltage determines if battery is charged in C.C. mode or C.V. mode. If the battery is charged in C.V. mode, the Coulomb counting is used to estimate SOC, otherwise the ECM based EKF is used.

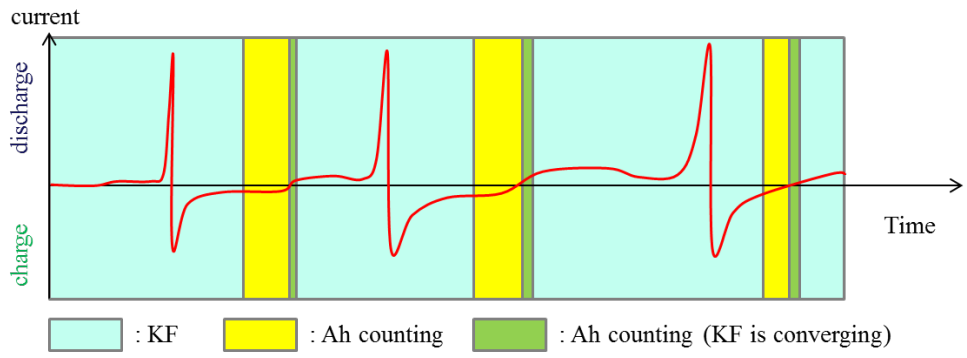

Figure 55: Principle of the novel combined SOC estimation method.

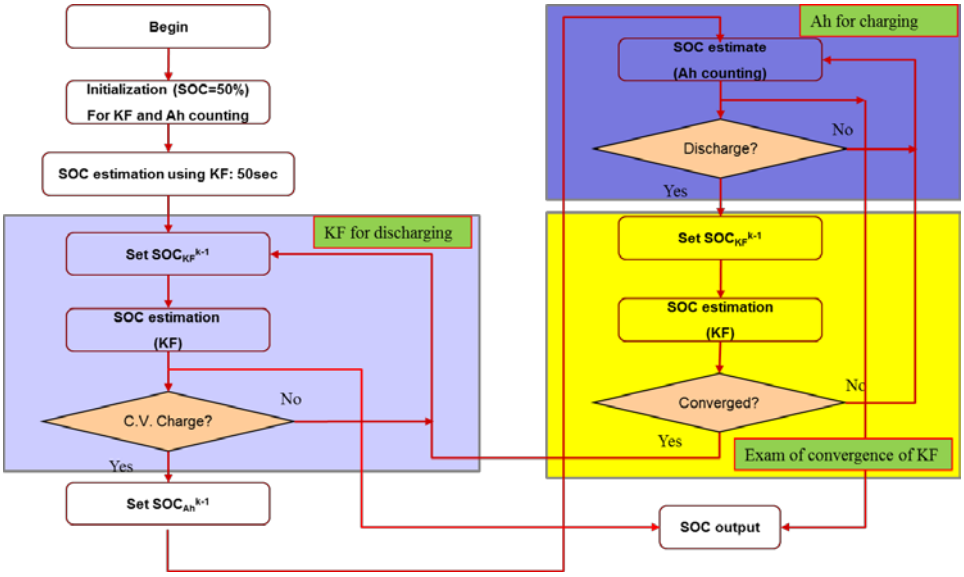

Figure 56: Flowchart of the combined SOC estimation method.

3.2 Effects of temperature on SOC estimation

Although the RC parameters in the ECM can be identified with the KF online, the model shows a large discrepancy when there is a significant change in battery temperature. The change of the temperature leads to not only change of the activation overpotentials that the RC parameter represents, but also the capacity of the battery.

To measure the capacity dependence on temperature, an experiment has been set up according to the following procedures:

1. Fully charge the battery with C.C. and C.V. mode in twenty four hours at room temperature, followed by four hour rest to relax the battery.
2. Set the thermal chamber to a specific temperature.
3. Put the battery in the thermal chamber for four hours to make sure that the working temperature reaches that specific temperature.
4. Completely discharge the battery with a constant current of 3.5A, and record the data.

Repeat steps 1 through 4 with all of the temperatures. The maximum capacity at that specific temperature is measured according to Coulomb counting. The measured maximum capacity at various temperatures is shown in Table 1 and plotted in Figure 57. The red point in Figure 57 is the experimental data and the blue line is a fitted curve by a second order polynomial that can be written in Equation (41). The coefficients of the second order polynomial are listed in Table 8.

Table 8: Measured capacity of fresh battery at different temperatures

Temperature (ºC)	**Capacity (Ah)**
-15	56.14
-10	57.73
-5	60.26
0	63.31
5	66.39
10	68.72
15	72.07
20	72.83
25	73.74

30	75.59
35	76.94
40	76.2
45	74.51
50	73.82
55	72.46
60	71.84

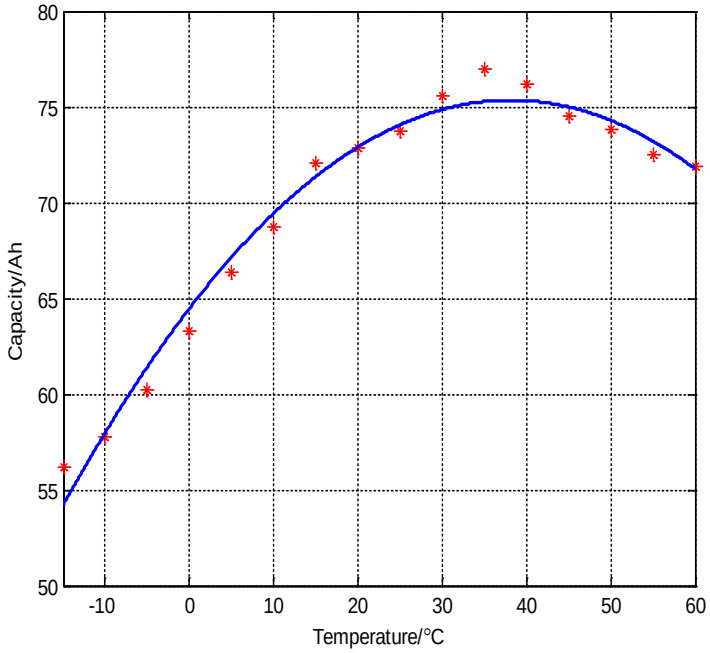

Figure 57: Capacity of a battery at different temperatures.

The empirical equation (41) shows that the capacity is a function of temperature.

$$Q(T) = d_1 T^2 + d_2 T + d_3, \tag{41}$$

where the coefficients of the second order polynomial are summarized in Table 9.

Table 9: Coefficients of the empirical equation for capacity at different temperatures

Coefficient	**Value**

d_1	-7.49×10^{-3} [Ah/^{o}C^2]
d_2	0.5718 [Ah/^{o}C]
d_3	64.44 [Ah]

If the Q_{max25} is known, the capacity at a current temperature is adjusted using equation (42). The $Q(T)$ in equation (42) is an empirical equation (41). Likewise, if the Q_{max25} and temperature T are known, the current capacity can be modified using equation (42).

$$Q_{\max}(T) = Q_{\max 25}\frac{Q(T)}{73.74} = \left(-1.0157\times10^{-4}T^2 + 7.8\times10^{-3}T + 0.8739\right)Q_{\max 25} \quad (42)$$

3.3 Results and analysis

3.3.1 SOC estimation of a fresh battery during C.V. charging

In order to test the method that combines the ECM based EKF with the Coulomb counting method, simulation results are compared with those of experiments during two drive cycles. The load profiles of drive cycle I and II are shown in Figure 57 and Figure 59, respectively. The corresponding SOC estimation with the new algorithm are shown in Figure 58 and Figure 60, respectively. The results show that even with a big initial error, the ECM based EKF can correct the error by measuring the terminal voltage, the error can be reduced to 5% quickly. Although the SOC range is very wide during both drive cycle I and II, and the battery is operated at C.V. charging mode, the estimation error becomes less than 5%. Compared with the results from the model without Coulomb counting in Figure 44, its performance is much better. From the results in Figure 58 and Figure 60, both methods are complemented, the disadvantages of both methods can be minimized.

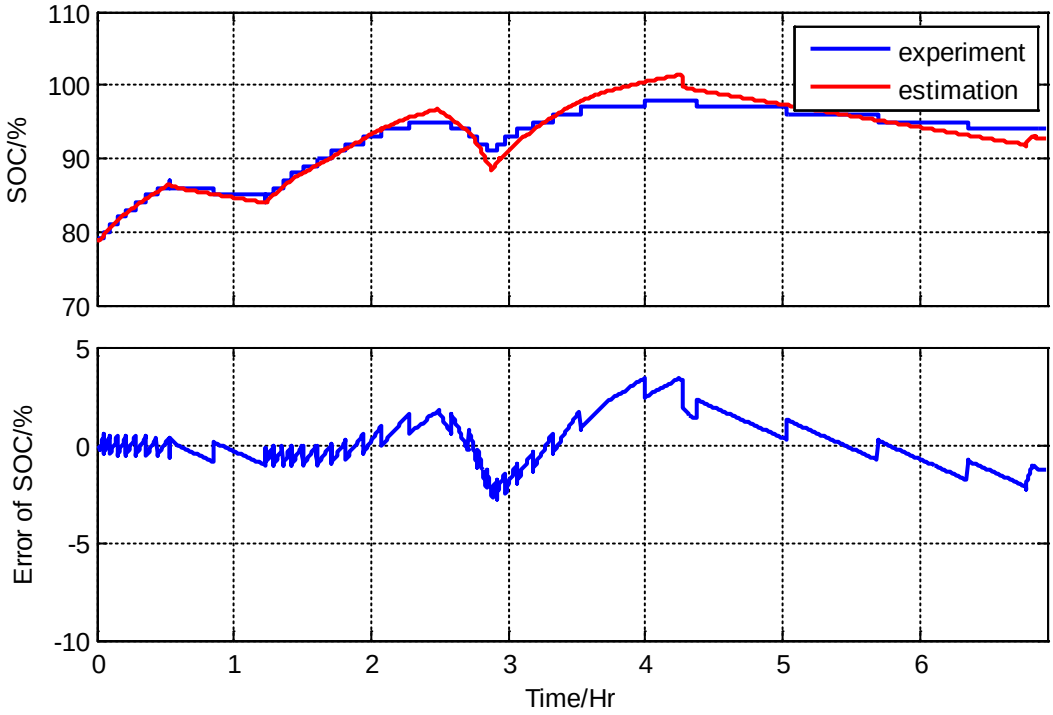

Figure 58: Simulated SOC and its error of a fresh battery using the combined method during drive cycle I at 25ºC.

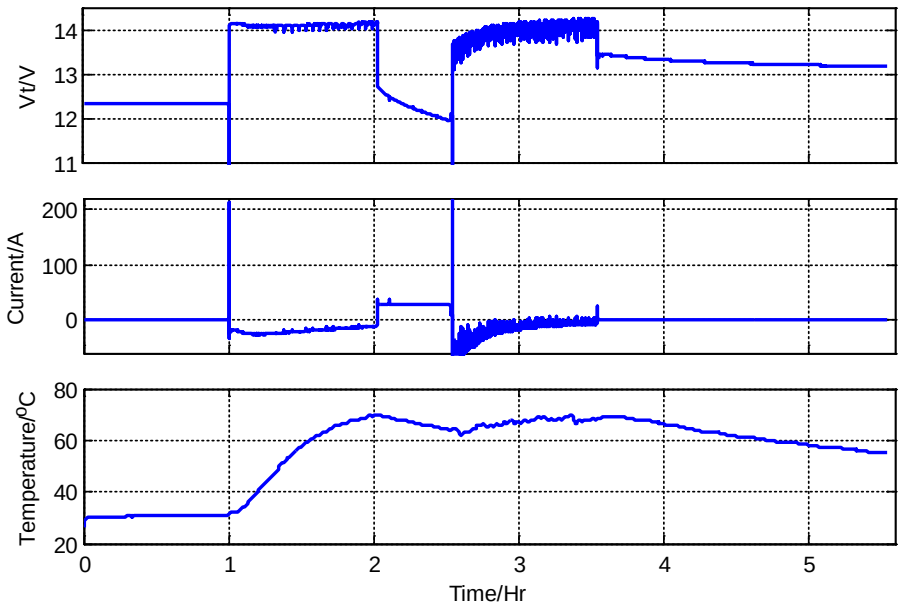

Figure 59: Drive cycle II.

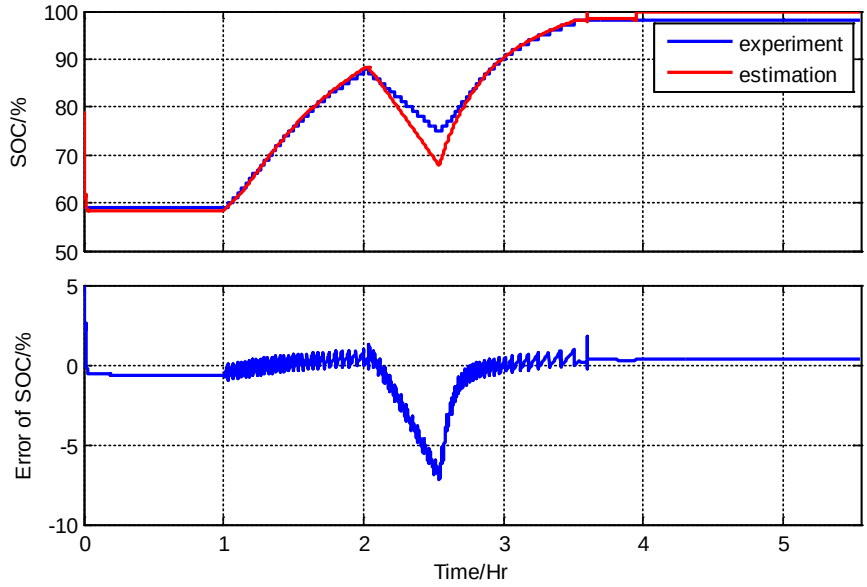

Figure 60: Simulated SOC and its error of a fresh battery using the combined method during drive cycle II at 25°C.

However, the maximum error in the drive cycle II is larger than 5%. During the period where the SOC error is large, the battery temperature is very high. Similar conclusions can also be

obtained from the results of a full charge-rest-discharge-rest cycle, and the results are shown in Figure 61. Since the RC parameters are identified online, the temperature dependence of capacity needs to be considered to improve the model.

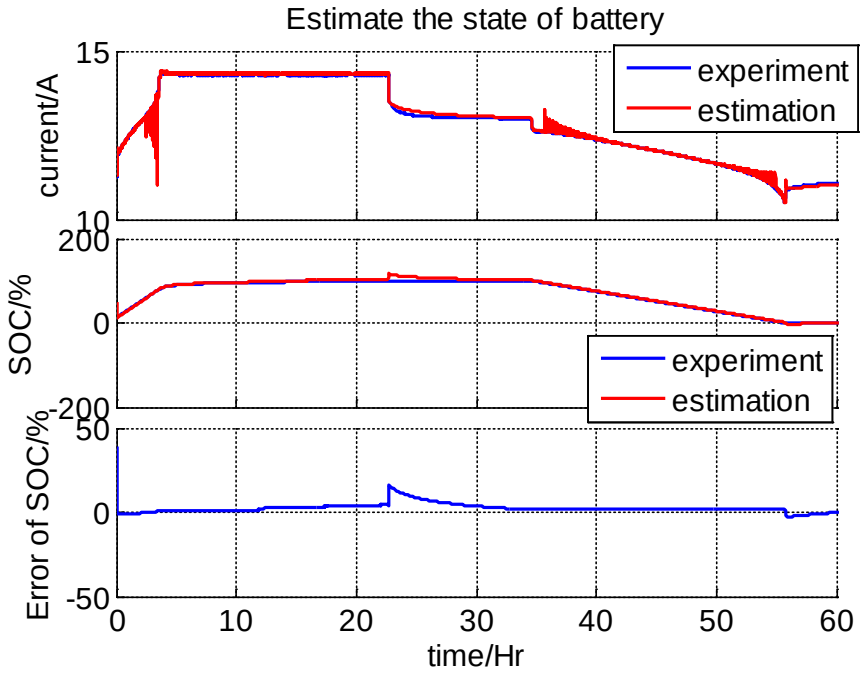

Figure 61: Simulated and experimented terminal voltage, SOC, and error of SOC of a fresh battery using the combined algorithm during a full cycle at 25°C.

3.3.2 Effects of temperature on capacity for SOC estimation of a fresh battery

The effects of temperature on capacity are considered using the empirical equation. The same drive cycle tests are conveyed as those in3.3.1, and the results are shown in Figure 62 and Figure 63. The initial condition for the SOC estimation is listed as shown in Table 10, where the model is significantly improved by considering the capacity that depends upon temperature. The error can be further reduced to less than 2%. One more drive cycle is used to test this method, where the experiment and simulation results are compared as shown in Figure 64 and Figure 65. During pulse charging and discharging, the SOC estimation error remains also stays below 2%.

Table 10: Initial condition of SOC estimation

Variables	**Values**
SOC	79%
R_0	5mΩ
R_1	30 mΩ
C_1	20kF
R_2	15 mΩ
C_2	10kF
Q_{max}	68.81Ah

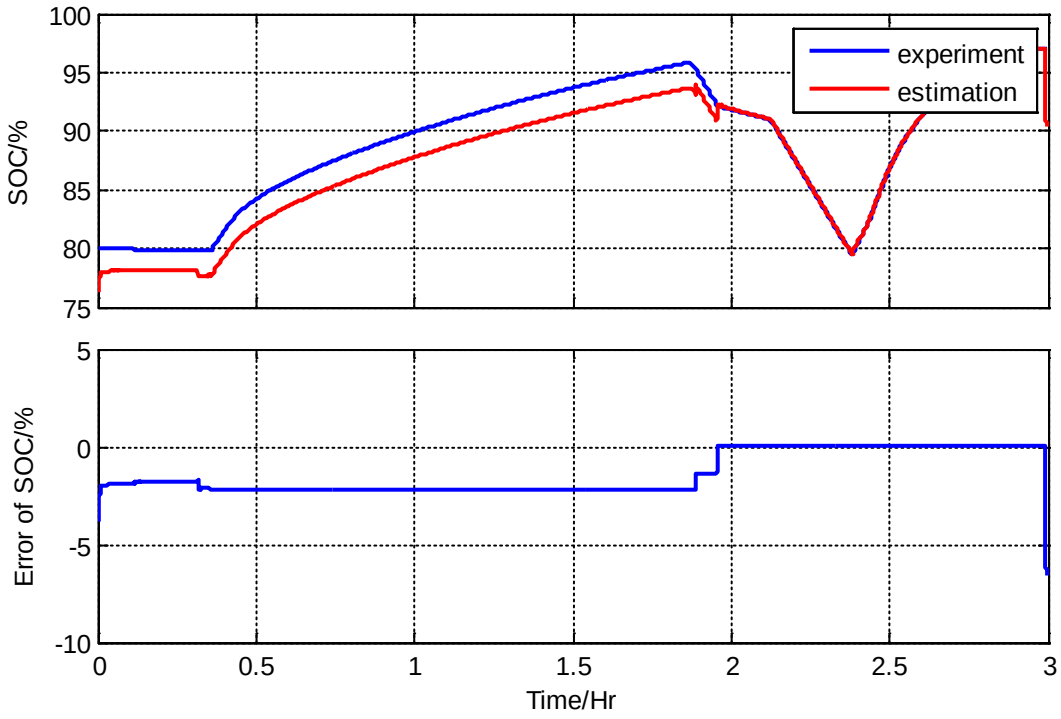

Figure 62: Simulated SOC and its error of a fresh battery using the combined method during drive cycle II at 25^{o}C without considering capacity variation.

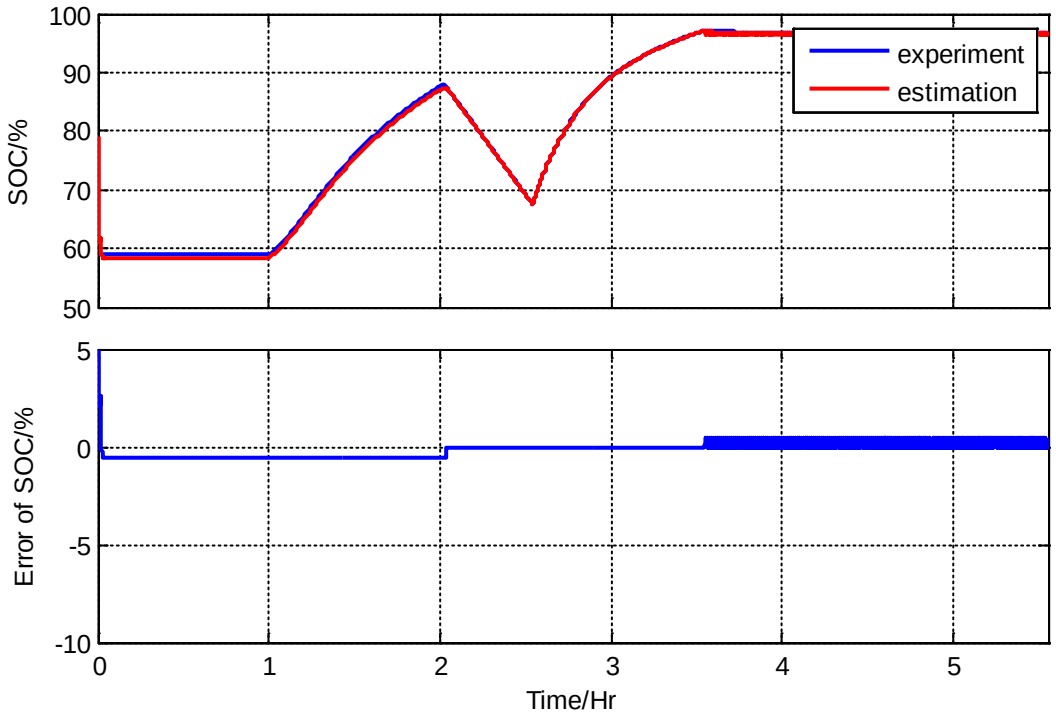

Figure 63: Simulated SOC and its error of a fresh battery using the combined method during drive cycle I at 25ºC with the capacity update.

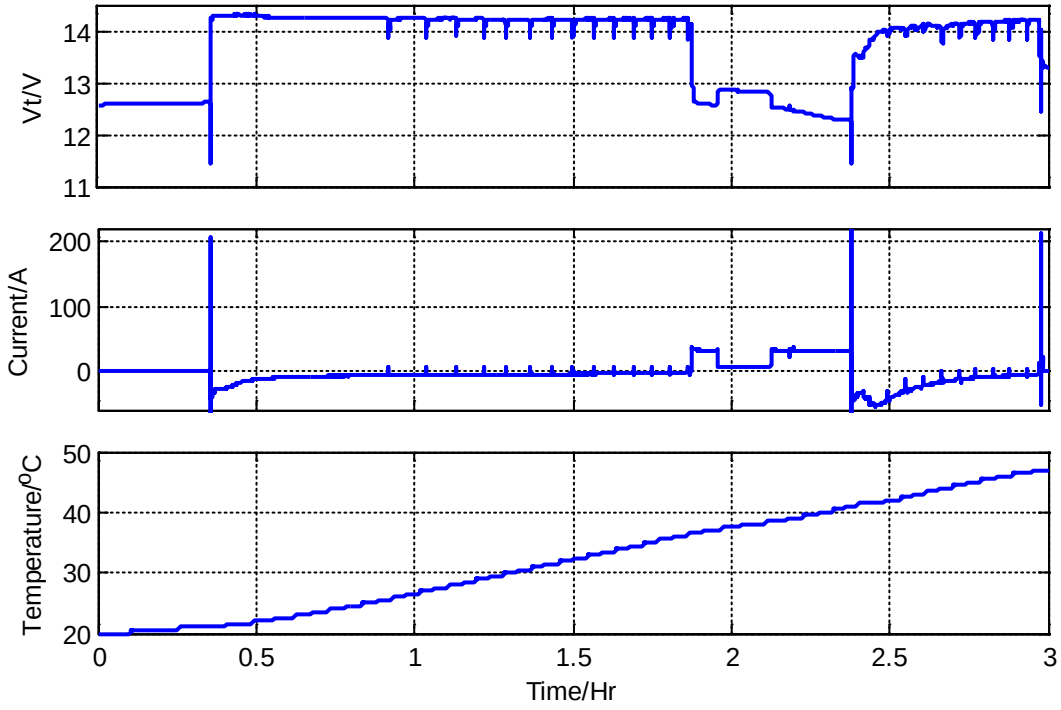

Figure 64: Drive cycle III at 25°C, including the response of voltage, current, and temperature.

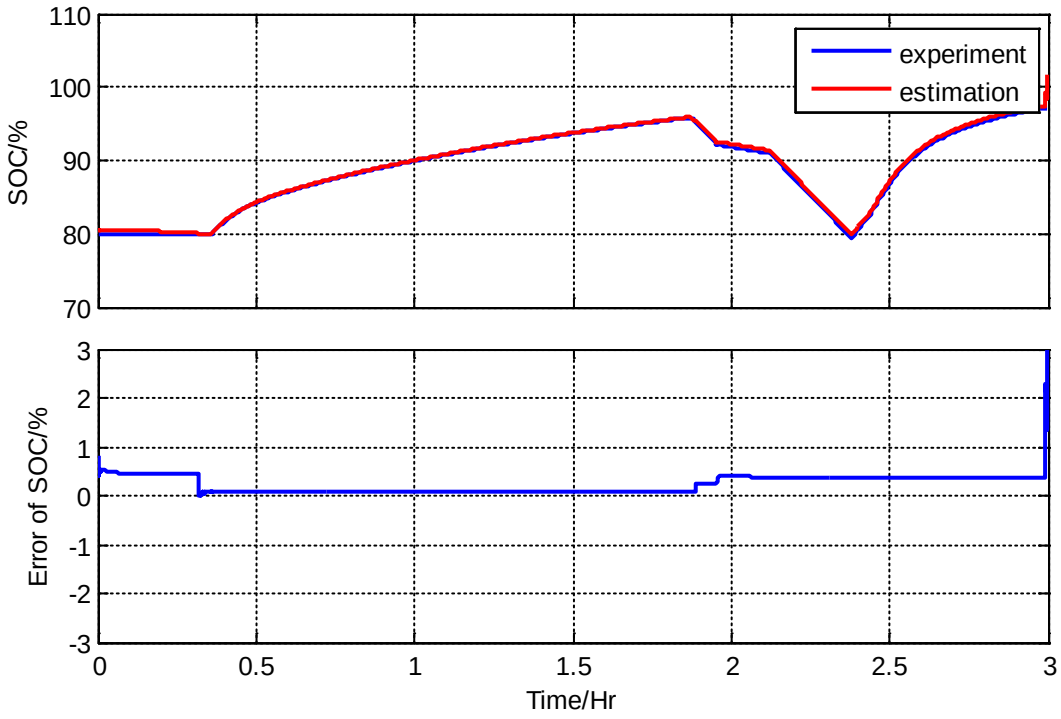

Figure 65: Simulated SOC and its error of a fresh battery using the combined method during drive cycle III at 25^{o}C with capacity update.

3.3.3 Effects of temperature and aging on the SOC estimation

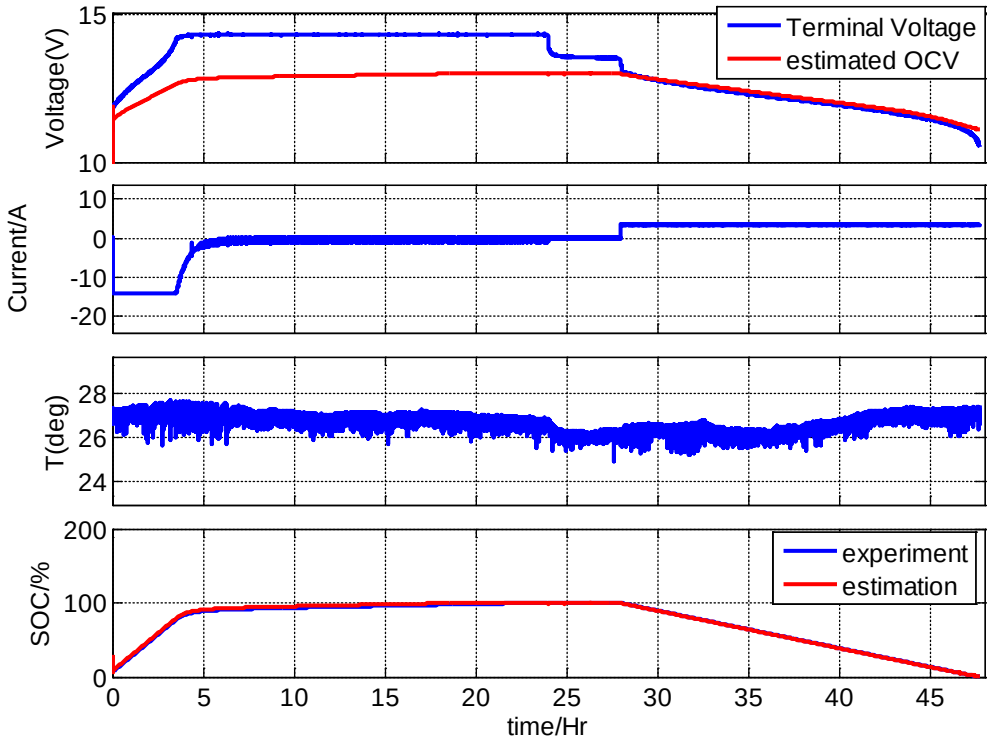

Figure 66: Simulated and experimented response of voltage, current, temperature and SOC.

The RC parameters of the ECM are affected not only by battery SOC and, temperature, but also by degradation. In order to test the effectiveness of the online parameter identification algorithm, the model is tested at different levels of degradation. For a fresh battery, the maximum capacity is measured at 25^{o}C which is 72.8Ah. The battery is then set to 0% SOC and a full cycle is applied to the battery, including a full charging at CC/CV mode, a five hours' rest, and a full discharge at C.C. mode. The current, temperature and voltage waveforms are shown in Figure 66. The true SOC of the battery is calculated by integration of current with respect to time, the estimated SOC is calculated from the combined model using the ECM based EKF and Coulomb counting method. The comparison between experimented and estimated SOC is shown in blue and red curves in (d) of Figure 66. The results show that even with a 20% initial SOC error, the model

can correct the error and reach the true SOC within 50s with the feedback of the measured terminal voltage.

After the battery is cycled, the maximum capacity is measured at 25ºC for every 20 cycles. The battery is then cycled under the load condition shown in the above analysis. After 20 cycles, the battery capacity is faded to 95%, which is 69Ah. At the same time, the active materials inside of the battery also changes, the RC parameters of the ECM should also be updated to meet the changes caused by degradation. With the online parameter identification algorithm, the model can estimate the battery SOC accurately, and the results are shown in Figure 67. The comparison shows that the model can identify the parameters and estimate SOC accurately, even when the battery is aged.

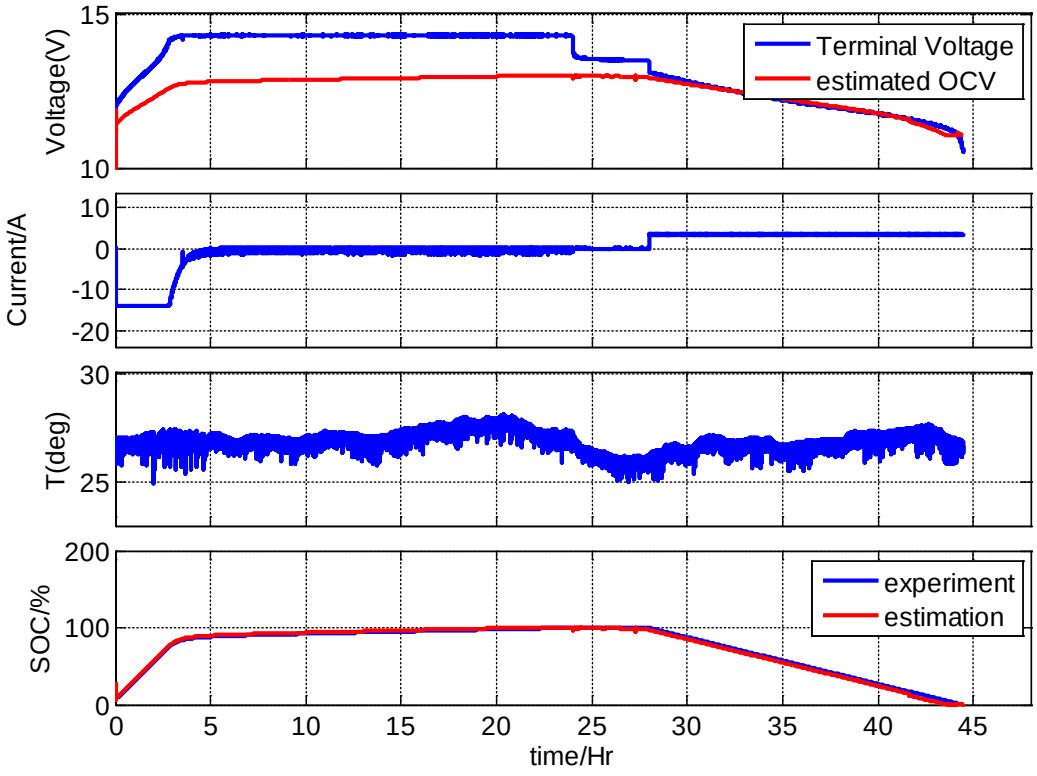

Figure 67: Simulated response of voltage, current, temperature, and SOC of an aged battery with 5% capacity fade.

Finally, the battery is cycled for another 50 cycles. Similar to the previous test, the maximum capacity is measured, and the capacity is faded to 51%, which is 37.5Ah. The battery is then cycled under the load condition shown in Figure 67. The SOC estimation results are shown in Figure 68. Even with a large capacity fade, the method can still accurately estimate the SOC with the online parameter identification method.

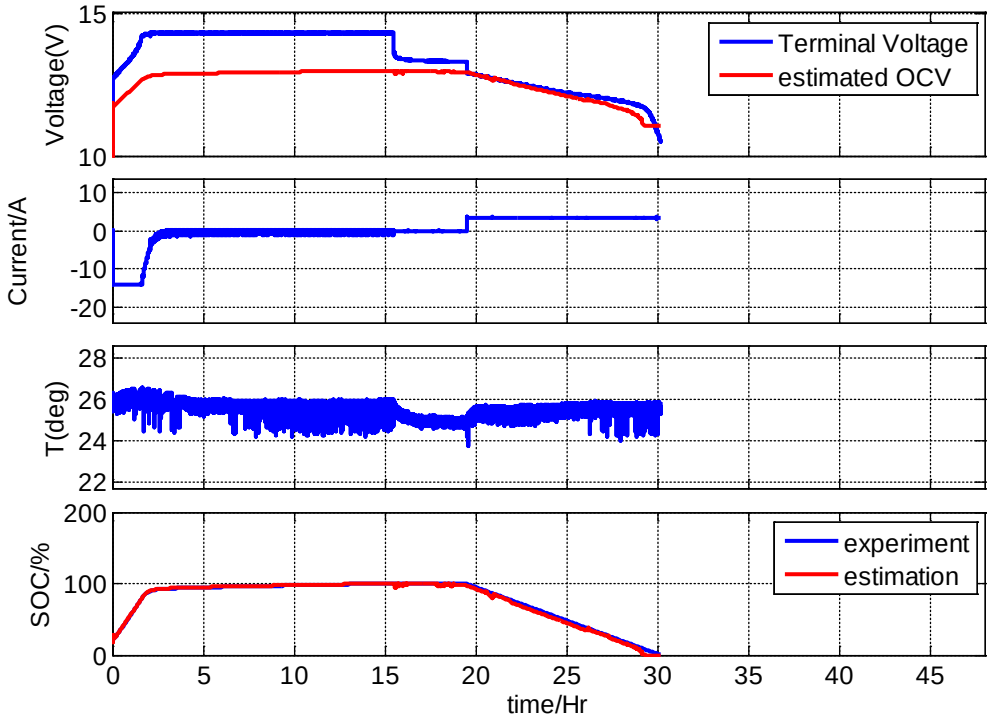

Figure 68: Simulated response of voltage, current, temperature, and SOC of an aged battery with 49% capacity.

In this section, the SOC estimation results of the method are tested with a battery at different stages of degradation, including 0%, 5%, and 41% capacity fades. Although the dynamics of the battery changes when the battery is aged, the ECM based EKF can still accurately estimate the battery SOC with the online parameter identification algorithm considering temperature and aging effects.

Chapter 4: Water loss

Water loss in the electrolyte caused by side reaction is one of the disadvantages of an AGM lead acid battery, and decreased ion conductivity. Thus, estimation of water loss is very desirable to keep the same performance of the battery at the beginning state. In this chapter, reasons for water loss and a method to measure water loss are analyzed. The amount of the water loss will be measured experimentally and also be estimated with a mathematical model.

4.1 Theory

The following three subsections focus on the theoretical aspects which are the main side reactions that lead to water loss. Section 4.1.1 deals with the general lead acid battery design and working principles of an AGM lead acid battery that includes absorbent glass mat and safety valve. Section 4.1.2 discusses the side reactions which lead to water loss. Lastly, section 4.1.3 will focus on the rate of the side reaction.

4.1.1 Design and working principles of an AGM lead acid battery

Two electrodes of different materials immersed in electrolyte can comprise an electrochemical power source, whereby the different potentials are formed at the two electrodes. Similarly, this potential difference generates the electromotive force of the electrochemical power source that makes the electric current flow between the two electrodes (anode and cathode) that are connected to a conductor with a load. Electrochemical reactions proceed at the interfaces of electrodes and electrolyte; it involves electrons transfer between the electrode surface and ions from the solution.

The lead acid battery as an electrochemical power source, includes lead dioxide (PbO_2) as the anode, lead (Pb) as the cathode and a solution of sulfuric acid (H_2SO_4) as the electrolyte. The reaction of lead dioxide reduction ($Pb^{4+} + 2e^- \rightarrow Pb^{2+}$) and of lead oxidation ($Pb \rightarrow Pb^{2+} + 2e^-$)

are utilized in lead acid batteries. As a rechargeable electrochemical power source, the reactions in lead acid battery are reversible. Therefore, the reaction of the lead acid battery can be described as,

Positive electrode: $$PbO_2 + SO_4^{2-} + 4H^+ + 2e^- \underset{charge}{\overset{discharge}{\rightleftharpoons}} PbSO_4 + 2H_2O \quad (43)$$

Negative electrode: $$Pb + SO_4^{2-} \underset{charge}{\overset{discharge}{\rightleftharpoons}} PbSO_4 + 2e^- \quad (44)$$

Cell reaction: $$Pb + PbO_2 + 2H_2SO_4 \underset{charge}{\overset{discharge}{\rightleftharpoons}} 2PbSO_4 + 2H_2O \quad (45)$$

.

The equilibrium potential of negative electrode can be calculated by Nernst equation,

$$E_{Pb/PbSO_4} = E^0_{Pb/PbSO_4} + \frac{RT}{nF}\ln\kappa, \quad (46)$$

where, R is the universal (or ideal) gas constant; T is temperature; n is the number of electrons; F is the Faraday constant; E^0 is the standard potential of the electrode; and κ is the equilibrium constant of the electrochemical reaction. According to the law of mass action, κ is equal to the ratio between the concentrations (or more precisely the activities, α) of the oxidized and reduced products of the reaction. The activity of the solid phase is equal to 1. For this action the κ is,

$$\kappa = \frac{\alpha_{PbSO_4}}{\alpha_{Pb}\cdot\alpha_{SO_4^{2-}}}. \quad (47)$$

The standard potential of the Pb/$PbSO_4$ electrode ($E^0_{Pb/PbSO_4}$) is equal to the electrode potential at $\alpha_{SO_4^{2-}} = 1$. According to the principles of electrochemical thermodynamics, the standard potential corresponds to the increase in Gibbs free energy (ΔG^0 cal),

$$E^0_{Pb/PbSO_4} = \frac{\Delta G^0}{nF}. \tag{48}$$

The sign of ΔG^0 is determined by convention. It is negative when a reduction process takes place at the electrode. We obtain that,

$$E^0_{Pb/PbSO_4} = \frac{-\Delta G^0_{PbSO_4} - \left(\Delta G^0_{SO_4^{2-}} + \Delta G^0_{Pb}\right)}{nF}. \tag{49}$$

The values for $\Delta G^0_{PbSO_4}$, $\Delta G^0_{SO_4^{2-}}$ and ΔG^0_{Pb} are form the Table 2.1 of references [1]. Finally, the equilibrium potential of negative electrode is calculated as,

$$E_{Pb/PbSO_4} = -0.358 - 0.029 \lg \alpha_{SO_4^{2-}}, \tag{50}$$

Similarly, the equilibrium potential of positive electrode can be calculated though the same way,

$$E_{PbO_2/PbSO_4} = 1.683 - 0.118\,pH - 0.059 \lg \alpha_{H_2O} + 0.029 \lg \alpha_{SO_4^{2-}}. \tag{51}$$

The electromotive force (EMF) of the lead acid battery can be calculated by equation (52).

$$EMF = 2.041 + 0.059 \lg\left(\frac{\alpha_{H_2SO_4}}{\alpha_{H_2O}}\right). \tag{52}$$

The EMF of the lead acid battery is the difference in equilibrium potentials of positive and negative electrodes. It is also called the open circuit voltage (OCV).

4.1.2 The side reactions leading to water loss

The electrolyte of the lead acid battery is a solution of sulfuric acid that is composed of sulfuric acid and water. Therefore, the side reaction of water must be considered. The reaction of the decomposition of water are shown equations (53) and (54),

$$2H^+ + 2e^- \rightarrow H_2, \tag{53}$$

$$2H_2O \rightarrow O_2 + 4H^+ + 4e^- . \tag{54}$$

According to the Nernst equation (46), $E^0_{O_2}$ can be calculated by equation (48), where the Gibbs free energy is listed in Table 2.1 of references [1], $E^0_{O_2} = 1.228V$. $E^0_{H_2}$ is defined to be 0V in electrochemical theory. The equilibrium constant κ in the reaction of decomposition of water is only affected by the pressure of the gas, because the concentration of water is constant.

The equilibrium potential of water can be calculated by equations (55) and (56),

$$E_{O_2} = 1.228 - 0.059\,pH + 0.015 \lg P_{O_2}, \tag{55}$$

$$E_{H_2} = -0.059\,pH - 0.029 \lg P_{H_2}. \tag{56}$$

Finally, the decomposition voltage of water in the electrolyte can be calculated with equation (57),

$$E_{H_2/O_2/H_2O} = 1.228 - 0.015 \lg P_{O_2} + 0.029 \lg P_{H_2}. \tag{57}$$

where, P_{O_2} and P_{H_2} are the pressures of hydrogen and oxygen inside of the battery, respectively. For the safety of the battery, the pressure is low, usually less than 2 psi. The decomposition voltage of water is less than 1.22V which is far below the manufactory's minimum voltage of the battery ($V_{\min}$=1.75V). Water decomposition and lead corrosion are to be accepted as unwanted secondary reactions in lead-acid batteries.

The lead acid battery is a $Pb/H_2SO_4/H_2O$ system. The lead compounds involved in this system are lead oxide (PbO), lead sulfate ($PbSO_4$), monobasic lead sulfate ($PbO{\cdot}PbSO_4$), tribasic lead sulfate ($3PbO{\cdot}PbSO_4{\cdot}H_2O$), tetrabasic lead sulfate ($4PbO{\cdot}PbSO_4$), lead dioxide (PbO_2) and red lead (Pb_3O_4). Although the solubilities of lead sulfate and lead dioxide in the electrolyte are very low, the Pb^{2+} and Pb^{4+} ions remain in the electrolyte. The relationships of transformations of lead compounds are shown in Figure *69*.

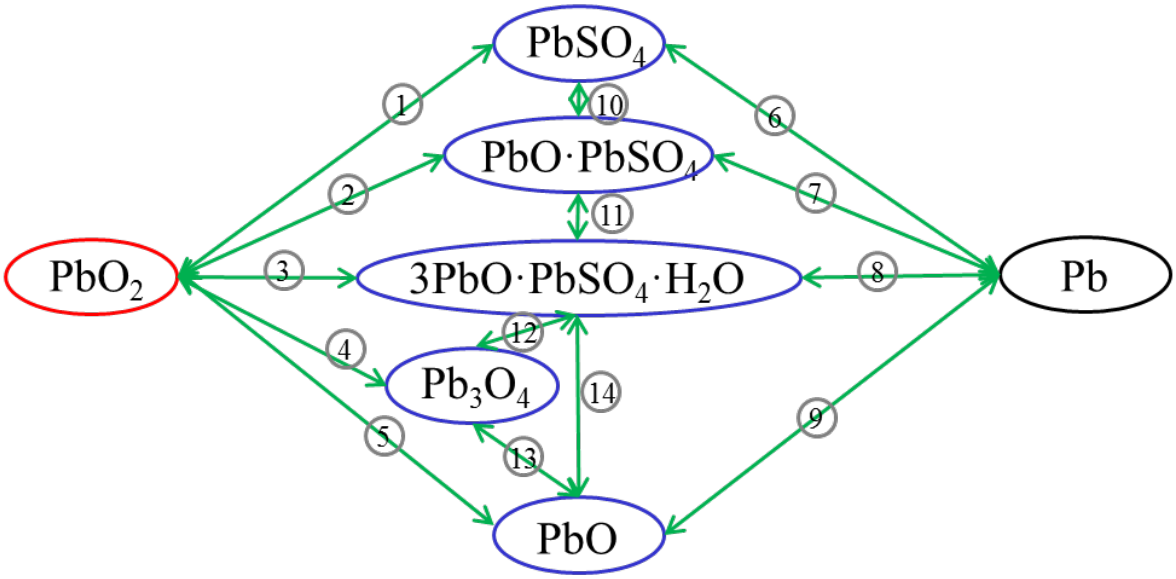

Figure 69: Relationships of transformations of lead compounds in $Pb/H_2SO_4/H_2O$ system.

The involved chemical and electrochemical reactions and their equilibrium states in the $Pb/H_2SO_4/H_2O$ system are presented in Table 11.

None of these electrochemical or chemical reactions leads to water loss. Only water direct decomposition causes water loss. The operating voltage is always larger than the potential that causes water loss and the water loss take places all the time.

In charging, the electrons in water decomposition come from the power supply. The action equations are shown in equation (53) and (54). While at rest, the electrons come from the discharge of the battery. Which is called self-discharge. The action equations can be written as equations (58) and (59).

$$PbO_2 + H_2SO_4 \xrightarrow{self-discharge} PbSO_4 + H_2O + \frac{1}{2}O_2 \tag{58}$$

$$Pb + H_2SO_4 \xrightarrow{self-discharge} PbSO_4 + H_2 \tag{59}$$

The valve-regulated lead acid battery (VRLA) has small gas channels in the electrolyte allowing the gas phase transport of oxygen to the negative electrode where it is reduced. The AGM lead acid battery achieves this characteristic by the application of absorbent glass mat separators which are soaked in the acid so that no liquid acid is left in the cell.

In conclusion, there are two side reactions that lead to water loss. One is hydrogen evolution at the negative electrode, and the other is oxygen evolution at the positive electrode. These side reactions take place during all operations of the battery charging, discharging and rest.

4.1.3 Speed of side reaction

The reaction of water decomposition is also called gassing. Two kinds of gases (hydrogen and oxygen) are generated by this reaction. In charging, the overall side reaction equation can be written as,

$$2H_2O \rightarrow 2H_2 + O_2. \tag{60}$$

Table 11: Electrochemical and chemical reactions that proceed in the system $Pb/H_2SO_4/H_2O$ [1]

	Reaction	**Equilibrium potential**
1	$PbO_2 + SO_4^{2-} + 4H^+ + 2e^- = PbSO_4 + 2H_2O$	$E_h = 1.685 - 0.118\,pH + 0.029 \lg \alpha_{HSO_4^-}$
	$PbO_2 + HSO_4^- + 3H^+ + 2e^- = PbSO_4 + 2H_2O$	$E_h = 1.628 - 0.088\,pH + 0.029 \lg \alpha_{SO_4^{2-}}$
2	$2PbO_2 + SO_4^{2-} + 6H^+ + 4e^- = PbO \cdot PbSO_4 + 2H_2O$	$E_h = 1.468 - 0.088\,pH + 0.015 \lg \alpha_{SO_4^{2-}}$
3	$4PbO_2 + SO_4^{2-} + 10H^+ + 8e^- = 3PbO \cdot PbSO_4 \cdot H_2O + 4H_2O$	$E_h = 1.325 - 0.074\,pH + 0.007 \lg \alpha_{SO_4^{2-}}$
4	$3PbO_2 + 4H^+ + 4e^- = Pb_3O_4 + 2H_2O$	$E_h = 1.122 - 0.059\,pH$
5	$PbO_2 + 2H^+ + 2e^- = PbO + H_2O$	$E_h = 1.107 - 0.0591\,pH$
6	$PbSO_4 + H^+ + 2e^- = Pb + HSO_4^-$	$E_h = -0.302 - 0.029\,pH - 0.029 \lg \alpha_{HSO_4^-}$
	$PbSO_4 + 2e^- = Pb + SO_4^{2-}$	$E_h = -0.358 - 0.029 \lg \alpha_{SO_4^{2-}}$
7	$PbO \cdot PbSO_4 + 2H^+ + 4e^- = 2Pb + SO_4^{2-} + H_2O$	$E_h = -0.13 - 0.029\,pH - 0.015 \lg \alpha_{SO_4^{2-}}$
8	$3PbO \cdot PbSO_4 \cdot H_2O + 6H^+ + 8e^- = 4Pb + SO_4^{2-} + 4H_2O$	$E_h = 0.030 - 0.044\,pH - 0.007 \lg \alpha_{SO_4^{2-}}$
9	$PbO + 2H^+ + 2e^- = Pb + H_2O$	$E_h = 0.028 - 0.059\,pH$
10	$PbO \cdot PbSO_4 + SO_4^{2-} + 2H^+ = 2PbSO_4 + H_2O$	$E_h = 8.4 + 0.5 \lg \alpha_{SO_4^{2-}}$
11	$3PbO \cdot PbSO_4 \cdot H_2O + SO_4^{2-} + 2H^+ = 2(PbO \cdot PbSO_4) + 2H_2O$	$E_h = 9.6 + 0.5 \lg \alpha_{SO_4^{2-}}$
12	$4Pb_3O_4 + 3SO_4^{2-} + 14H^+ + 8e^- = 3(3PbO \cdot PbSO_4 \cdot H_2O) + 4H_2O$	$E_h = 1.730 - 0.103\,pH + 0.007 \lg \alpha_{SO_4^{2-}}$
13	$Pb_3O_4 + 2H^+ + 2e^- = 3PbO + H_2O$	$E_h = 1.076 - 0.059\,pH$
14	$4PbO + SO_4^{2-} + 2H^+ = 3PbO \cdot PbSO_4 \cdot H_2O$	$E_h = 14.6 + 0.5 \lg \alpha_{SO_4^{2-}}$

It is a first-order reaction. According to the reaction rate law, the reaction rate can be written as,

$$r_c = \kappa_c \alpha_{H_2O}^2 . \tag{61}$$

where, $\alpha_{H_2O}^2$ expresses the activity of the water, and the constant κ is the rate coefficient of the reaction.

Similarly, the overall side reaction of self-discharging can be written as,

$$PbO_2 + Pb + 2H_2SO_4 \longrightarrow 2PbSO_4 + H_2O + H_2 + \frac{1}{2}O_2 \tag{62}$$

Since the PbO_2 and Pb are both in the solid phase, the activities of both are 1. Therefore, the reaction rate of the overall side reaction of self-discharging is

$$r_s = \kappa_s \alpha_{H_2SO_4}^2 \tag{63}$$

The OCV is the electromotive force that is based on the equilibrium potential of electrodes. The equilibrium potential of electrodes is a function of activity. According to the Nernst equation, the relationship between OCV and activity is built. $\alpha = f(OCV)$.

If the SOC is known, the concentration of H_2SO_4 at 25°C can be calculated by SOC definition, such as $C_{H_2SO_4} = f(SOC)$.

The effect of temperature on the OCV can be expressed as a function based on temperature, OCV at 25°C and concentration of H_2SO_4. $OCV = g(T, C_{H_2SO_4})$

The reaction rate of the side reaction causing water loss is,

$$r_c = \kappa_c \alpha_{H_2O}^2 = \kappa_c [f(T, SOC)]^2 \quad (64)$$
$$r_s = \kappa_s \alpha_{H_2SO_4}^2 = \kappa_s [f(T, SOC)]^2$$

In this thesis, because the range of operating temperature of the battery and algorithm operation speed are considered, we ignore the effect of temperature. Therefore, the reaction rate of side reaction is,

$$r_c = \kappa_c \alpha_{H_2O}^2 = \kappa_c [f(SOC)]^2 \quad (65)$$
$$r_s = \kappa_s \alpha_{H_2SO_4}^2 = \kappa_s [f(SOC)]^2$$

The amount of water loss can be calculated by the following equations,

Charging:
$$m_{H_2O} = M_{H_2O} \int_0^t r_c dt = M_{H_2O} \int_0^t \kappa_c \alpha_{H_2O}^2 dt \quad (66)$$

Self-discharge:
$$m_{H_2O} = \frac{M_{H_2O}}{2} \int_0^t r_s dt = \frac{M_{H_2O}}{2} \int_0^t \kappa_s \alpha_{H_2SO_4}^2 dt \quad (67)$$

where, M_{H_2O} is the molar mass of water, which is 18 g/mol.

4.2 Experiments

The following three subsections focus on finding out the reaction rates of side reactions. Section 4.2.1 introduces the measurement system of pressure. Section 4.2.2 discusses the maximum pressure of the battery and the free inner volume of the battery. Finally, section 4.2.3 describes how to calculate the reaction rate.

4.2.1 Pressure measurement system

Figure 70 shows the measurement system of pressure. It is comprised of a pressure sensor, electronic valve, manual valve, injector, sample bag, connectors and hose. This system is designed to test the reaction rate of water decomposition during charging, discharging and rest (κ_c and κ_s

in equation (65)). In this system, as the original safety valve of the battery cannot be controlled, is replaced by an electric valve. When the current pressure is larger than maximum pressure (P_{max}), the electronic valve will reduce the pressure. The P_{max} should be measured, the electronic valve can be set to work exactly the same as the original valve.

The manual valve and injector works to test the maximum pressure of the battery and the inner volume of the battery. The pressure sensor can convert the air pressure into a voltage signal that can be measured and recorded by a PC. The sample bag collects the gas for gas analysis.

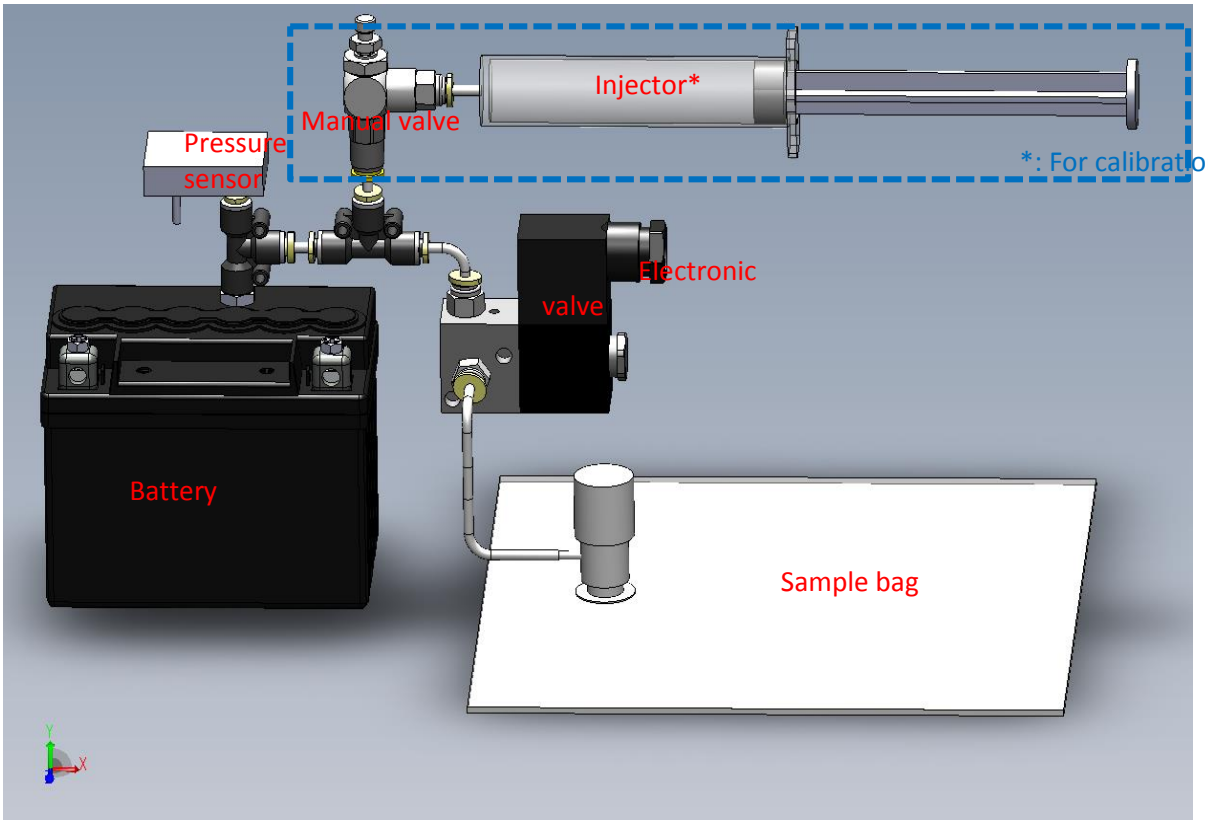

Figure 70: Measurement system of pressure.

4.2.2 Maximum pressure and inner volume of the battery

The application of small gas channels in the electrolyte cannot completely eliminate the gassing. In order to avoid the lead acid battery exploding due to water evaporation of electrolyte, the lead acid battery should install a sealed shell that has a safety valve.

This valve release gas, when the inner pressure is too high. According to the design requirement of different manufacturers, this value of the limit pressure of the valve usually is 1.0-2.0 psi. The pressure limit is called the maximum pressure of the battery (P_{max}).

Before the calculation of the reaction rate, the maximum pressure should be tested. The steps to measure it are as follows.

1. Turn off the electronic valve;
2. Turn on the manual valve;
3. Push piston, inject air;
4. Turn off the manual valve;
5. Remove injector, Pull piston;
6. Repeat step 3~6;
7. Record the max pressure (maximum allowable pressure of the safety valve: P_{max}).

Another important parameter of the system is the inner free space of the battery (V_{sys}) which is used to calculate the amount of water that decompose.

When the electric valve is cut off, the manual valve is turned on. In the initial conditions, the pressure is P_1, the temperature is T_1, the volume of injector is V_{in}, and the inner free space of the battery is V_{sys}. According to the ideal gas equation of the state, the state of the system is,

$$P_1\left(V_{sys}+V_{in}\right)=nRT_1 \tag{68}$$

After V_{air} air is injected in a battery, the pressure and temperature are changed to P_2 and T_2. The state of the system is,

$$P_2\left(V_{sys} + V_{in} - V_{air}\right) = nRT_2 . \tag{69}$$

The inner free space of the battery can be calculated by equation (70),

$$V_{sys} = V_{in} - \frac{P_2 T_1}{P_1 T_2 - P_2 T_1} V_{air} . \tag{70}$$

Table 12 is the experimental data collected during this process. According to equation (70), using the least square method (LS), the inner free space (V_{sys}) is calculated. V_{sys} = 83.1 m*l*.

Table 12: Experimental data of inner free space of the battery

Injected volume (ml)	0	1	2	3	4	5	6	7	8	9	10
ΔP (psi)	0	0.019	0.056	0.100	0.144	0.189	0.231	0.276	0.318	0.365	0.405

4.2.3 Reaction rate

The experimental data of voltage, current, temperature, and change in pressure are shown in Figure 71. The goal of this experiment is to calculate the water loss by measuring the pressure change during battery operation. Terminal voltage and current of the battery are plotted in Figure 71 (a) and (b).. First, this battery is charged by C.C. and C.V. The current in C.C. mode is 45A and then rested for two hours. Temperature and difference between air pressure and battery pressure and is shown in Figure 71 (c) and (d) is shown in.

The pressure change (Figure 71 (d)) is used to calculate water loss. The flowchart of the calculation is shown in Figure 72, where n_{out} and n_{gen} denote the molar quantity of the released

gas the generated gas. Before the test, the initial pressure (P_0) and temperature (T_0) are measured and the pressure and temperature are measured during charging and discharging. If the pressure is less than P_{max}, the n_{gen} is calculated by equation (71), otherwise the n_{out} is calculated by equation (72). Finally, the mass of water loss is calculated by equation (73), where M_{gas} is the molar mass of oxygen and hydrogen.

$$n_{gen} = n_{out} + \frac{V_{sys}}{R}\left(\frac{P_k}{T_k} - \frac{P_0}{T_0}\right) \tag{71}$$

.

$$n_{out} = n_{out} + \frac{V_{sys}}{R}\left(\frac{P_k}{T_k} - \frac{P_0}{T_0}\right) \tag{72}$$

$$m_{loss} = n_{gen} M_{gas} \tag{73}$$

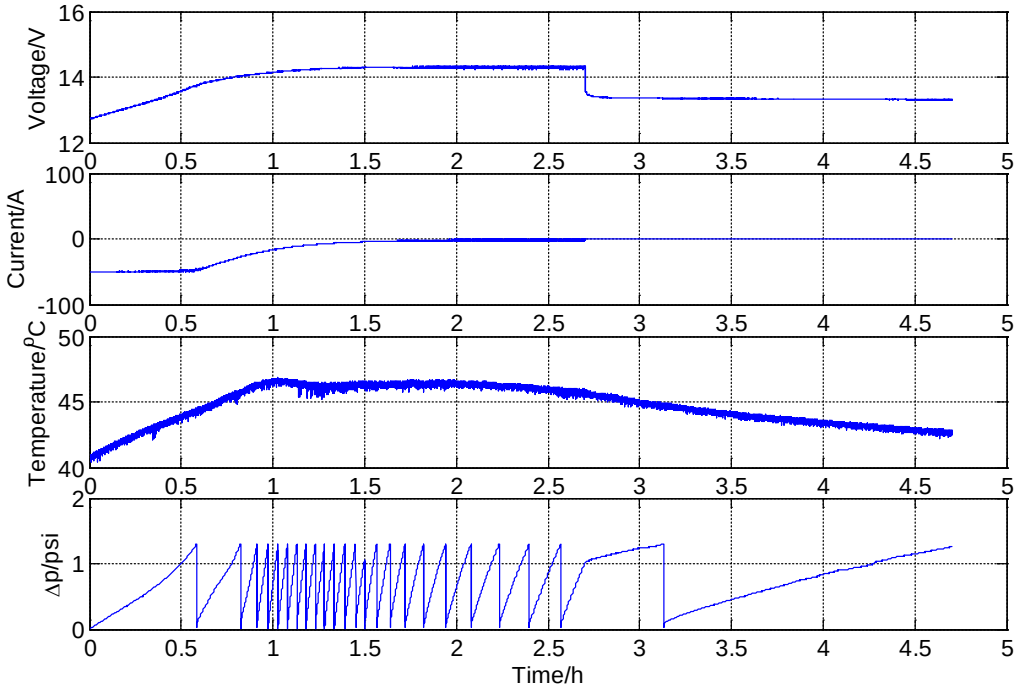

Figure 71: Experimental data of voltage, current, temperature and pressure change.

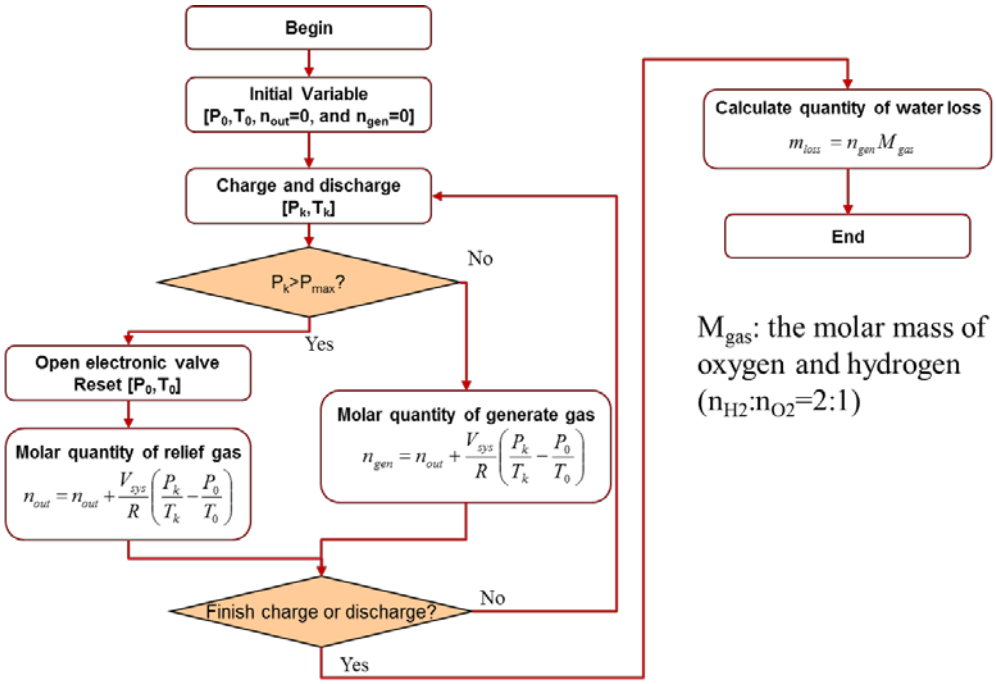

Figure 72: Flowchart of the measurement of water loss.

The amount of water loss is shown in Figure 73. Using equation (65) and the results of the amount of water loss, the reaction rate of water loss can be fitted. $\kappa_c = 8.21\times10^{-9}$ and $\kappa_s = 1.43\times10^{-11}$.

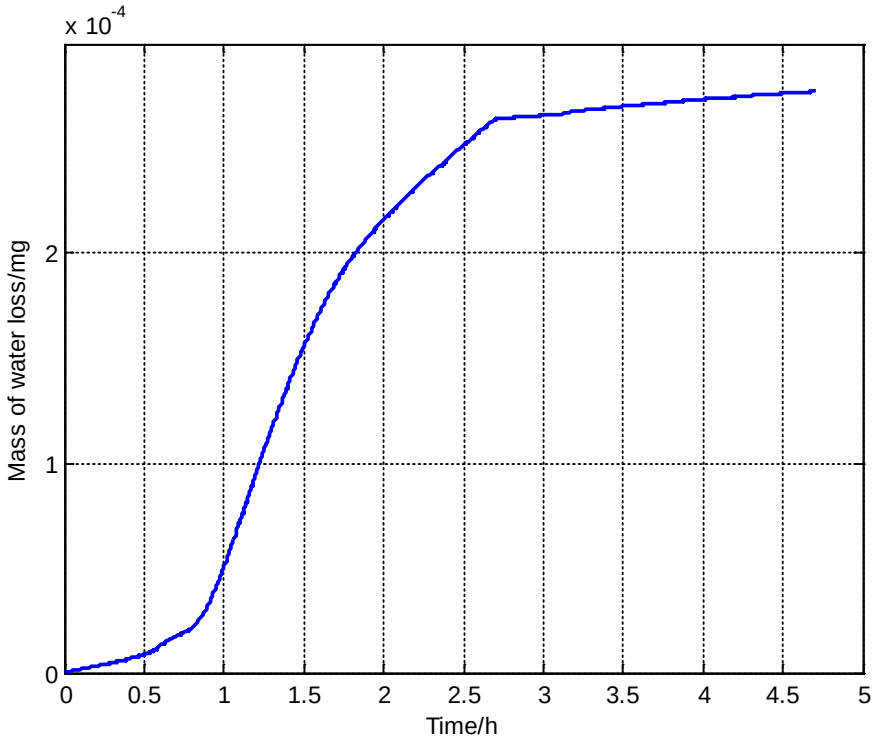

Figure 73: Amount of water loss in charging and rest.

4.3 Results of water loss

Figure 74 shows the voltage, current, temperature, and the change in pressure of a fresh battery during a full cycle that consists of constant current charging, constant voltage charging, rest, constant current discharging, constant voltage discharging, and another rest. The estimation of water loss is shown in Figure 75. After about nine hours' test, predicted water loss was 0.42μg. Most of the water loss takes place at the end of C.C. charging and the beginning of C.V. charging, where the SOC, voltage, and temperature are very high.

The voltage, current, temperature, and the change of the pressure of an aged battery during multi-cycles is shown in Figure 76. Every single cycle consists of constant current charging, constant voltage charging, rest, constant current discharging, constant voltage discharging, and

another rest. Figure 77 shows the result of water loss estimation. After 4 cycles, the total water loss was 1.8μg, and 0.45μg in each cycle, which matches the test results in a single cycle of Figure 75. Similar to the previous tests, most of the water loss takes place at the end of C.C. charging and the beginning of C.V. charging, where all the SOCs, voltages, and temperatures are very high.

Figure 78 shows the voltage, current, temperature, and the change in pressure of a used cell during a random current. It is testing the algorithm in normal application. The result of water loss in this process is shown in Figure 79. Different from the previous two tests, the water loss is not much, the temperature keeps 40^{o}C, and the voltage is less than 13V.

The results of water loss estimation plotted in Figure 75, Figure 77, and Figure 79 show good match with measurements, although there are some errors, because the effect of temperature is ignored in this algorithm. Consideration of the effect of temperature could make the algorithm more accurate. Moreover, all the results show that high SOC, over temperature and voltage leads to more water loss, which results in fast battery degradation. Therefore, the BMS should monitor the SOC, voltage, and temperature of the battery, and control the battery usage in real application to prolong the battery's cycle life.

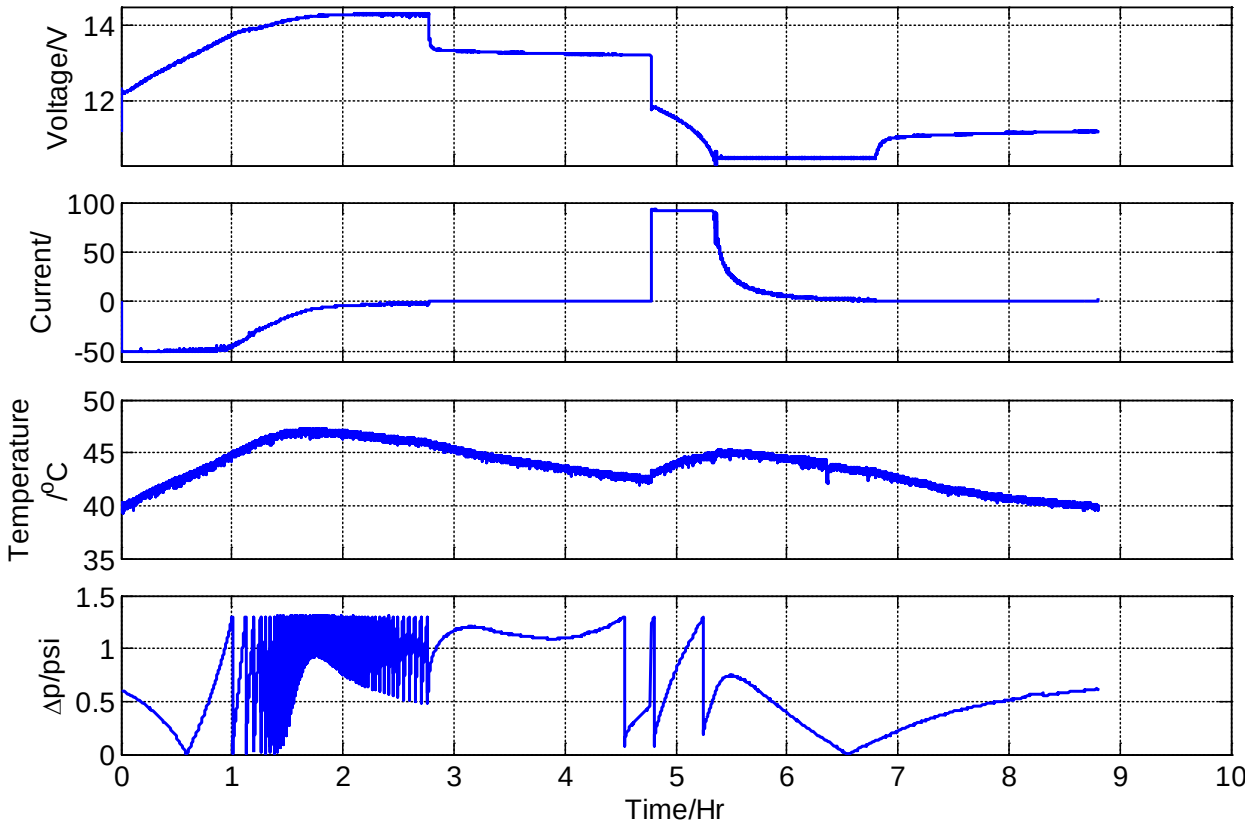

Figure 74: Experimental data of a fresh battery during a full cycle (C.C. charging, C.V. charging, rest, C.C. discharging, C.V. discharge and rest) at 40°C, including voltage, current, temperature, and change of pressure.

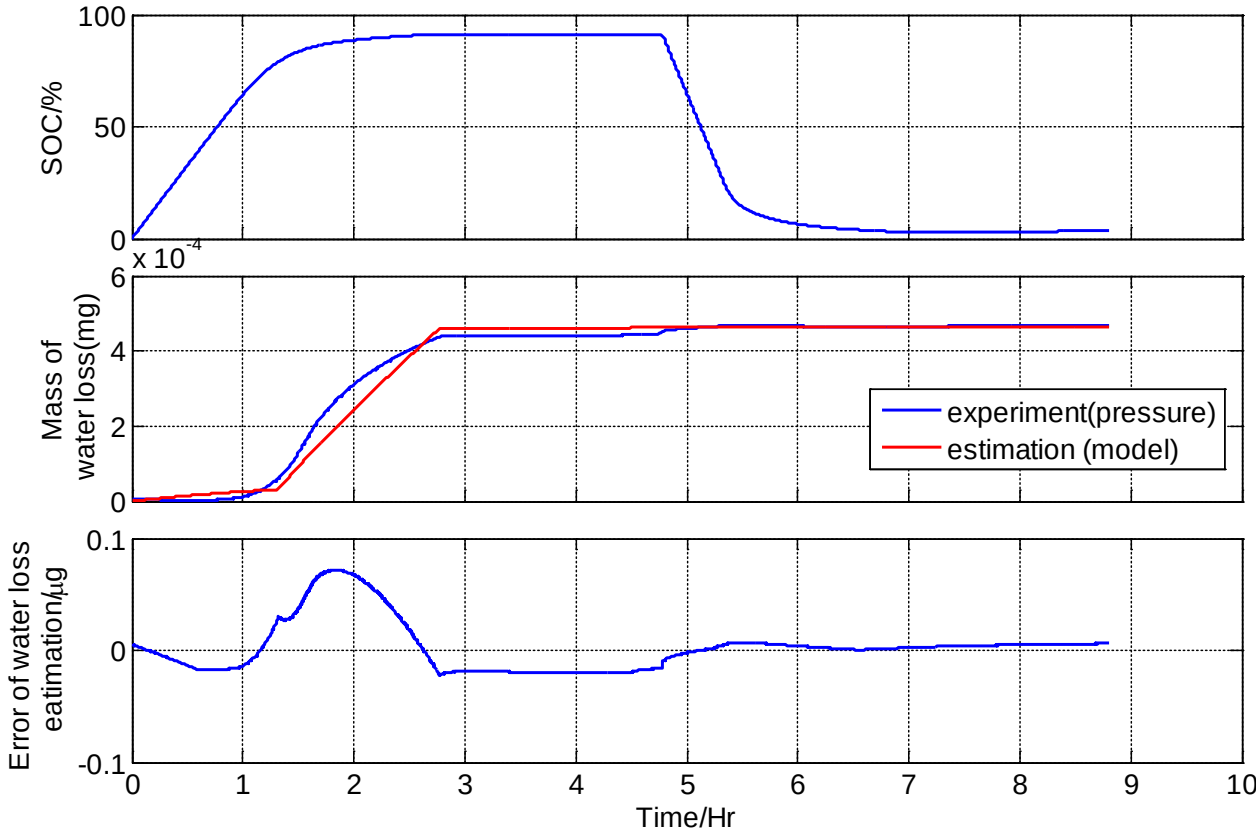

Figure 75 Estimation of water loss during a full cycle at 40°C.

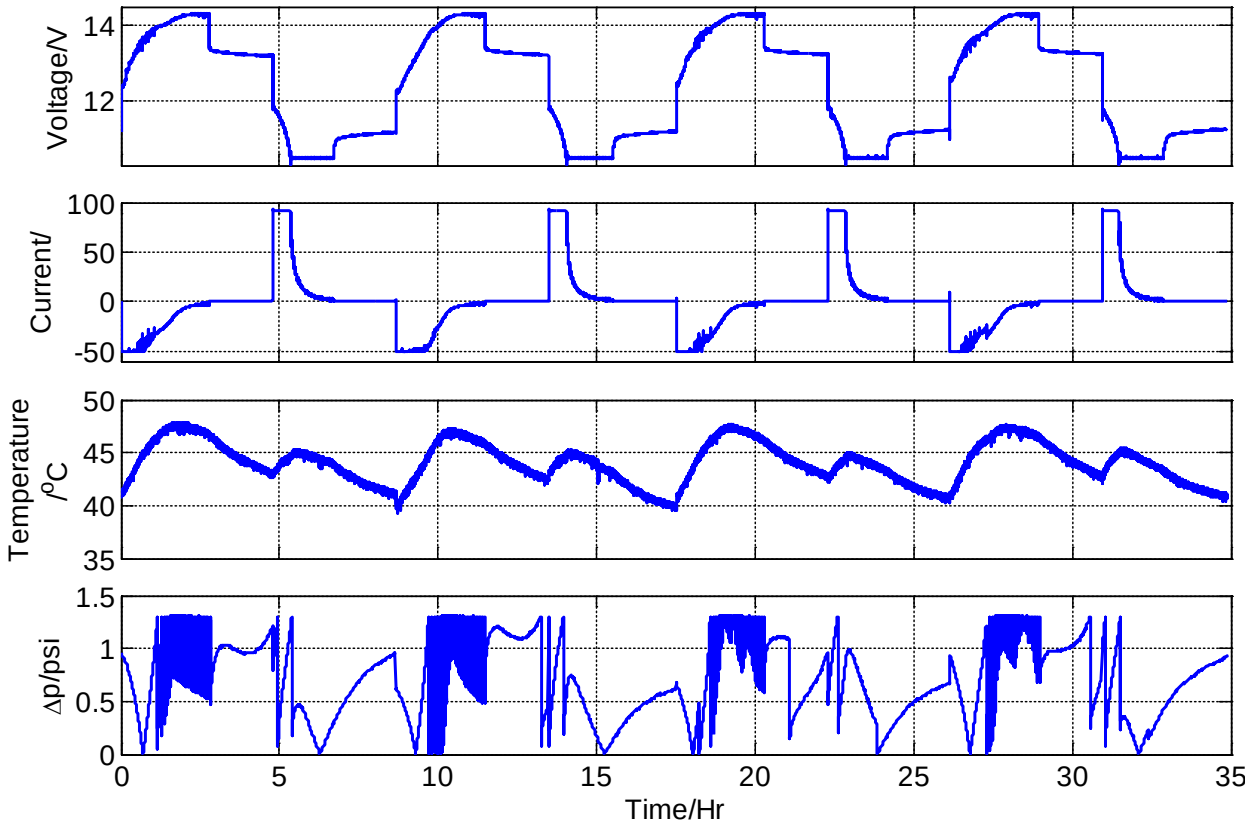

Figure 76: Experimental data of an aged battery during multi-cycle test at 40°C, including voltage, current, temperature, and change of pressure.

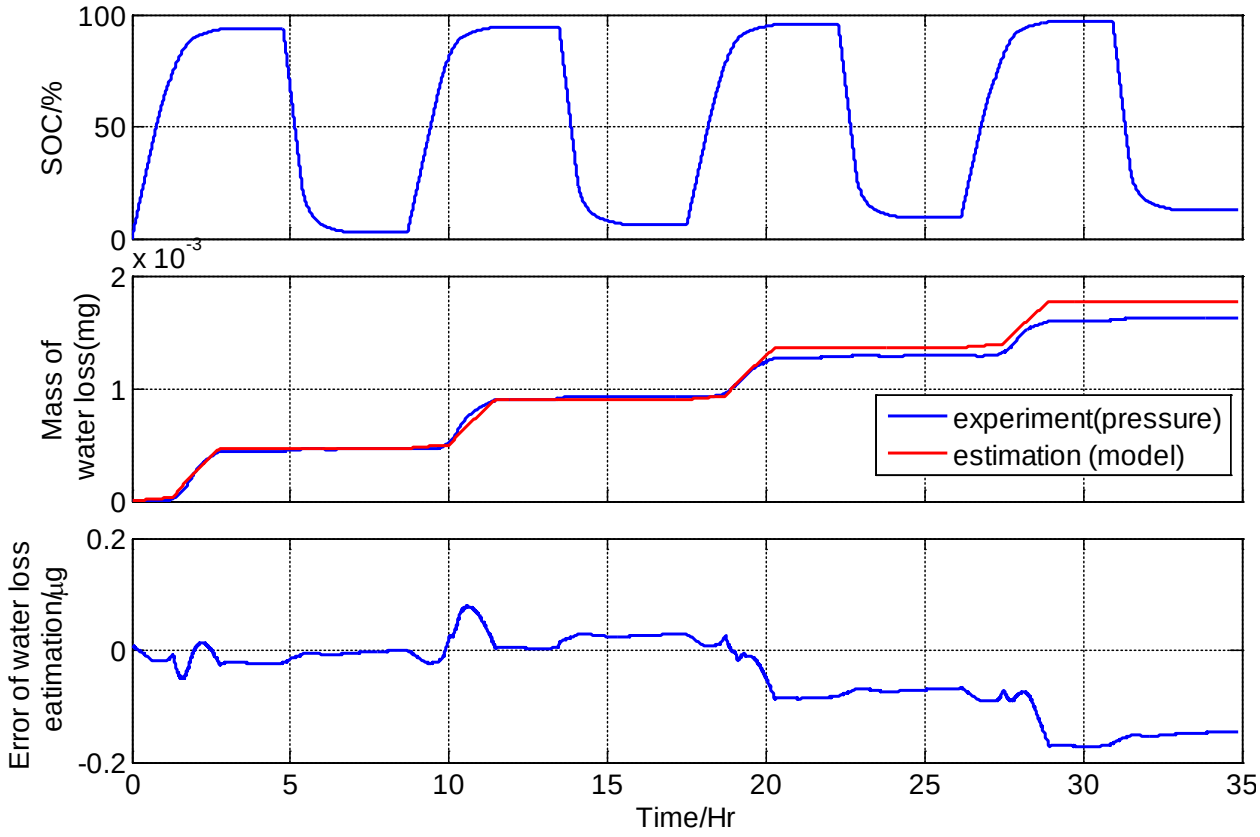

Figure 77: Estimation of water loss during multi-cycle test at 40°C.

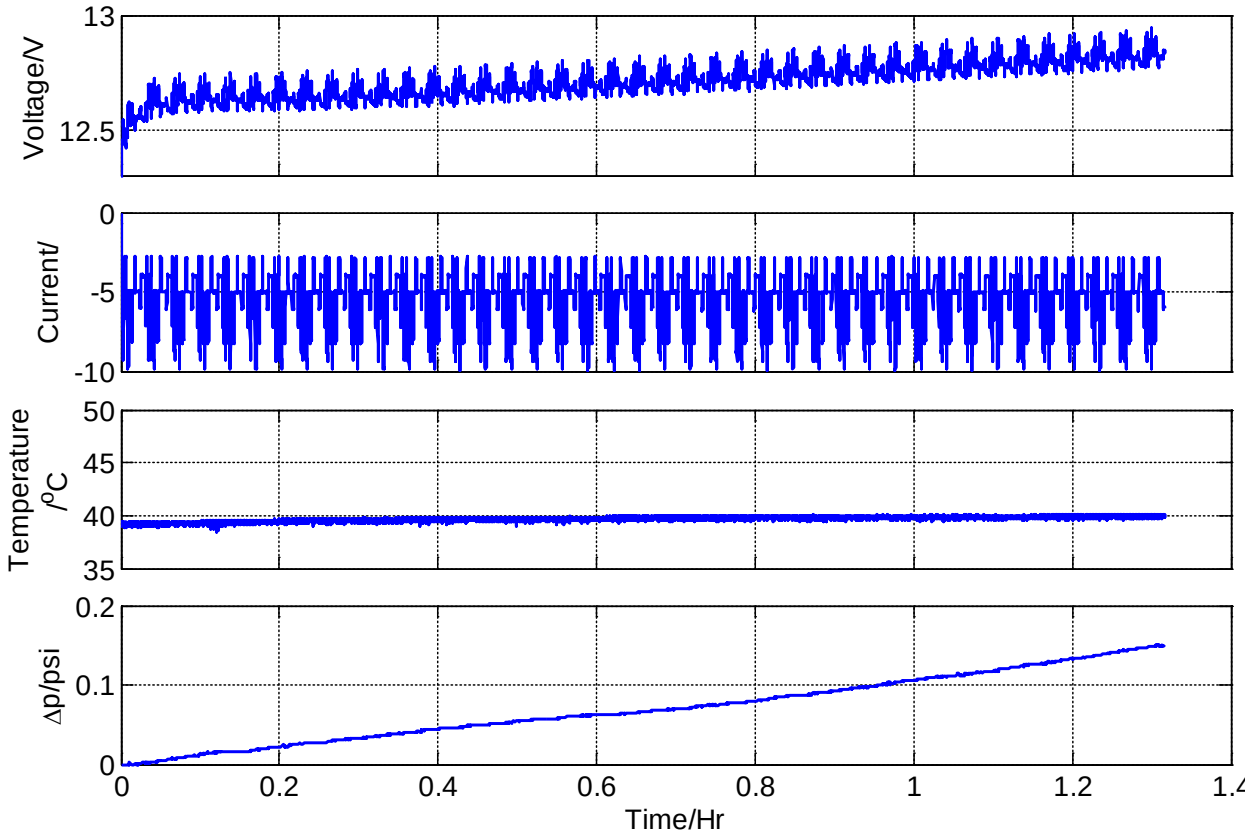

Figure 78: Experimental data of a fresh battery during random charge and discharge at 40°C, including voltage, current, temperature, and change of pressure.

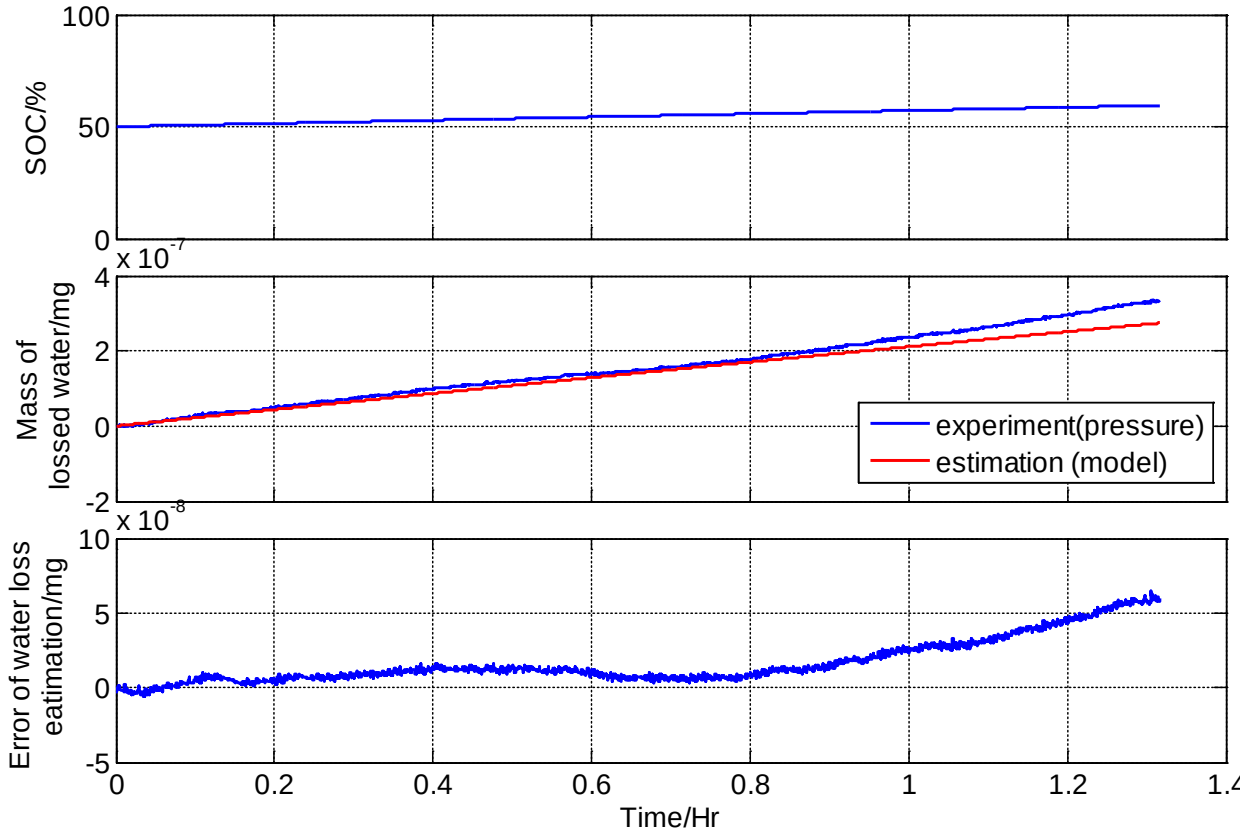

Figure 79: Estimation of water loss in a randomly charging and discharging cycle.

Chapter 5: Conclusion and future work

5.1 Conclusion

5.1.1 SOC estimation

This work focuses on developing an SOC estimation method for the AGM lead acid battery operating at various temperatures and aging states. The proposing SOC estimation method combined two methods. One is Coulomb counting that works in C.V. charging and is improved by a capacity-temperature model. The other method is based on second order ECM, where the EKF is used for error correction. The state of the system includes the SOC and the parameters of the ECM. The parameters are identified online. The new method works well in C.C. charging, C.V. charging, and C.C. discharging at various temperatures.

Through a set of drive cycle data, the simulation results show the accuracy, practicability, and reliability of the novel SOC estimation method.

5.1.2 Water loss estimation

This thesis proposes a new method to measure water loss of an AGM lead acid battery. The mass of water loss is calculated based on the measured pressure change taking place inside the battery. Using this method, the side reaction rate is also calculated. The mass of water loss, which becomes hydrogen and oxygen gas after decomposition, is estimated by the reaction rate. The comparison between simulation and experiment results shows accurate estimation of the water loss.

5.2 Future work

- For SOC estimation, further development of ECM for CV mode is needed.
- For estimation of water loss, effects of temperature and aging process should be considered. In addition, effects of water loss should be considered for efficiency of

charging, estimation of capacity and aging process including OCV. The effects of water loss can be explain in three categories.

First, the gases are generated from water in electrolyte, which process dissipates a lot of energy, particularly when charging and affects charging efficiency.

Second, oxygen produced by the gassing plays a very important role in the positive plate. During gassing, the oxygen evolved at the positive plate surface penetrates through the corrosion layer to the lead grid and oxidizes its surface to PbO_2. The obtained PbO_2 layer has a high Ohmic resistance. If the rate of PbO_2 formation is higher than the rate of its oxidation to PbO_2, a thick layer of PbO_2 with a high Ohmic resistance forms on the grid surface which leads to a high polarization of the plate on discharge and eventually causes a capacity loss [1].

Third, when gassing occurs, the concentration of the electrolyte increases because of water loss. Effects of the electrolyte concentration of H_2SO_4 on aging process are summarized in Figure 80.

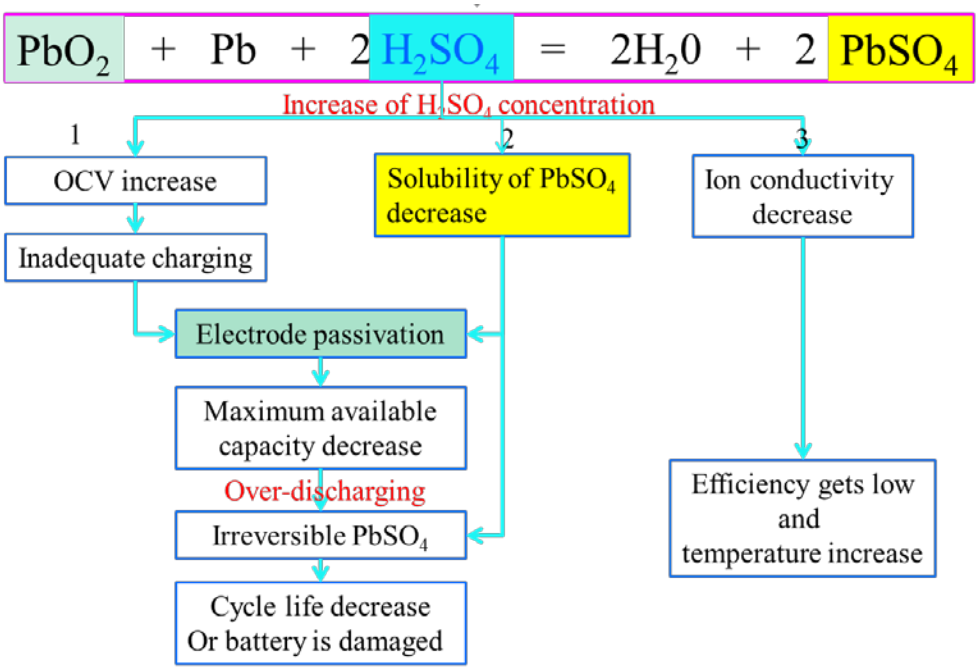

Figure 80: Effects of concentration of H_2SO_4 on lead acid degradation.

The most important effect of water loss is the change of OCV that V is directly related to the electrolyte concentration (See Chapter 4). When the concentration increases, the OCV tends to increase, which is shown in equation (52). For SOC estimation, the OCV-SOC curve is assumed to be unchangeable with battery conditions. Considering water loss, the OCV-SOC curve should be updated during aging.

Reference

[1] D. Pavlov, *Lead-acid batteries: science and technology: science and technology*: Elsevier, 2011.

[2] F. Sun, X. Hu, Y. Zou, and S. Li, "Adaptive unscented Kalman filtering for state of charge estimation of a lithium-ion battery for electric vehicles," *Energy,* vol. 36, pp. 3531-3540, 2011.

[3] Y. Hu and S. Yurkovich, "Battery state of charge estimation in automotive applications using LPV techniques," in *American Control Conference (ACC),* pp. 5043-5049, 2010.

[4] V. Pop, H. Bergveld, J. O. het Veld, P. Regtien, D. Danilov, and P. Notten, "Modeling battery behavior for accurate state-of-charge indication," *Journal of The Electrochemical Society,* vol. 153, pp. A2013-A2022, 2006.

[5] F. Codecà, S. M. Savaresi, and G. Rizzoni, "On battery state of charge estimation: A new mixed algorithm," in *Control Applications, 2008. CCA 2008. IEEE International Conference on*, pp. 102-107, 2008.

[6] P. Mauracher and E. Karden, "Dynamic modelling of lead/acid batteries using impedance spectroscopy for parameter identification," *Journal of power sources,* vol. 67, pp. 69-84, 1997.

[7] S. Rodrigues, N. Munichandraiah, and A. Shukla, "A review of state-of-charge indication of batteries by means of ac impedance measurements," *Journal of power Sources,* vol. 87, pp. 12-20, 2000.

[8] S. Piller, M. Perrin, and A. Jossen, "Methods for state-of-charge determination and their applications," *Journal of power sources,* vol. 96, pp. 113-120, 2001.

[9] H. Chaoui and P. Sicard, "Accurate state of charge (SOC) estimation for batteries using a reduced-order observer," in *Industrial Technology (ICIT), 2011 IEEE International Conference on*, pp. 39-43, 2011.

[10] H. He, R. Xiong, X. Zhang, F. Sun, and J. Fan, "State-of-charge estimation of the lithium-ion battery using an adaptive extended Kalman filter based on an improved Thevenin model," *Vehicular Technology, IEEE Transactions on,* vol. 60, pp. 1461-1469, 2011.

[11] N. K. Bullock and W.-H. Kao, "Lead-acid battery," ed: Google Patents, 1991.

[12] W. Gu, C. Wang, and B. Liaw, "Numerical Modeling of Coupled Electrochemical and Transport Processes in Lead‐Acid Batteries," *Journal of The Electrochemical Society,* vol. 144, pp. 2053-2061, 1997.

[13] G. L. Plett, "Sigma-point Kalman filtering for battery management systems of LiPB-based HEV battery packs: Part 2: Simultaneous state and parameter estimation," *Journal of Power Sources,* vol. 161, pp. 1369-1384, 2006.

[14] G. L. Plett, "Sigma-point Kalman filtering for battery management systems of LiPB-based HEV battery packs: Part 1: Introduction and state estimation," *Journal of Power Sources,* vol. 161, pp. 1356-1368, 2006.

[15] E. Wan and R. Van Der Merwe, "The unscented Kalman filter for nonlinear estimation," *Adaptive Systems for Signal Processing, Communications, and Control Symposium 2000. AS-SPCC. The IEEE* , pp. 153-158, 2000.

[16] H. Dai, X. Wei, Z. Sun, J. Wang, and W. Gu, "Online cell SOC estimation of Li-ion battery packs using a dual time-scale Kalman filtering for EV applications," *Applied Energy,* vol. 95, pp. 227-237, 2012.

[17] G. L. Plett, "Extended Kalman filtering for battery management systems of LiPB-based HEV battery packs: Part 3. State and parameter estimation," *Journal of power sources,* vol. 134, pp. 277-292, 2004.

[18] L. Wang, L. Wang, and C. Liao, "Research on improved EKF algorithm applied on estimate EV battery SOC," *Power and Energy Engineering Conference (APPEEC), 2010 Asia-Pacific*, pp. 1-4, 2010

[19] G. L. Plett, "Extended Kalman filtering for battery management systems of LiPB-based HEV battery packs: Part 2. Modeling and identification," *Journal of power sources,* vol. 134, pp. 262-276, 2004.